

Response to Review n.1

November 25, 2019

General comments

General comments: The abstract is very long and contains too many information. Suggest to re-write it in a more concise way. The same comment is valid for the chapter 3.3.1 Window of opportunities, here there are interesting observations, but sometimes slightly verbose. The authors indicate that the active sediments are influenced by “deep methane source”, then at the end of the paper they define that the deep methane source is ca 3 m below the seafloor, which is not exactly very deep. Would it be possible to find another term instead of “deep”? In any case, this has to be better defined at the beginning of the manuscript

Response

We would like to thank the reviewer for the overall positive comment and suggestions. We will revise the abstract and the section 3.3.1 *Window of opportunity* for the final version of the paper.

In addition, we will also clarify the term “deep”. We used the term “deep” to refer to methane sources below the simulated sediment column (*i.e.* > 3 m) not investigating the precise origin of this methane (permafrost/hydrates/thermogenic sources/in situ production) at the base of the sediment column (which could also come from even deeper depths). But we do agree that we must refer more clearly to the base of the sediment column.

Specific comments

1. Page 2 Lines 17-18: “Under these conditions, permafrost aggraded on the shelf and was subsequently submersed when rising sea level flooded the shelf during the Holocene sea transgression (12 and 5 kyr BP)”. Reference is needed
Response: We added a reference to Romanovskii and Hubberten, 2001; Romanovskii, Hubberten, et al., 2005, for the thickness after submer-sion and Bauch et al., 2001 for the sea transgression.

2. Page 2 Line 19: explain what is “gas hydrate”
Response: a state of matter in which a low molecular weight gas (like CH₄) is trapped in a “cage” of water molecules and whose structure is thermodynamically stable under specific temperature-pressure-salinity conditions that are found either in oceanic depths or beneath the permafrost (Sloan Jr et al., 2007). We will integrate a definition in the revised version of the manuscript..
3. Page 2 Lines 29-30: “The increasing influx of warmer Atlantic water into the Arctic Ocean - the so-called Atlantification”. This term need to be explained and relevant papers need to be cited. In both “Zhang et al., 1998; Biastoch et al., 2011” the term Atlantification is not mentioned.
Response: the influence of warmer and saltier waters of Atlantic origins has been identified and brought up to the attention of the scientific community already in Biastoch et al., 2011; Carmack et al., 1995; Zhang et al., 1998, but the term “Atlantification” appears only in Polyakov et al., 2017 and Barton et al., 2018. These reference will be added in the revised version of the manuscript.
4. “Page 2 Line 2: what destabilize gas hydrate? Pressure changes or temperature increase? Or what?”
Response: both pressure and temperature change are responsible of gas hydrates destabilization as reported in paragraph 3.3 of Shakhova, Semiletov, and Chuvilin, 2019. It has been suggested that in the case of subsea permafrost associated gas hydrates, temperature plays a more important role gas hydrate destabilization (Chuvilin et al., 2018; Mako-gon et al., 2007).
5. Page 4 Line 6: which are the “changes in environmental condition” mentioned here?
Response: The transient change in lower CH₄ boundary conditions and, in case of the seasonal scenario n.2, also the change in the upper boundary conditions of SO₄²⁻. We will clarify this point in the revised version of the manuscript.
6. Page 4 Line 12: for methane emissions and fractures, it might be useful to read a recently published paper in Biogeosciences “Yao et al., 2019”. Biogeosciences, 16, 2221-2232, 2019.
Response: Thanks for the suggestion. The recommend paper indeed supports our understanding of methane transport and biogeochemistry in fracture-affected sediments and we will add a reference to the revised version of the manuscript.
7. Page 4 Line 19: What are the “passive and active sediment”? Although there is some explanation later in the manuscript, these concepts need to be explained here, as soon as they are mentioned in the text.

Response: “Passive sediments” are sediments characterized by the absence of an advective water flow. In contrast, “active sediments” are subject to a non-zero water flow pointing upwards towards the sediment-water interface. The definition in the paper is reported at page 5, line 18-19. We will define these terms earlier in the revised version of the manuscript.

8. Page 6 Line 15: what about the anaerobic oxidation of methane?

Response: The aerobic and the anaerobic oxidation of methane have been regarded as secondary redox reaction, as they are not directly involved in the degradation of the organic matter. They are described in detail later on (page 6, line 32 and page 7).

9. Page 9 Line 10: why the authors have assumed both baseline scenarios a water depth of 30 m when the average water depth of the ESAS is ~ 45 m (data from James et al., 2016)?

Response: mainly for two reasons:

- We do not expect a large difference in the results between 30 or 45 meters, as well as if we had used 60 m. The mechanisms we identify and the sensitivity we explore is expected to be largely unaffected by such small changes in the water depth. Results indicate that one of the main controls on non-turbulent methane escape is the sedimentation rate ω . Applying the formulation of Burwicz et al., 2011, ω has basically the same value for 30 m and 45 m water depth. The only factor which is sensitive to water depth is the saturation value of methane ($[\text{CH}_4]^*$). At a water depth of 30 m, $[\text{CH}_4]^* = 5.45 \mu\text{M}$ as opposed to $\sim 10 \mu\text{M}$ at 45 m. This last value might increase even more the efficiency of the biofilter, leading in case simply to a reduction of the maximum CH_4 we identified.
- The observed increase in summer temperature (Dmitrenko et al., 2011) occurs at shallower depths (~ 10 m). We wanted to investigate even shallower shelves, as they are the ones expected to be more delicate and active from the biogeochemical point of view. For this reason we set a depth halfway between the average value of 45 m (which takes into account also deeper depths, not really important for methane emissions) and shallower shelves closer to the coast.

10. Page 10 Line 28: is the trawling in the area affecting gas hydrate stability also? Is the gas hydrate close to the seafloor? Where is the real sediment depth? Which is the thickness of the sediments that is affected by trawling? Few cm or maybe 1 meter?

Response: On the Siberian shelf, gas hydrates are often associated with subsea permafrost (the so called subsea permafrost associated gas hydrates, Ruppel et al., 2017) and are located below the subsea

permafrost. Trawling can affect sediments: from centimeters to meters to a few meters (Shakhova, Semiletov, Gustafsson, et al., 2017) and, thus, is not expected to exert a significant effect on hydrate stability. In any case, we do not simulate subsea permafrost thawing or hydrate destabilization explicitly, but rather explore the fate of plausible methane fluxes from such deep sources and therefore do not make assumptions about release mechanisms and drivers.

11. Page 17 Line 13: “rapidely”.
Response: Thanks. Typo corrected
12. Page 23 lines 26-29: Would it be possible to better explain this concept here? I found very difficult to follow the reasoning here and related gas saturation concentration with precipitation of authigenic carbonates.
Response: Thanks. We will revise this section to clarify these aspects.
13. Page 24 Line 28: Lena river and Moustakh Island in the Buor-Khaya Gulf need to be included in Figures and captions. As a general rule, all the locations that are mentioned in the main text need to be reported in location maps and relative captions.
Response: The revised version of the manuscript will include a map reporting the mentioned locations.
14. Page 26 Lines 16-17: The authors indicate that Additional physical reworking such as ice scouring or dredging, or the absence of bioirrigation, which is known to be patchy in Arctic sediments could even further reduce estimated methane efflux. I would assume that these processes might enhance the methane fluxes instead since they remobilize sediments. More elaboration is needed here.
Response: The effects of non-local mixing processes are complex. They can indeed increase fluxes by enhancing transport through the sediment. However, they can also reduce fluxes of methane (and other reduced species) by increasing the flux of oxygen and sulfate into the sediment. We will revise this section to clarify this point.
15. Page 26 Line 25: “Artic’s”.
Response: Thanks. Typo corrected
16. How does it happen that “increasing sedimentation rates occur through coastal erosion”? please clarify.
Response: Coastal erosion and the erosion of coastal ice complex provide an input of debris and sediments which are sink rapidly to the sea floor (Vonk et al., 2014). Areas close to the coast are affected by coastal erosion and will thus receive a higher input of terrigenous material.
17. Page 28 Lines 33-34: “we show that methane from deep sources (ca. 3 m) reaches the sediment water interface within 7 to 20 years.” A comment on the fact that

3 meters is considered deep has been previously reported.

Response: see comment above

18. Page 29 Line 29: wording “which is in turn is determined”.

Response: Thanks. Corrected.

19. Chapter 3.3.1 this chapter is not very well organized and it is difficult to follow.

Response: We will carefully revise this section.

20. Page 33 Lines 25-26: “On the ESAS, AOM is a transport-limited process and transport parameters thus exert an important control on the efficiency of the AOM biofilter and, thus, on methane efflux”. Please rewrite in a more clear way.

Response: Since AOM is a transport-limited process, transport processes and parameters exert a dominant control on the efficiency of the AOM biofilter and, ultimately, on the methane efflux at the SWI. We will revise the section accordingly.

21. Page 33 line27: what does “sedimentation and active fluid flow” in brackets mean respect the advective transport?

Response: We simply list the two possible types of advective transport considered.

References

- Barton, Benjamin I, Yueng-Djern Lenn, and Camille Lique (2018). “Observed Atlantification of the Barents Sea causes the Polar Front to limit the expansion of winter sea ice”. In: *Journal of Physical Oceanography* 48.8, pp. 1849–1866.
- Bauch, Henning A, Thomas Mueller-Lupp, Ekaterina Taldenkova, Robert F Spielhagen, Heidemarie Kassens, Peter M Grootes, Jörn Thiede, J Heinemeier, and VV Petryashov (2001). “Chronology of the Holocene transgression at the North Siberian margin”. In: *Global and Planetary Change* 31.1-4, pp. 125–139.
- Biastoch, Arne, Tina Treude, Lars H Rüpke, Ulf Riebesell, Christina Roth, Ewa B Burwicz, Wonsun Park, Mojib Latif, Claus W Böning, Gurvan Madec, et al. (2011). “Rising Arctic Ocean temperatures cause gas hydrate destabilization and ocean acidification”. In: *Geophysical Research Letters* 38.8.
- Burwicz, Ewa B, LH Rüpke, and Klaus Wallmann (2011). “Estimation of the global amount of submarine gas hydrates formed via microbial methane formation based on numerical reaction-transport modeling and a novel parameterization of Holocene sedimentation”. In: *Geochimica et Cosmochimica Acta* 75.16, pp. 4562–4576.
- Carmack, Eddy C, Robie W Macdonald, Ronald G Perkin, Fiona A McLaughlin, and Richard J Pearson (1995). “Evidence for warming of Atlantic water in the southern Canadian Basin of the Arctic Ocean: Results from the Larsen-93 expedition”. In: *Geophysical Research Letters* 22.9, pp. 1061–1064.
- Chuvilin, Evgeny, Boris Bukhanov, Dinara Davletshina, Sergey Grebenkin, and Vladimir Istomin (2018). “Dissociation and self-preservation of gas hydrates in permafrost”. In: *Geosciences (Switzerland)* 8.12. ISSN: 20763263. DOI: [10.3390/geosciences8120431](https://doi.org/10.3390/geosciences8120431). URL: <https://www.mdpi.com/2076-3263/8/12/431>.
- Dmitrenko, Igor A, Sergey A Kirillov, L Bruno Tremblay, Heidemarie Kassens, Oleg A Anisimov, Sergey A Lavrov, Sergey O Razumov, and Mikhail N Grigoriev (2011). “Recent changes in shelf hydrography in the Siberian Arctic: Potential for subsea permafrost instability”. In: *Journal of Geophysical Research: Oceans* 116.C10.
- Makogon, Y. F., S. A. Holditch, and T. Y. Makogon (2007). “Natural gas-hydrates - A potential energy source for the 21st Century”. In: *Journal of Petroleum Science and Engineering* 56.1-3, pp. 14–31. ISSN: 09204105. DOI: [10.1016/j.petrol.2005.10.009](https://doi.org/10.1016/j.petrol.2005.10.009). URL: <https://www.sciencedirect.com/science/article/pii/S0920410506001859>.
- Polyakov, Igor V, Andrey V Pnyushkov, Matthew B Alkire, Igor M Ashik, Till M Baumann, Eddy C Carmack, Ilona Goszczko, John Guthrie, Vladimir V Ivanov, Torsten Kanzow, et al. (2017). “Greater role for Atlantic inflows on sea-ice loss in the Eurasian Basin of the Arctic Ocean”. In: *Science* 356.6335, pp. 285–291.
- Romanovskii, Nikolai N and H-W Hubberten (2001). “Results of permafrost modelling of the lowlands and shelf of the Laptev Sea region, Russia”. In: *Permafrost and periglacial processes* 12.2, pp. 191–202.
- Romanovskii, Nikolai N, H-W Hubberten, AV Gavrilov, AA Eliseeva, and GS Tipenko (2005). “Offshore permafrost and gas hydrate stability zone on the shelf of East Siberian Seas”. In: *Geo-marine letters* 25.2-3, pp. 167–182.

- Ruppel, Carolyn D and John D Kessler (2017). “The interaction of climate change and methane hydrates”. In: *Reviews of Geophysics* 55.1, pp. 126–168.
- Shakhova, Natalia, Igor Semiletov, and Evgeny Chuvilin (2019). “Understanding the Permafrost–Hydrate System and Associated Methane Releases in the East Siberian Arctic Shelf”. In: *Geosciences* 9.6, p. 251.
- Shakhova, Natalia, Igor Semiletov, Orjan Gustafsson, Valentin Sergienko, Leopold Lobkovsky, Oleg Dudarev, Vladimir Tumskoy, Michael Grigoriev, Alexey Mazurov, Anatoly Salyuk, et al. (2017). “Current rates and mechanisms of subsea permafrost degradation in the East Siberian Arctic Shelf”. In: *Nature communications* 8, p. 15872.
- Sloan Jr, E Dendy and Carolyn Koh (2007). *Clathrate hydrates of natural gases*. CRC press.
- Vonk, Jorien E, Igor P Semiletov, Oleg V Dudarev, Timothy I Eglinton, August Andersson, Natalia Shakhova, Alexander Charkin, Birgit Heim, and Örjan Gustafsson (2014). “Preferential burial of permafrost-derived organic carbon in Siberian-Arctic shelf waters”. In: *Journal of Geophysical Research: Oceans* 119.12, pp. 8410–8421.
- Zhang, Jinlun, D Andrew Rothrock, and Michael Steele (1998). “Warming of the Arctic Ocean by a strengthened Atlantic inflow: Model results”. In: *Geophysical Research Letters* 25.10, pp. 1745–1748.

Response to Review n.2: Volker Brüchert

November 25, 2019

General comment

“I have a lot of respect for the sophisticated details of the diagenetic reaction-transport model BRNS described in the manuscript by Puglini et al. It is a sophisticated, well-established model framework and has been used in many important publications, not the least already in the sensitivity analysis of anaerobic oxidation of methane in many different marine settings. This study takes advantage of the long developmental work that has been done previously with respect to AOM with this model. Here it is used to simulate sediment methane cycling for one of the big hotspots for potential future marine methane emissions - the East Siberian shelf sea, with its potential for thawing submarine permafrost and the potential presence of gas hydrates (although the presence of both is often contested in the literature for good reasons).”

Response: We would like to thank the reviewer for his appreciative, extremely constructive and insightful comment that not only sheds light on some critical aspects of our manuscript and helps to improve the quality of the manuscript, but also provides an opportunity to provide important clarifications and/or further detail.

Here we would like to stress that we included in the model a methane source from below (assuming different methane concentration spanning the range from 0 to the saturation concentration) which is supposed to resemble any kind underlying source. Our focus is in the upper 3 m of the sediments and we do not investigate and/or specify any explicit origin of the methane coming from below nor the model is, in such a version, sensitive to this origin. Since the area of interest is the ESAS, we hypothesize that subsea permafrost or gas hydrates may be the origin of such methane, but no results rely on this specific assumption. In fact we just wanted to stress the potential character of the non-turbulent methane emissions we found.

“The model uses the conventional setup of a network of biogeochemical reactions directly or indirectly coupled to the degradation of organic matter deposited at the sea floor. The paper is mostly not about the Siberian shelf, but is a very thorough assessment of AOM dynamics with explicit treatment of upward flow, bioenergetics controls of AOM, and a complex reaction network of biogeochemical redox reactions

as they may occur in Siberian shelf sediment”

Response: While the reviewer is absolutely right in pointing out that the results of the comprehensive sensitivity study described in the manuscript are universally valid, we would like to stress that the model setup and the sensitivity study have been specifically designed with the aim of assessing the fate of dissolved methane released from a deep source (*e.g.* dissociating hydrates or thawing subsea permafrost) in warming Siberian Shelf sediments. More specifically:

- The model is forced with a variable flux of dissolved methane potentially originating from dissociating methane hydrates and/or thawing permafrost in the deeper sediment. The methane flux is constrained by assuming lower model boundary methane concentrations ranging from 0 to a maximum concentration that is constrained by the saturation of dissolved CH₄ under pressure, temperature and salinity conditions encountered on the Siberian shelf.
- All model boundary conditions, forcings and parameters (Tables S5 and S6) are chosen to be representative of environmental conditions encountered on the Siberian shelf.
- The range of boundary conditions and parameters tested in the steady state sensitivity study are constrained based on data compiled for the Siberian shelf.

As a consequence, the study presented here does not cover the entire range of possible conditions (*e.g.* methane fluxes, active fluid flow, organic carbon concentrations etc.) encountered at the global ocean seafloor, but is representative for conditions (likely) encountered on the present and future Siberian Shelf.

“The manuscript is well written up section 3.3.1., after which it deteriorates conspicuously”

Response: We agree that the logical structure of section 3.3.1 could be improved and have carefully revised this part.

“In principle, there were two objectives: 1. BROADSCALE simulation of AOM dynamics: It does a very good job at simulating a range of broadly set environmental conditions with direct impact on the filter efficiency of anaerobic methane-oxidizing microbial consortia that use methane and sulfate. The range of the environmental conditions is set broad enough to encompass conditions that may be encountered on the East Siberian shelf. However, this part is not very novel and AOM dynamics and filter efficiency have been reviewed by Regnier et al. (2011) previously. Therefore all sections of the manuscript that relate to the simulation tests should be significantly shortened.”

Response: We strongly disagree with this comment. Regnier et al., 2011 present a comprehensive review of previously developed models that have

been applied to investigate a large employed to simulate a large set of diverse depositional environments affected by intense methane cycling, ranging from mud volcanoes and active seeps to passive sediments experiencing groundwater discharge or high organic matter inputs. The review explicitly explores how different model implementations/formulations (with increasing complexity of the biogeochemical network) perform in simulating methane-affected sediments, as well as explore simulated AOM efficiency in response to a discrete, non-specific set of environmental conditions considered in these models.

However, the analysis of AOM filter efficiency and CH_4 effluxes presented has a completely different focus and goes well beyond the analysis presented in Regnier et al., 2011. As pointed out above, the main aim of this model study is to specifically investigate the potential escape of dissolved methane released from a deep source (*e.g.* dissociating hydrates or thawing subsea permafrost) from warming Siberian Shelf sediments. It thus assesses the efficiency of the microbial AOM filter in attenuating potential dissolved permafrost/hydrate methane fluxes under a continuous and specifically chosen range of environmental conditions/scenarios (likely) encountered on the present and (idealized) future Siberian shelf using an identical model set-up and thus offering not only more robust theoretical consistency and comparability. The main focus of the presented sensitivity analysis lies on identifying environmental conditions (and thus potential areas on the Siberian Shelf) that favor non-turbulent dissolved methane fluxes across the sediment-water interface.

We further emphasized this point in the manuscript by modifying the introduction and abstract accordingly.

“2. Regional application: The second part of the manuscript is the application of the model to the East Siberian shelf. I found this part the more relevant one, given the title, but unfortunately also less well constrained due to the paucity of data used to constrain their model in face of the diversity and size of the targeted marine region. For reference, my guess is that the authors would certainly not model the whole of the North Sea or the Baltic Sea with this model, two marginal seas of similar size or even smaller than the Laptev Sea”

Response: We also disagree with this statement. One strength of a models is that it can provide the explorative means to assess dynamics at spatial/temporal scales that cannot easily be assessed by observations alone. In particular, transfer functions, simple look-up tables and/or neural networks that are derived from or trained on a large ensemble of individual model simulations over a broad range of plausible boundary conditions have been frequently and successfully used to investigate regional and even global dynamics.

For instance, Gypens et al., 2008, Dale, Nickelsen, et al., 2015, Dale, Graco, et al., 2017, Capet et al., 2016 use simple transfer functions derived from a large ensemble of 1D diagenetic model simulations to predict benthic

nutrient recycling fluxes for the coastal North Sea (Gypens et al., 2008), the Peruvian Upwelling system (Dale, Graco, et al., 2017), the entire global ocean (Bohlen et al., 2012; Dale, Nickelsen, et al., 2015) or the entire Black Sea (Capet et al., 2016). Marquardt et al., 2010 used a transfer function to estimate the global gas hydrate inventory in marine sediments. In addition, Bourgeois et al., 2017 used a generalized additive model to calculate oxygen fluxes through the sediment-water interface for the entire Arctic Ocean and Artificial Neural Networks have been used to estimate sulfate (Bowles et al., 2014) fluxes through the sediment-water interface on a global scale.

These approaches are similar to the regional assessment presented here and illustrate the power of such transfer functions. We now highlight this in the introduction.

“My specific critique relates to the following points, which to my opinion are important in controlling the biogeochemical rates and flux output of the model, but that are not or too poorly constrained in the model to substantially further our understanding of how efficient anaerobic methane oxidation is and will be in the Siberian shelf sediments. Even with the reduction of the investigated area to the Laptev Sea only, the depositional environments and geological settings are so much more variable that a simple sedimentation rate/bathymetry-based prediction of present-day organic carbon accumulation gives a starting condition for the model that is too simplifying to be acceptable.”

Response: The results of the extensive sensitivity study presented here clearly indicate the sedimentation rate and active fluid flow exert the dominant control on the escape of methane derived from thawing permafrost and/or disintegrating methane gas hydrates through the Siberian shelf sea floor across a wide range of contrasting environmental conditions encountered in this depositional environment. Results show that additional environmental conditions, such as OM content or AOM efficiency (*i.e.* k_{AOM}) play a minor or negligible role. Sedimentation rate can thus be used to predict the non-turbulent of methane escape on the Siberian Shelf.

The extensive sensitivity study presented here, thus also confirms the general approach that underlies the ensemble of studies listed in the previous response: single benthic biogeochemical characteristics, such as seafloor fluxes, redox horizons or inventories are often controlled by a limited set (1-2) of dominant factors that can then be used to robustly predict these characteristics on a regional/global scale.

“For example, the authors rely on a selected handful of Pb-210 data (there are more available in the literature for better coverage (see Bröder et al., 201; Strobl et al., 1988) for sedimentation rates”

Response: We thank the reviewer for the suggestions. Bröder et al., 2016 reports values for two sites in the East Siberian Sea and can thus unfortunately not be used to improve data coverage in the Laptev Sea. However, the reported linear sedimentation rate ($0.14 - 0.15 \text{ cm yr}^{-1}$) is not only sim-

ilar to the sedimentation rate used in our local model application (0.12 cm yr^{-1}), but would also not change flux calculations if applied (see sensitivity study). We now include the values reported by Strobl et al., 1998. They show that sedimentation rate in the Laptev sea is of the same order (0.15 cm yr^{-1})- a value that falls well in the range we explored.

“The model doesn’t consider the regionally diverse sediment types, permeabilities and rates in the Siberian Shelf Sea (see for example Dudarev et al., 2006 Oceanology; Rekant et al., 2015). The model doesn’t consider known clay/sand/sand grain size variation and their influence of carbon concentration, permeability, transport, and resulting biogeochemical rates.”

Response: We would like to stress again that the presented study does account for the regional variability of sedimentation rate: 1) in the sensitivity study considering a large range spanning almost two orders of magnitude ($0.03 - 1.5 \text{ cm yr}^{-1}$), and 2) in the regional analysis that applies a spatially variable sedimentation rate. In addition, the influence of the amount of degradable OM has also been tested in the sensitivity study and, because it is of secondary importance, is qualitatively discussed in the regional study.

It is however correct that we assume a porosity profile, which is representative for fine-grained shelf sediments. This is in agreement with Dudarev et al., 2006 (although they focus on the East Siberian Sea and not the Laptev Sea). They suggest that: “*The distribution of sediments demonstrates that they sustain fine-grained texture in the major part of the continental shelf regardless of the distance from the shore*”. Considering that the overall geomorphological characteristics of the East Siberian Sea and Laptev Sea are similar, we can assume that a 3 m sediment column with a prescribed porosity (dependent on depth) and a uniform texture and sediment type might be a decent representative for a large setting of the ESAS. We added a comment to the methods section.

“The model assumes Barents Sea depositional conditions as a good analog, however, these are unlike those of the Siberian shelf, since the Barents Sea is much deeper, has higher marine productivity, less ice cover, and much less input of terrestrial organic matter. In addition, it does not have terrestrial permafrost underneath the recent Holocene sediments. It is therefore not a particularly good analog. If the authors are interested, I can provide porewater methane, sulfate and ammonium data from this region.”

Response: We would like to thank the reviewer for this offer. We have been in contact with the reviewer for porewater methane, sulfate and ammonium data and now include an additional model test case for this Laptev Sea site. We would however also like to stress that we do not consider the Barents Sea shelf offshore Versterålen as a good analog for the ESAS. Due to the paucity of observational data from the Laptev Sea for model testing, we used this Arctic site to illustrate the performance of our model set-up in simulating biogeochemical dynamics in high-latitude shelf sediments.

“The reactive continuum approach employed here probably overestimates the reactive organic carbon amount that is available to organic carbon degradation at depth. In reality, the reactivity of the organic matter below the oxic horizons is one to two orders of magnitude lower than commonly observed in marine shelf sediments (see Figure 9, Brüchert et al., 2018). Given the very low reactivity of carbon in these sediments (See Brüchert et al., 2018; Bröder et al., 2016; Tesi et al., 2014), sulfate is likely never exhausted and methanogenesis and AOM may not even take place in these sediments at all. I am therefore not surprised at all that the authors arrive at such low regional dissolved benthic methane fluxes, seemingly at odds with the broadly published claims of extensive methane emission from the Siberian shelf.”

Response: This is a misunderstanding which we would like to clarify. First of all, we would also like to emphasize again that, according to our findings, the organic matter reactivity only exerts a secondary effect on our conclusions and therefore does not alter the overall picture of our results. In addition, we would like to stress again that the focus of the presented analysis centers on the fate of methane fluxes from thawing permafrost and/or disintegrating methane gas hydrates and not in-situ biogenically produced methane for which OM reactivity may play a more important role. The presence of a deep methane flux from thawing permafrost and/or disintegrating methane gas hydrates also ensures the presence of an AOM and the depletion of sulfates.

However, apart from this, we also disagree with the overall comment that the reactive continuum model (RCM) overestimates reactivity in these sediments. In fact, the RCM accounts for the decrease of OM reactivity with sediment depth/degradation state. Here, we test a wide range of RCM parametrizations (*i.e. a*) including those that result in a rapid decrease of OM reactivity by 1-2 orders of magnitude. Moreover the two papers cited actually support the use of a reactive-continuum model.

1. Bröder et al., 2016 show that the half-life of the organic matter deposited at two sites in the East Siberian Sea is 19 – 27 yr. These half-life are represented by our RCM parametrizations in the intermediate range. Assuming $\nu = 0.125$ the corresponding *a* for the two samples would be $a = 3.4 - 4.8$ yr - values that are well within the range explored in our sensitivity analysis.
2. Tesi et al., 2014 in their conclusions clearly state: “*Therefore our results suggest that TerrOC is made of several allocthonous pools each with distinct reactivity toward the oxidation (i.e., reactive continuum)*”.

We modified the method section to clarify this point and also added the two references.

“In fact, these fluxes confirm my own direct measurements of porewater methane concentrations and methane fluxes from a range of stations investigated in the summer of 2014 during the SWERUS expedition with the Swedish icebreaker Oden. If the authors are interested, I am willing to share these data with them to better constrain their model.”

Response: We are really thankful for this offer and have been in contact with the reviewer.

“The model doesn’t consider Holocene sealevel change to elaborate on the mass of sediment available for methane generation since the last glacial maximum, which is the time since reactive sedimentary organic carbon accumulation began.”

Response: This is a misunderstanding. Again, the focus of the presented paper is on the fate of methane released from subsea permafrost/gas hydrates on the present-day and future Siberian shelf. We do not intend to simulate the historical evolution of the SSPF and of related historical methane emission, but only a plausible range of current/future ones. Furthermore, our model analysis is based on the simulation of the first 3 meters of sediment and the Holocene sedimentation rates we explored ($0.03 - 1.5 \text{ cm yr}^{-1}$) indicate that the sediment layer overlying the subsea permafrost always exceeds 3 m.

“The model design relies on a sequence of thermodynamically regulated terminal electron acceptor reactions driven by fresh carbon accumulation at the top of the model domain. In reality, non-biogenic or old Pre-Holocene-produced methane transport from below (of thermogenic or Pleistocene age, i.e., terrestrial) is the key unique characteristic of the Siberian shelf with respect to methane cycling. This carbon is old and uncoupled to recent carbon accumulation. In addition, carbon accumulation varied greatly through time on the Siberian shelf. The model appears to assume continuity of recent depositional conditions back in time and space, which is most certainly incorrect.”

Response: This is a misunderstanding. In fact, the model analysis focus on this “non-biogenic or old Pre-Holocene-produced methane transport from below (of thermogenic or Pleistocene age, i.e., terrestrial)” and not on the in-situ produced biogenic methane. Because it is impossible to reconstruct depositional conditions over the Holocene for the entire region, we indeed assume broadly similar depositional conditions during the Holocene. This is an acceptable simplification, in particular because:

1. Early diagenetic rates are highest in the shallow, young sediment layers and decrease rapidly with depth. As a consequence, biogeochemical dynamics are mostly affected by recent depositional conditions. This is especially true in the light of the fast decrease in OM reactivity reported by broder 2016; Brüchert et al., 2018; Tesi et al., 2014.
2. Our comprehensive sensitivity study indicates that OM degradation and biogenic methane production in the Holocene sediment layer ex-

erts a minor control on non-turbulent methane fluxes across the sediment-water interface. Holocene fluctuations in environmental conditions will thus exert a negligible effect on our results.

We clarify this throughout the manuscript (see previous replies).

“Only the section with the transient model scenarios therefore applies to the Siberian shelf and only scenarios with an explicit upward flux of methane are relevant for investigating AOM dynamics in these sediments. However, because of the difficulties in constraining the regional distribution of seeps, flux rates cannot be reliably extrapolated and one should refrain from a regional flux estimate.”

Response: This is a misunderstanding. All steady-state simulations also apply an upward flux of methane (as outlined in the method section for details). They are thus relevant for investigating the fate of permafrost/hydrate derived methane in the Holocene sediment column and its possible escape through the sediment water interface. They also allow to derive the transfer function for possible non-turbulent methane escape that has been used to establish a regional estimate. We clarify this point throughout the manuscript (see previous replies).

Because our steady state analysis shows that AOM acts as an efficient biofilter and mostly prevents non-turbulent methane escape from the sediment, we also explored a number of plausible transient scenarios to explore if microbial dynamics could possibly create “windows of opportunity” for methane escape and assess their importance. We further clarify this in the introduction and method section. in the transient analysis we performed we actually refrained from an upscale estimate and we just explained the result of the flux out of simulated sediment column.

“My objections to the present manuscript are therefore not whether the model’s capabilities are useful to the scientific community in general, which it certainly is, but a critique of the attempt to mimic biogeochemical as well as recent and past depositional conditions on the Siberian shelf to better predict sediment methane emissions from this region.”

Response: see responses above.

“I am fully aware of the infected discussion of the relevance of the Siberian shelf sea’s role as a potentially huge methane source to the atmosphere put forward by Shakhova and co-authors. The outcome of the model simulations presented here, even in their most generous state (high advective upward flow and moderately to high sedimentation rates), would imply that the emissions proposed by Shakhova and coauthors are very hard to achieve without invoking massive gas emissions (which are not seen regionally in atmospheric measurements).”

Response: This is indeed one of the conclusions of our analysis.

“However, the inability of this 1D model to encapsulate environmental conditions

that are found in the Laptev and East Siberian Sea make it impossible to use its scaled model output to the current system or to use the model to make reliable assessments of how the shelf environment may change methane fluxes in the future. Particularly the latter requirement is key to the use of a reaction transport model such as this one in climate science. [...] The study and conclusions give the false impression that this particular model is capable, with certainty, to predict the non-gaseous methane flux emanating from this 1.5 million square kilometer large region, if one only knows the sedimentation rate and water depth. The authors may therefore consider a new title for their manuscript for the first section and resubmit it under this new title without much reference to dissolved methane emissions on the East Siberian shelf, since this is not what they can model reasonably with the data they have available. [...] Alternatively, the model simulations can be tested with actual data from the Siberian shelf, which I am willing to share. In this case, I would suggest to reduce the first part of the manuscript and focus on the application of the BRNS to the Siberian shelf sea rather than a broad treatment of the model's performance."

Response: This comment reflects a string of misunderstandings. We do not aim at quantifying, "*with certainty*" the exact evolution of present and future methane emissions from the Siberian shelf. As highlighted in the title, abstract, introduction, the presented study assesses the potential for non-turbulent methane escape (derived from deep sediment sources such as permafrost/gas hydrates) from Siberian shelf sediments. As pointed out in the results and conclusion section, it thus provides a robust, quantitative framework suitable to make first order estimates and draw conclusions with respect to present and potential future emissions, as well as methane gas emissions required to support previous estimates of Arctic Ocean methane emissions to the atmosphere. Given the urgent need to assess this potentially ticking time bomb, but the paucity of observational data, it represents a feasible and robust quantitative first step towards a better assessment of the threat methane emissions from thawing subsea permafrost/ disintegrating methane hydrates pose for our climate.

Therefore, we are convinced that the title, as well as the approach of the presented study adequately reflect its scope and do not give a false impression. However, we have adapted the abstract, introduction, method and conclusion sections to further clarify these points. In addition, we have also included a new case study for the Laptev sea site based on the data provided by the reviewer.

Specific comments

Page 8: "This is a crude overgeneralization. The authors must provide more references on the physical oceanography of the Laptev Sea and its sediment distribution and bathymetry to justify this comparison. The Norwegian setting has much higher primary productivity, is up to 8 times deeper and has substantially less ice cover over the year. If anything, the Vesterålen site shares very few similarities with the Laptev

Sea or the East Siberian Shelf Sea.”

Response: This is a misunderstanding. As pointed out in the response to general comments, we used the Hola trough sediments merely to assess the ability of the model to simulated carbon and sulfur dynamics in high latitude shelf sediments porewater profiles in a Northern shelf. No calibration of the BRNS or other following results relies on the simulations performed to reproduce the Vesterålen site, nor do we claim any similarity with the shelf areas of the East Siberian Arctic shelf. However, we do agree that our statement could be misunderstood and have now modified this section accordingly.

Page 12: “Please correct, not for methane”

Response: “Simulation results show an overall satisfactory agreement with measurements except for methane.”

Page 13:

- “It is not correct to make reference to the ESAS, since the range of the environmental conditions applied here is sufficiently broad to be applied to a wide range of shelf and slope margin settings with possible AOM. One condition worthwhile exploring and not done here is whether at low OM reactivities, the consumption of sulfate may not be completed for the time span of Holocene sediment accumulation on the ESAS (i.e., since ca 7000 years ago).”

This is a misunderstanding. As stated earlier, we investigate the fate of methane from deep sources (permafrost/hydrate) rather than in-situ produced methane (although the model also accounts for biogenic production in the Holocene sediment layer). As a consequence, we apply a range of methane fluxes from below that ensure a consumption of sulfate. With respect to the comment on the environmental conditions, we would like to repeat our response to a similar general comment here.

“While the reviewer is absolutely right in pointing out that the results of the comprehensive sensitivity study described in the manuscript are universally valid, we would like to stress that the model setup and the sensitivity study have been specifically designed with the aim of assessing the fate of dissolved methane released from a deep source (e.g. dissociating hydrates or thawing subsea permafrost) in warming Siberian Shelf sediments. More specifically:

- *The model is forced with a variable flux of dissolved methane potentially originating from dissociating methane hydrates and/or thawing permafrost in the deeper sediment. The methane flux is constrained by assuming lower model boundary methane concentrations ranging from 0 to a maximum concentration that is constrained by the saturation of dissolved CH₄ under pressure,*

temperature and salinity conditions encountered on the Siberian shelf.

- *All model boundary conditions, forcings and parameters (Tables S5 and S6) are chosen to be representative of environmental conditions encountered on the Siberian shelf.*
- *The range of boundary conditions and parameters tested in the steady state sensitivity study are constrained based on data compiled for the Siberian shelf.*

As a consequence, the study presented here does not cover the entire range of possible conditions (e.g. methane fluxes, active fluid flow, organic carbon concentrations etc.) encountered at the global ocean seafloor, but is representative for conditions (likely) encountered on the present and future Siberian Shelf.”

- “Please correct to : ’to the SWI’ The model does not provide any constraint on the SWI flux, i.e., the benthic flux itself, because here other processes play an important that are modelled here.”

Response: We are not sure which processes the reviewer refers to, but in addition to diffusion and advection, the model explicitly accounts for bioturbation and non-local transport (through bioirrigation or ice scouring). It thus provides a robust representation of transport through the SWI.

- “Referencing this study to other studies that show a range of 5 orders of magnitude in methane fluxes to justify its applicability seems odd. Please clarify how exactly each of the referenced studies supports the model findings in your simulation.”

Response: The referenced studies offer a comparison with respect to the fluxes, as well as the flux variability in response to different environmental conditions we simulated.

- “Which value was that? Not clear from the text. Apart from that, I deeply object to the use of one value to the whole of the ESAS. What is the purpose of this upscaled value? The original model value doesn’t gain any more legitimacy from upscaling and the fact that the upscaled value may be in the range of expected values neither. Please delete this section”

The maximum value we found was $27.48 \mu\text{molCH}_4 \text{ cm}^{-2} \text{ yr}^{-1}$. We added the exact value to the respective section. As pointed out in the earlier response, model results provide a robust quantitative framework to evaluate the potential for non-turbulent methane escape from the Siberian Shelf. The purpose of upscaling the maximum value to the ESAS is simply to offer an upper limit for this possible non-turbulent methane flux and show that, even if the most favorable conditions for methane escape were to be found over large shelf areas (note, this is

different from claiming that they are), non-turbulent methane fluxes would still be negligible and would not be able to support earlier estimates of methane emissions to the atmosphere.

Page 14:

- “This is an interesting conclusion. How can one reconcile the observation that methane concentrations in the methanogenic zone generally tend to increase with depth, i.e., their transport away from the zone of formation is too slow relative to the methanogenesis rate?”

Response: The Damköhler numbers are defined in such a way that the transport process considered occurs in the same region as the reaction, *i.e.* we considered the methane transport within the methanogenic zone for the evaluation of Da_{MG} and the SMTZ for the evaluation of the Da_{AOM} . Simulation results reveal that methane transport is efficient within the methanogenic zone. However, comparison with Da_{AOM} shows that methane consumption within SMTZ is slower than its transport. In other words, methane can be efficiently transported to SMTZ but it is not quickly consumed there. As a consequence, methane accumulates below the SMTZ because at the SMTZ level it is not consumed and below the SMTZ no AOM occurs.

- “This is a curious assertion for the Siberian shelf system. It is wellknown that the sediments of the Siberian shelf are not reactive enough to yield significant methane. It is instead supposed that externally introduced methane from the thawing permafrost that serves as the methane source. The current model does not take external sources into account and this is the major flaw of this paper. It is actually not suited in the current version to model the processes on the Siberian shelf.”

Response: Deep (external) sources of methane are the main focus of the presented study. See response to general comments for details on biogenic methane production, methane fluxes from permafrost/hydrates.

- “This introduction paragraph is rather wordy and doesn’t say much. Can it be shortened?”

Response: we will shorten it in the finalized version of the paper, although we value the fact that an introduction might already provide the main message of what is described in detail later.

- “Please provide a reference to the ‘traditional views’. The view proposed here is not new.”

Response: We replaced “traditional” with “intuitive”. Our findings give further evidence of the dominant role of transport processes for non-turbulent methane effluxes also in modeling scenario compatible with ESAS settings.

Page 15: “What is meant by ‘margin’?”

Response: the continental margin. We could replaced “margin” with “shelf” to avoid confusion.

Page 17: “The authors should avoid trivial sentences such as this one.”

Response: it is not necessarily trivial, since a high methanogenesis might also be expected to foster a higher oxidation process and therefore accumulation of methane is not necessarily a triviality

Page 19: “I wonder whether the reactivity of organic matter in large parts of the Siberian Shelf isn’t even lower than 100 years. More 1000 years.”

Response: we also explored the $a \geq 100$ yr. As already stated in the reply to the general comment, the reactivity of the organic matter reported in other studies (*e.g.* Bröder et al., 2016) shows that a is < 5 , not far from the value $a = 10$ yr we used for the baseline simulation. In addition, a -values > 1000 years are characteristic for deep sea sediments underlying extremely oligotrophic gyres, such as the deep South Pacific. Shelf, slope and most deep sea environments are generally characterized by $a < 1000$ years.

Page 23: “The authors are conflating to independent processes into one.”

It is not clear which processes the reviewer refers to. We guess they are, on one hand, the actual AOM and, on the other hand, the precipitation of authigenic carbonate. We do not claim or mix them up and we are aware that they are two different processes but it is well established that they are not independent, since the alkalinity produced during the AOM can drive precipitation of authigenic carbonates as reported in many site all over the globe (*e.g.* Aloisi et al., 2004; Crémière, Lepland, Chand, Sahy, Condon, et al., 2016; Crémière, Lepland, Chand, Sahy, Kirsimäe, et al., 2016; Karaca et al., 2010; Luff et al., 2005; Meister et al., 2018; Pierre et al., 2012). We are simply hinting at an indirect effect supporting our findings, aware that the two processes are however well distinct and not trivially connected.

Page 24: “These calculated active and passive fluxes are so low that they are empirically not verifiable with currently available measurement techniques.”

Response: We are aware of this limit and acknowledge it in the study. However, we would also like to point out that the exact quantity of these small fluxes is of minor importance. What is important here is that the potential for non-turbulent methane fluxes from Siberian Shelf sediments, even under the most favorable environmental conditions, is extremely limited and previous estimates of methane emissions to the atmosphere would thus require the build up of large quantities of methane gas.

Page 26: “The question is more, whether biogenic methane ever forms in these sediments, as the authors likely overestimate the reactivity of the organic matter. Altogether I think that the authors arrive at the right conclusion for the wrong reasons.”

As stated previously, we disagree with this comment. Please see reply to general comment for details.

Page 28: “From this section on the manuscript becomes distinctly less well written, more typographic errors and less succinct writing. At the same time, the discussion of transient conditions is most relevant to the Siberian shelf system. This section needs to be carefully revised and improved in its writing.”

Response: We will carefully revise and improve this section.

Page 29: “A better way of explaining the discrepancy between the two methane fluxes at steady state and the transient condition would be to show the AOM rate for the two rate laws.”

Thanks for the suggestion. We add the AOM rate profile to fig. 11.b

Page 31:

- “This is hard to understand. It should be possible to extract the instantaneous apparent k_{AOM} value throughout the simulation. Ultimately of relevance is not what the k_{AOM} is at the end of the simulation, but its time-integrated AOM rate throughout the modelled transient run.”

It is actually possible to extract the k_{AOM} at each simulated time step. However, here we wanted to explain why the final, new steady-state flux in the bioenergetic formulation is different from the simulation with the bimolecular formulation and that is the reason we focused on the final k_{AOM} , its shape and values.

- “Poor English makes this paragraph hard to understand, most importantly it is not clear how the authors arrive at their conclusion with this argument”

Response: We will carefully revise and improve this section.

- “thermodynamical”

Response: Corrected

Page 32:

- “19 years”

Response: Corrected

- “The role of sulfide was not mentioned previously. Is sulfide generally an important player for thermodynamic calculations done here?”

Sulfide influences AOM it appears in the formulation of F_T , which controls the AOM in the bioenergetic approach as shown in Eq. 11. Bicarbonate appears as well, but it is rarely a limiting factor.

Page 33:

- “The wording should be reversed. An AOM biomass accounts for an AOM filter, not the other way round”

Response: we agree but we wanted to stress that in order to have an efficient AOM filter a minimum AOM biomass is needed and this quantity has been estimated to be $> 10^{10}$ cells cm^{-3} , which is of the same order of magnitude as the value we found.

- “Overall, this is irrelevant. The supply from below is what counts for the Siberian shelf, not the in-situ production, which is negligible in almost all settings except for the Eastern East Siberian Sea and the Chukchi Sea. In addition, the statement is also irrelevant in a general sense. As the supply from below is increased, so must the proportional contribution of in-situ produced methane decrease. This is not worth mentioning.”

Response: We will edit this sentence accordingly in the final version of the paper.

- “typo here: from ... to..”

Response: Corrected

- “I am getting lost with the abbreviations”
[CH₄]₋ is the methane concentration at the bottom of the sediment column.

- “As stated this is not true and must be corrected. Never did you investigate ESAS shelf sediments in this study. Modeling scenarios were investigated, of which some conditions may apply to selected environmental setting on the ESAS. The passive/active terminology strictly applies to theoretical scenarios of system behavior.[...] Seriously, the authors have not investigated these sediments directly at all and should not make a claim to have investigate them.”

Response: This is a misunderstanding. The focus of this study is not a regional simulation of ESAS shelf sediments, but to develop a robust, quantitative framework that can be used to evaluate the potential for non-turbulent methane escape driven by thawing subsea permafrost and/or disintegrating methane gas hydrates on the warming Siberian shelf. We would again like to repeat our response to one of the general comments.

“This comment reflects a string of misunderstandings. We do not aim at quantifying, “with certainty” the exact evolution of present and future methane emissions from the Siberian shelf. As highlighted in the title, abstract, introduction, the presented study assesses the potential for non-turbulent methane escape (derived from deep sediment sources such as permafrost/gas hydrates) from Siberian shelf sediments. As pointed out in the results and conclusion section, it thus provides a robust, quantitative framework suitable to make first order estimates and draw conclusions with respect to present and potential future emissions, as well as methane gas emissions required to support previous estimates of Arctic Ocean methane emissions to the atmosphere. Given the urgent need to assess this potentially ticking

time bomb, but the paucity of observational data, it represents a feasible and robust quantitative first step towards a better assessment of the threat methane emissions from thawing subsea permafrost/disintegrating methane hydrates pose for our climate.

Therefore, we are convinced that the title, as well as the approach of the presented study adequately reflect its scope and do not give a false impression.

However, we also modified this section accordingly to avoid misunderstandings.”

- “first or first-order?”

Response: Actually both first and first-order. Modified accordingly.

References

- Aloisi, Giovanni, Klaus Wallmann, RR Haese, and J-F Saliege (2004). “Chemical, biological and hydrological controls on the ^{14}C content of cold seep carbonate crusts: numerical modeling and implications for convection at cold seeps”. In: *Chemical Geology* 213.4, pp. 359–383.
- Bohlen, Lisa, Andrew W Dale, and Klaus Wallmann (2012). “Simple transfer functions for calculating benthic fixed nitrogen losses and C: N: P regeneration ratios in global biogeochemical models”. In: *Global Biogeochemical Cycles* 26.3.
- Bourgeois, Solveig, Philippe Archambault, and Ursula Witte (2017). “Organic matter remineralization in marine sediments: A Pan-Arctic synthesis”. In: *Global Biogeochemical Cycles* 31.1, pp. 190–213.
- Bowles, Marshall W, José M Mogollón, Sabine Kasten, Matthias Zabel, and Kai-Uwe Hinrichs (2014). “Global rates of marine sulfate reduction and implications for sub-sea-floor metabolic activities”. In: *Science* 344.6186, pp. 889–891.
- Bröder, Lisa, Tommaso Tesi, August Andersson, Timothy I Eglinton, Igor P Semiletov, Oleg V Dudarev, Per Roos, and Örjan Gustafsson (2016). “Historical records of organic matter supply and degradation status in the East Siberian Sea”. In: *Organic Geochemistry* 91, pp. 16–30.
- Brüchert, Volker, Lisa Bröder, Joanna E Sawicka, Tommaso Tesi, Samantha P Joye, Xiaole Sun, Igor P Semiletov, and Vladimir A Samarkin (2018). “Carbon mineralization in Laptev and East Siberian sea shelf and slope sediment”. In: *Biogeosciences* 15.2, pp. 471–490.
- Capet, Arthur, Filip JR Meysman, Ioanna Akoumianaki, Karline Soetaert, and Mari-laure Grégoire (2016). “Integrating sediment biogeochemistry into 3D oceanic models: a study of benthic-pelagic coupling in the Black Sea”. In: *Ocean Modelling* 101, pp. 83–100.
- Crémière, Antoine, Aivo Lepland, Shyam Chand, Diana Sahy, Daniel J Condon, Stephen R Noble, Tonu Martma, Terje Thorsnes, Simone Sauer, and Harald Brunstad (2016). “Timescales of methane seepage on the Norwegian margin following collapse of the Scandinavian Ice Sheet”. In: *Nature communications* 7, p. 11509.
- Crémière, Antoine, Aivo Lepland, Shyam Chand, Diana Sahy, Kalle Kirsimäe, Michael Bau, Martin J Whitehouse, Stephen R Noble, Tõnu Martma, Terje Thorsnes, et al. (2016). “Fluid source and methane-related diagenetic processes recorded in cold seep carbonates from the Alvheim channel, central North Sea”. In: *Chemical Geology* 432, pp. 16–33.
- Dale, Andrew W, Michelle Graco, and Klaus Wallmann (2017). “Strong and dynamic benthic-pelagic coupling and feedbacks in a coastal upwelling system (Peruvian shelf)”. In: *Frontiers in Marine Science* 4, p. 29.
- Dale, Andrew W, Levin Nickelsen, Florian Scholz, Christian Hensen, Andreas Oschlies, and Klaus Wallmann (2015). “A revised global estimate of dissolved iron fluxes from marine sediments”. In: *Global Biogeochemical Cycles* 29.5, pp. 691–707.

- Dudarev, Oleg Victorovich, Igor Petrovich Semiletov, Alexander Nikolaevich Charkin, and AI Botsul (2006). “Deposition settings on the continental shelf of the East Siberian Sea”. In: *Doklady earth sciences*. Vol. 409. 2. Springer, pp. 1000–1005.
- Gypens, Nathalie, Christiane Lancelot, and Karline Soetaert (2008). “Simple parameterisations for describing N and P diagenetic processes: Application in the North Sea”. In: *Progress in oceanography* 76.1, pp. 89–110.
- Karaca, Deniz, Christian Hensen, and Klaus Wallmann (2010). “Controls on authigenic carbonate precipitation at cold seeps along the convergent margin off Costa Rica”. In: *Geochemistry, Geophysics, Geosystems* 11.8.
- Luff, Roger, Jens Greinert, Klaus Wallmann, Ingo Klaucke, and Erwin Suess (2005). “Simulation of long-term feedbacks from authigenic carbonate crust formation at cold vent sites”. In: *Chemical Geology* 216.1-2, pp. 157–174.
- Marquardt, Mathias, Christian Hensen, Elena Pinero, Klaus Wallmann, and Matthias Haeckel (2010). “A transfer function for the prediction of gas hydrate inventories in marine sediments”. In: *Biogeosciences* 7.9, pp. 2925–2941.
- Meister, Patrick, Johanna Wiedling, Christian Lott, Wolfgang Bach, Hanna Kuhfuß, Gunter Wegener, Michael E Böttcher, Christian Deusner, Anna Lichtschlag, Stefano M Bernasconi, et al. (2018). “Anaerobic methane oxidation inducing carbonate precipitation at abiogenic methane seeps in the Tuscan archipelago (Italy)”. In: *PLoS one* 13.12, e0207305.
- Pierre, Catherine, Marie-Madeleine Blanc-Valleron, Jérôme Demange, Omar Boudouma, Jean-Paul Foucher, Thomas Pape, Tobias Himmler, Noemi Fekete, and Volkhard Spiess (2012). “Authigenic carbonates from active methane seeps offshore southwest Africa”. In: *Geo-Marine Letters* 32.5-6, pp. 501–513.
- Regnier, Pierre, Andy W Dale, S Arndt, DE LaRowe, J Mogollón, and P Van Cappellen (2011). “Quantitative analysis of anaerobic oxidation of methane (AOM) in marine sediments: a modeling perspective”. In: *Earth-Science Reviews* 106.1-2, pp. 105–130.
- Strobl, C, V Schulz, S Vogler, S Baumann, Heidemarie Kassens, PW Kubik, M Suter, and A Mangini (1998). “Determination of depositional beryllium-10 fluxes in the area of the Laptev Sea and beryllium-10 concentrations in water samples of high northern latitudes”. In: *Land-Ocean Systems in the Siberian Arctic*. Springer, pp. 515–532.
- Tesi, Tommaso, Igor Semiletov, Gustaf Hugelius, Oleg Dudarev, Peter Kuhry, and Örjan Gustafsson (2014). “Composition and fate of terrigenous organic matter along the Arctic land–ocean continuum in East Siberia: Insights from biomarkers and carbon isotopes”. In: *Geochimica et Cosmochimica Acta* 133, pp. 235–256.

Assessing the potential for non-turbulent methane escape from the East Siberian Arctic Shelf

Matteo Puglini^{1,2}, Victor Brovkin^{1,3}, Pierre Regnier², and Sandra Arndt²

¹Land in the Earth System, Max Planck Institute for Meteorology, Hamburg, Germany

²BGeosys, Department Geoscience, Environment & Society (DGES), Université Libre de Bruxelles, Brussels, Belgium

³CEN, Universität Hamburg, Hamburg, Germany

Correspondence: Matteo Puglini (matteo.puglini@mpimet.mpg.de)

Abstract. The East Siberian Arctic Shelf (ESAS) hosts large, yet poorly quantified reservoirs of subsea permafrost and associated gas hydrates. It has been suggested that the global-warming induced thawing and dissociation of these reservoirs is currently releasing methane (CH₄) to the shallow shelf-coastal ocean and ultimately the atmosphere. However, a major unknown in assessing the contribution of this CH₄ flux to the exact contribution of permafrost thaw and methane gas hydrate destabilization to benthic methane efflux from the warming shelf and ultimately methane-climate feedbacks remains controversial. A major unknown global CH₄ cycle and its climate feedbacks is the fate of permafrost and/or gas hydrate-derived methane-CH₄ as it migrates towards the sediment-water interface. In marine sediments, (an)aerobic oxidation reactions generally act as extremely efficient biofilters that often consume close to 100% of the upward migrating methane. However, it has been shown that a very efficient methane sink. Yet, a number of environmental conditions can reduce the efficiency of this biofilter, thus allowing methane to escape to the overlying ocean. Here, we used a reaction-transport model to assess the efficiency of the benthic methane filter and, thus, the potential for permafrost and/or gas hydrate derived methane to escape shelf sediments under benthic methane escape across a wide range of environmental conditions encountered on that could be encountered on the East Siberian Arctic Shelf. Results of an extensive sensitivity analysis show that, under steady state conditions, anaerobic oxidation of methane (AOM) acts as an efficient biofilter that prevents the escape of dissolved methane from shelf sediments for a wide range of environmental conditions. Yet, high CH₄ escape comparable to fluxes reported from mud volcanoes is simulated for rapidly accumulating (sedimentation rate > 0.7 cm yr⁻¹) and/or active (active fluid flow > 6 cm yr⁻¹) sediments and can be further enhanced by mid-range organic matter the presence of organic matter with intermediate reactivity and/or intense local transport processes, such as bioirrigation. In addition, in active settings, the sudden onset of CH₄ flux triggered by, for instance, permafrost thaw or hydrate destabilization can also drives a high non-turbulent methane escape of up to 19 μmolCH₄ cm⁻² yr⁻¹ can also occur during a transient, multi-decadal period following the sudden onset of CH₄ flux triggered by, for instance, permafrost thaw or hydrate destabilization. This "window of opportunity" arises due to the time needed by the delayed response of the resident microbial community to build up an efficient AOM biofilter. In contrast, seasonal variations in environmental conditions (e.g. bottom water SO₄²⁻, suddenly changing CH₄ flux) exert a negligible effect on CH₄ efflux through the Sediment-Water-Interface (SWI). Our results indicate that present and future methane efflux from ESAS sediments is mainly supported by methane gas and non-turbulent CH₄ efflux from rapidly accumulating and/or active sediments (e.g.

coastal settings, portions close to river mouths or submarine slumps). In particular active sites on the ESAS may release methane in response to the onset or increase of permafrost thawing or CH_4 gas hydrate destabilization rates. Model results also reveal that AOM generally acts as an efficient biofilter for upward migrating CH_4 under environmental conditions that are representative for the present-day ESAS with potentially important, yet unquantified implications for the Arctic ocean's alkalinity budget and, thus, CO_2 fluxes. The results of the model sensitivity study are used as a quantitative framework to derive fluxes. A first-order estimates estimate of non-turbulent, benthic methane efflux from the Laptev Sea is derived as well. We find that, under present day conditions, AOM is an efficient biofilter and non-turbulent methane efflux from Laptev Sea sediments does not exceed $1 \text{ GgCH}_4 \text{ yr}^{-1}$. As a consequence, we state conclude that previously published estimates of fluxes from ESAS water into atmosphere ocean-atmosphere CH_4 fluxes from the ESAS cannot be supported by non-turbulent methane escape from the sediments, but require the build-up and preferential escape of benthic methane gas from the sediments to the atmosphere that matches or even exceeds such estimated fluxes, benthic methane escape.

1 Introduction

The Siberian Shelf represents the largest shelf on Earth (~ 3 millions km^2 Wegner et al. (2015)) and spreads from the Kara Sea to the Laptev, the East Siberian and the Chuckhi Sea. The East Siberian Arctic Shelf (ESAS) corresponds to the broad area beneath the shallow (~ 45 m water depth, James et al. (2016)) Laptev and East Siberian Arctic Sea (Romanovskii et al., 2004; Shakhova et al., 2010a) and represents the largest region on the Siberian Shelf (Romanovskii et al., 2005), covering about 25% of the total Arctic shelf (Shakhova et al., 2010a).

Although similar in many aspects to other shelf environments, a distinguishing feature of the ESAS is the presence of subsea permafrost and associated gas hydrates buried in the sediment (Sloan Jr and Koh, 2007; Romanovskii et al., 2005). Subsea permafrost is a terrestrial relict that mainly formed during glacial periods, when Arctic shelves were exposed due to sea level retreating, down to retreating sea levels (with a minimum of 120 m below the current level around the Last Glacial Maximum) exposed Arctic shelves (Fairbanks, 1989; Bauch et al., 2001). Under these conditions, permafrost aggraded on the shelf and was subsequently submersed when rising sea level flooded the shelf (Romanovskii and Hubberten, 2001; Romanovskii et al., 2005) by rising sea levels during the Holocene sea transgression (12 and 5 kyr BP) (Bauch et al., 2001). Gas hydrates are solid, methane concentrated states of matter, in which a gas molecule is trapped in a cage of water molecules (Ruppel and Kessler, 2017). They are thermodynamically stable under specific temperature-pressure-salinity conditions in the ocean floor including areas beneath the subsea permafrost (Sloan Jr and Koh, 2007).

Little is known about the total amount of carbon stored in subsea permafrost, as well as its partitioning between subsea permafrost itself, gas hydrates and free gas. Published estimates of carbon reservoir sizes diverge by orders of magnitude. For instance Shakhova et al. (2010a) estimate that 1175 PgC are locked in subsea permafrost on the ESAS alone, while McGuire et al. (2009) calculate that, across the entire Arctic shelf, 9.4 PgC reside in upper sediments and 1.5-49 PgC ($2\text{-}65 \text{ PgCH}_4$) in methane gas hydrates. Thus, the size of the Arctic subsea permafrost reservoir, its spatial distribution, as well as its biogeochemical and physical characteristics remain poorly known.

These knowledge gaps are critical as climate change is amplified in polar regions. The Arctic is currently warming at a rate twice as fast as the global mean (Trenberth et al., 2007; Bekryaev et al., 2010; Jeffries and Richter-Menge, 2012; Christensen et al., 2013). Recent observations indicate that bottom water temperatures in the coastal and inner shelf regions of the ESAS (water depth < 30 m, Dmitrenko et al. (2011)) are rising, while the central shelf sea may be subject to intense episodic warming (Janout et al., 2016). The increasing influx of warmer Atlantic water into the Arctic Ocean - the so-called Atlantification (Polyakov et al., 2017; Barton et al., 2018) - will not only further enhance this warming, but will also influence circulation and salinity patterns on the shelf (Zhang et al., 1998; Biastoch et al., 2011)(Carmack et al., 1995; Zhang et al., 1998; Biastoch et al., 2011). At the same time, it has been long recognized that the Arctic is a potential hotspot for methane emissions. Extensive methane gas bubbling has been observed in the Laptev Sea and has been directly linked to these environmental changes (Shakhova et al., 2010b, 2014). Shakhova et al. (2014) suggest that warming induced subsea permafrost thaw and hydrate destabilization may support methane emissions of up to 17 TgCH₄ yr⁻¹ from the ESAS alone. Projected ~~climate change will~~ change in temperature (Shakhova et al., 2017, 2019) due to climate change is expected to further destabilize Arctic subsea permafrost and gas hydrate reservoirs and might thus enhance further methane emissions (Piechura and Walczowski, 1995; Westbrook et al., 2009; Reagan and Moridis, 2009; Biastoch et al., 2011; Hunter et al., 2013; Drake et al., 2015; Ruppel and Kessler, 2017). However, a number of recent studies have questioned the significance of subsea permafrost thaw and hydrate destabilization for methane efflux from Arctic sediment (Thornton et al., 2016; Ruppel and Kessler, 2017), for methane concentrations in Arctic Ocean waters (Overduin et al., 2015; Sapart et al., 2017) and, ultimately, for methane emissions from the Arctic waters (Ruppel and Kessler, 2017; Sparrow et al., 2018). Thus, the contribution of subsea permafrost thaw and gas hydrate destabilization to methane emissions from the warming Arctic shelf and, ultimately, methane-climate feedbacks remains poorly quantified (James et al., 2016; Saunio et al., 2016). As a consequence, it has not received much attention in the recent IPCC special report (Masson-Delmotte et al., 2018). At present, a major unknown is the strength of methane sinks in Arctic sediments and waters and their influence on methane emissions (Ruppel and Kessler, 2017). Therefore, improved assessments of the present and future climate impact of permafrost thaw and hydrate destabilization require not only a better knowledge Arctic subsea permafrost and hydrates distribution, reservoir size and characteristics, but also a better quantitative understanding of Arctic methane sinks.

In marine sediments, upward migrating methane is generally efficiently consumed by the anaerobic oxidation of methane (AOM) and, to a lesser extend, the aerobic oxidation of methane (AeOM) (Hinrichs and Boetius, 2002; Reeburgh, 2007; Knittel and Boetius, 2009). Although the exact AOM process has not been fully understood yet (James et al., 2016; McGlynn et al., 2015; Milucka et al., 2012; Wegener et al., 2015; Dean et al., 2018), it is thought that AOM is mediated by methane oxidizing archaea that use water (or bicarbonate) as electron acceptor (Hinrichs and Boetius, 2002; Dale et al., 2006):



The electrons are then shuttled (Krüger et al., 2003; Hinrichs and Boetius, 2002), via H₂, to sulfate reducing bacteria (eq. (2))



the overall reaction being



The first catabolic step is thermodynamically favourable only under a limited range of environmental conditions, while the second step is subject to weaker thermodynamic constraints (LaRowe et al., 2008). A recent assessment indicates that, in global sediments, around 45-61 TgCH₄ yr⁻¹ (Egger et al., 2018) are consumed by AOM, thus significantly reducing previously published estimates of 320-360 PgCH₄ yr⁻¹ (Hinrichs and Boetius, 2002; Reeburgh, 2007).

AOM generally acts as a particularly efficient biofilter for upward migrating methane and oxidizes up to 100% of the methane flux coming from below (*e.g.* Regnier et al. (2011)). However, a number of environmental conditions can reduce the efficiency of this AOM biofilter, allowing methane to escape from the sediment (Iversen and Jørgensen, 1985; Piker et al., 1998; Jørgensen et al., 2001; Treude et al., 2005; Knab et al., 2008; Dale et al., 2008c; Thang et al., 2013; Egger et al., 2016). It has been shown that, in particular, high sedimentation rates (Egger et al., 2016), slow microbial growth (Dale et al., 2006, 2008c) or the accumulation of free gas can promote methane efflux from the sediment. These findings are particularly relevant for potential methane escape from Arctic shelf sediments. The Siberian shelf is the largest sedimentary basin in the world (Gramberg et al., 1983) and shelf areas close to the large Arctic rivers reveal sedimentation rates that can be up to 5 times faster than rates that are typically observed in the ocean (Leifer et al., 2017). In addition, the Arctic shelf is subject to large seasonal, as well as climate-induced longterm, changes in environmental conditions ~~that~~, namely SO₄²⁻ concentration in sea water and availability of CH₄ in the sediments coming from deeper strata. These factors may influence the efficiency of the AOM biofilter through their effect on microbial biomass dynamics. Finally, observations from the ESAS also indicate that methane gas accumulates in the sediments. When free gas pockets grow enough, methane tends to migrate upwards along pathways with higher permeability or where fractures occur (Yakushev, 1989; Boudreau et al., 2005; Wright et al., 2008; Shakhova et al., 2014, 2015, 2017; Leifer et al., 2017) and might even crack the sediments themselves (~~O'Connor et al., 2010; Overduin et al., 2016~~) (O'Connor et al., 2010; Overduin et al., 2016; Yao et al., 2019). However, despite a wealth of AOM-related research, a holistic, quantitative evaluation of the most important environmental controls on the efficiency of the AOM biofilter and its impact on methane escape from marine sediments is currently lacking. Thus our ability to understand and quantify AOM sink in ESAS sediments and thus the climate impact of subsea permafrost thaw and gas hydrate destabilization is seriously compromised.

Therefore, we here use a 1-D reaction-transport model approach to understand and quantify the efficiency of the AOM biofilter and its influence on the potential benthic release of methane ~~from ESAS sediments that bear in response to a plausible range of upward migrating dissolved methane fluxes from~~ thawing permafrost and/or dissociating methane gas hydrates on the warming ESAS shelf. The developed model accounts for the most pertinent primary and secondary redox processes, as well as mineral precipitation, methane gas formation and fast equilibrium reactions ~~that affect biogeochemical dynamics in both passive, as well as active sediments influenced by a deep methane source.~~ Both active sites (characterized by an upward water flow) and passive sites (without an upward water flow) are investigated. We limit our model analysis to non-turbulent methane efflux, because methane in gaseous form is not directly accessible for the AOM community. As a consequence, free gas bubbles

are less prone to be consumed by AOM and methane gas either sits in the sediments or rapidly migrates upcore through cracks, faults or fractures (Boudreau, 2012), bypassing the AOM biofilter.

The model is forced with a set of boundary conditions that are broadly representative of the conditions encountered on the ESAS. It is applied to conduct a comprehensive one-at-a-time, steady-state sensitivity study over the entire plausible range of 1) sedimentation rates, 2) active fluid flow velocities, 3) AOM rate constants, 4) organic matter reactivity and 5) non-local transport activity encountered on the ESAS. In addition, we also evaluated the influence of ~~environmental change induced by~~ 1) seasonal variability and 2) idealized, projected climate change on the efficiency of the AOM-biofilter and potential non-turbulent methane escape ~~at the seafloor from the ESAS~~ under transient conditions. For this purpose, the model is extended by adopting an explicit description of AOM biomass dynamics and a bioenergetic rate law for AOM (Dale et al., 2006, 2008c, 10 b). Finally, the the results of all sensitivity study runs are used to identify the most important controls on methane efflux and derive a transfer function that allows establishing a first-order estimate of methane escape from the ESAS.

The specific aims of this work are ~~to thus:~~ 1) to identify and quantitatively understand the most important environmental controls on the efficiency of the AOM biofilter, as well as 2) its significance ~~for non-turbulent methane escape from marine sediments on the ESAS under present-day environmental conditions and in response to idealized environmental variability in~~ reducing upward migrating methane fluxes originating from thawing subsea permafrost or destabilizing methane gas hydrates under a plausible range of environmental conditions encountered on the present and future Siberian Shelf. Model results ~~will then be~~ are then used to 3) ~~quantitatively assess the~~ identifying environmental conditions (and thus areas on the ESAS) that favour non-turbulent dissolved methane fluxes across the sediment-water interface and 4) derive transfer functions that allow estimating the potential for non-turbulent CH₄ escape from ESAS sediments ~~and set some,~~ thus providing first order constraints 20 on the Arctic methane budget.

2 Methods

2.1 BRNS: Reaction-transport model

The Biogeochemical Reaction Network Simulator (BRNS) (Regnier et al., 2002; Aguilera et al., 2005; Centler et al., 2010) - an adaptive simulation environment suitable for simulating large, mixed kinetic-equilibrium reaction networks in porous media (*e.g.* Jourabchi et al. (2005); Thullner et al. (2005); Dale et al. (2009)) - is used to quantitatively explore the fluxes and transformations of methane in ~~ESAS sediments~~ a sediment column representative for ESAS conditions. For this purpose, we set-up a reaction network (table S1, S2), model parameters (table ~~S5~~S6), as well as boundary conditions (table ~~S6~~) ~~that are broadly representative for~~ S7) that cover the conditions encountered on the present-day Siberian shelf.

In the BRNS, the general mass conservation for each solid and dissolved species is described by a a set of coupled advection-diffusion-reaction equations in porous media which are solved simultaneously (*e.g.* Berner (1980); Boudreau (1997); note that dependencies on z and t have been omitted for simplicity):

$$\frac{\partial \xi C_i}{\partial t} = \frac{\partial}{\partial z} \left[(D_i + D_{b,i}) \xi \frac{\partial C_i}{\partial z} \right] - \frac{\partial}{\partial z} (v \xi C_i) + \alpha_i \xi (C_i(0) - C_i) + \mathcal{S}_i. \quad (4)$$

C_i is the concentration of the species i (mass per porewater volume for dissolved species or mass per solid matrix volume for a solid species); ξ *i.e.* the porosity $\xi = \varphi$ for dissolved species and $\xi = \varphi_s = 1 - \varphi$ for solid species. D_i is the effective diffusion coefficient for species i and is affected by salinity, temperature and tortuosity (see Table S5S6). D_b denotes the bioturbation coefficient and v is the advective velocity. For solid species $v = \omega$ with ω being the burial rate, while the advective velocity for dissolved species is given by the sum of the burial rate and an advective flow velocity, v_{up} , *i.e.* $v = \omega + v_{up}$. A site where $v_{up} \neq 0$ is defined as an *active site*, while a site with no advective upward water flow is defined as *passive*. α_i is the bioirrigation coefficient ($\alpha_i = 0$ for solid species) and $C_i(0, t)$ is the concentration of the species i at the Sediment-Water Interface (SWI). The reaction term \mathcal{S}_i is written as:

$$\mathcal{S}_i = \sum_j \lambda_{ij} R_j \quad (5)$$

10 where λ_{ij} are the stoichiometric coefficients of all reaction rates R_j that affect species i .

2.1.1 Transport

The effective diffusion coefficients D_i are determined by correcting the diffusion coefficients in free solution D_i^0 (Boudreau, 1997) for tortuosity θ and temperature. Tortuosity is calculated by means of porosity φ according to a modified Weissberg relation (Boudreau, 1997): $\theta = 1 - \ln(\varphi^2)$. Note that the effective diffusion coefficients used in the model neglect pressure effects. Following Dale et al. (2008a), migration of methane gas is simply parameterized via a pseudo-diffusive term, with an apparent gas diffusion coefficient, $D_{CH_4}(g)$. Bioturbation in the upper decimeters of the sediment is simulated using a diffusive term (*e.g.*, Boudreau (1986)), with a constant bioturbation coefficient, D_b^0 . The model assumes that bioturbation ceases at the bioturbation depth, z_{bio} (Boudreau, 1997). Bioirrigation is included in the mass conservation equation as a source or a sink function analogous to a kinetic rate. It is calculated as the product of the irrigation intensity, α ($\alpha = 0$ for all solids), and the difference in concentration of species i relative to the concentration at the SWI, $C_i(0)$. The bioirrigation rate α , is evaluated from the bioirrigation coefficient at the sediment surface (α_0) and the bioirrigation attenuation depth (z_{irr}) and is given by eq. S9. Porosity is assumed to decrease with depth according to an exponential decay (Athy, 1930):

$$\varphi(z) = \varphi_0 e^{-c_0 z} \quad (6)$$

with φ_0 : porosity at the Sediment-Water Interface (SWI) and c_0 : typical length scale for compaction. ~~Table S5 provides a detailed overview of the transport parameter values applied in the model.~~

2.1.2 Biogeochemical network

The reaction network implemented here (33 species, 37 reactions) encompasses the most pertinent primary and secondary redox reactions, equilibrium reactions and mineral precipitation and adsorption reactions. A summary of the reactions, their stoichiometry and their rate formulations can be found in Table S2 and Table S3. The following section provides a short

description of the implemented reaction network, as well as a more detailed description of the reactions that affect the production/consumption of methane. A complete description can be found in the supplementary information.

The BRNS model accounts for the degradation of organic matter by aerobic degradation, denitrification, manganese oxide reduction, iron reduction, sulfate reduction and methanogenesis (Table S2). Organic matter degradation is described by means of the reactive continuum model (RCM) (Aris, 1968; Ho and Aris, 1987; Boudreau and Ruddick, 1991) that describes compound-specific reactivities (Tesi et al., 2014) and, thus, captures the widely observed decrease in apparent organic matter reactivity with degradation state. The relative importance of each metabolic pathway is simulated through a series of kinetic limitation terms, reflecting their sequential utilization in the order of their decreasing Gibbs energy yields (Table S1). After all terminal electron acceptors (TEAs) are consumed, the remaining organic matter may be degraded by methanogenesis. The rates of secondary redox reactions (Table S3), are described by bimolecular rate laws (*e.g.* Wang and Van Cappellen (1996)). Adsorption reactions are considered as fast equilibrium processes (Table S3, R28-R30). Mineral precipitation rates are simulated according to kinetic-thermodynamic rate laws (Table S3, R16-R24).

As described above, methane is produced during organic matter degradation by methanogens in deeper sediment layers, once all TEAs are depleted (Table S2, R6). If the concentration of dissolved methane exceeds the saturation concentration $[\text{CH}_4]^*$ methane gas forms. The transfer rate of methane between the dissolved and gaseous phase is linearly controlled by the departure of the simulated dissolved methane concentration from the saturation concentration (Haeckel et al., 2004; Hensen and Wallmann, 2005; Tishchenko et al., 2005; Mogollón et al., 2009; Graves et al., 2017). $[\text{CH}_4]^*$ is calculated according to Dale et al. (2008a), derived from the formulation proposed by Duan et al. (1992) for which $[\text{CH}_4]^*$ depends on *in situ* salinity, pressure and temperature. Here, we assume that the formed methane gas is inaccessible to microbial activity and hence bypasses anaerobic and/or aerobic oxidation zones. In contrast, dissolved methane can be consumed by anaerobic (AOM) or aerobic oxidation of methane (AeOM). Free gas can re-dissolve into porewater once porewater methane concentration fall below the saturation level and may then become available to methanotrophs. AeOM rate is simply described by a bimolecular rate law (Table S3, R14). The description of AOM depends on the model scenario. For steady state simulations, we apply a simple bimolecular rate:

$$\text{rate}_{AOM} = k_{AOM}[\text{CH}_4][\text{SO}_4^{2-}]. \quad (7)$$

It is the simplest and most commonly used formulation of the AOM rate in reaction-transport models (*e.g.* Regnier et al. (2011)). It accounts for kinetic controls and assumes that, under steady state conditions, bioenergetic controls are negligible (Dale et al., 2006; Regnier et al., 2011).

For transient model simulations, we apply a bioenergetic rate law in combination with an explicit description of the AOM-performing biomass (Dale et al., 2006, 2008c). It has been shown that the rates of redox reactions, whose energy yield is used by micro-organisms to grow, can be coupled to biomass growth rates via a kinetic Monod term and a thermodynamic Boltzmann term (*e.g.* Rittmann and VanBriesen (2019)). Hence, the time derivative of AOM-performing biomass (B) can be written as:

$$\frac{dB}{dt} = \mu_g B \cdot F_K \cdot F_T - \mu_d B^2 \quad (8)$$

where μ_g is the growth rate and μ_d is the decay rate. F_K is the kinetic constraint given by:

$$F_K = \frac{[\text{CH}_4]}{K_m^{\text{CH}_4} + [\text{CH}_4]} \cdot \frac{[\text{SO}_4^{2-}]}{K_m^{\text{SO}_4^{2-}} + [\text{SO}_4^{2-}]} \quad (9)$$

with $K_m^{\text{SO}_4^{2-}}$ half saturation constant of SO_4^{2-} and $K_m^{\text{CH}_4}$ half saturation constant of CH_4 , according to a typical Michaelis-Menten for enzymatically-catalyzed reactions. F_T represent the thermodynamic limitation and is given by

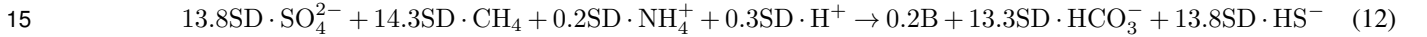
$$5 \quad \begin{cases} 1 - \exp\left(\frac{\Delta G_r + \Delta G_{BQ}}{\chi RT}\right), & \text{if } \frac{\Delta G_r + \Delta G_{BQ}}{\chi RT} < 0 \\ 0, & \text{if } \frac{\Delta G_r + \Delta G_{BQ}}{\chi RT} > 0 \end{cases} \quad (10)$$

where R is the gas constant, T is the absolute temperature, χ is the average number of electrons transferred per reaction per mole of ATP produced (Jin and Bethke, 2005), ΔG_r is the Gibbs free energy of the reaction and $\Delta G_{BQ} = 20 \text{ kJ (mol e}^{-})^{-1}$ is the minimum energy needed to support synthesis of $\sim \frac{1}{3} - \frac{1}{4}$ mol ATP (Dale et al., 2008c). In order to be thermodynamically favorable the total energy $\Delta G_r + \Delta G_{BQ}$ has to be negative, meaning the that Gibbs free energy provided by the catabolic reaction is sufficient to sustain the microbial biomass growth. ΔG_r is given by

$$\Delta G_r = \Delta G_r^0 + RT \ln \left(\gamma \frac{[\text{HS}^-] \cdot [\text{HCO}_3^-]}{[\text{CH}_4] \cdot [\text{SO}_4^{2-}]} \right) \quad (11)$$

with ΔG_r^0 : standard free energy of the reaction, the second term: deviations from standard conditions (temperature and reaction quotient) on Gibbs free energy and γ : a parameter representing departure from ideal behaviour.

The link between substrate consumption and microbial growth (anabolism) is given by Dale et al. (2006):



Assuming that the cellular composition of the biomass B is equal to $\text{C}_5\text{H}_7\text{O}_2\text{N}$ (Bruce and Perry, 2001; Dale et al., 2006, 2008c; Rittmann and McCarty, 2012). $SD = (1 - \varphi)/\varphi$ is the conversion factor between dissolved and solid species, here represented by microorganisms (which are assumed to be attached to the solid matrix). Catabolism is linked to biomass growth (anabolism) through the growth yield. We apply a yield of 0.0713 (Dale et al., 2006), which falls at the upper end of reported AOM growth yields, *i.e.* 0.05 – 0.07 (Dale et al., 2006; Nauhaus et al., 2007).

2.1.3 Boundary conditions

Boundary conditions place the model in its environmental context. For dissolved species, constant bottom water concentrations (Dirichlet boundary conditions) are applied at the sediment-water interface, while a known flux condition (Neumann boundary condition) are applied for solid species. At the lower boundary, a zero gradient flux boundary condition ($\partial C/\partial z = 0$) is considered for all species except methane, for which a Dirichlet condition is specified to account for methane supplied from thawing permafrost and/or dissociating gas hydrates below.

2.2 Model evaluation

~~In order to~~

To evaluate the performance of the BRNS set-up in capturing the main diagenetic patterns observed in Arctic marine ~~sediments we perform one steady state model case studies for an Arctic sites : a cold seep site off Vesterålen, Norway~~
5 ~~(68.9179~~shelf sediments we run the model for two case study sites in the area of interest: 1) a site offshore Kotelny Island
in the central region of the Laptev Sea, north of the Lena river delta (76.171°N, 14.2858129.333°E, 222-56 m water depth;
Sauer et al. (2015, 2016)) collected during the SWERUS-C3 expedition in summer 2014 (Brüchert et al., 2018; Brüchert, 2020)

~~Even though it is not located on the ESAS, the core offshore Norway (GC-51) is chosen because it was retrieved in~~

10 Although observations are merely available for the first 22 cm, the Høla trough, on the continental shelf of Vesterålen, and is
thus representative for the type of shelf sediments considered in our study. In addition, porewater data reveals a well-developed
Sulfate-Methane Transition Zone (SMTZ) first 3 m of sediment are simulated to allow for the full development of the early
diagenetic network, thus also accounting for biogeochemical processes (e.g. methanogenesis) in deeper sediment layers that
potentially affect biogeochemical cycling in the shallower sediment. Observations at the site indicate the absence of active
15 flow and the advective velocity v_{up} is thus set to zero. The site has already been subject of a modeling analysis by Sauer et al
2016, hence offering a benchmark for our simulation results. The Vesterålen site shows no sign of active water flow and, thus
represents a passive setting ($v_{up} = 0 \text{ cm yr}^{-1}$). Upper boundary conditions and model parameters are constrained on the basis of
observations reported by Sauer et al. (2016) the observations reported (Brüchert, 2020) (Table S4). In addition, we impose the
TOC depth-profile reported in Sauer et al. (2015) and evaluate the age of the organic matter using the sedimentology reported
20 in Sauer et al. (2016). The observed organic carbon profile is imposed in the first 19 cm (Table S5) and organic carbon contents
in deeper sediments are calculated on the basis of the reactive continuum model for organic matter degradation (described in
Sections S2 and S3) and the deepest observed value. In addition, the possibility of a source of methane is implemented at the
bottom of the modelled sediment column by applying a Dirichlet boundary condition, thus taking into account the possible
presence of methane seeping from deep sediments as results of destabilizing gas hydrates/subsea permafrost - a distinguishing
25 feature of the ESAS sediments. The methane boundary condition is determined by model fitting (see below).

When evaluating model performance, particular attention is given to sulfate, methane~~and~~, ammonium (NH_4^+), phosphates
(PO_4^{3-}) and dissolved inorganic carbon (DIC) depth profiles. While the former two species are of main interest for evaluating
simulated AOM dynamics, ~~NH_4^+ is a good indicator~~ the remaining three serve as indicators for OM degradation since it is
produced by the degradation of organic matter dynamics since they are metabolic byproducts of degradation (see Table S2)and
30 . Moreover NH_4^+ is only affected by nitrification (R7) and adsorption (R28). The latter, although important, acts homogeneously
throughout the ~~sediments~~ sediment (considering the slight variation in sediment porosity, LaRowe et al. (2017)). It can thus
only cause uniform shifts in $[\text{NH}_4^+]$ profile, but does not affect the overall shape of the NH_4^+ depth profile. Similarly, PO_4^{3-} is
only consumed by fluorapatite precipitation (R22) and adsorption processes (R29 and R31). Fluorapatite precipitation controls

maximum dissolved PO_4^{3-} concentrations, while the mineral adsorption process (R29) exerts a homogeneous influence and the interaction with $\text{Fe}(\text{OH})_3$ is expected to be minor and mainly affects PO_4^{3-} within the iron reduction zone.

OM reactivity parameters (a and ν), bottom methane concentration ($[\text{CH}_4]_-$) and reaction rates are varied to find the best fit between observed and simulated OM, $[\text{NH}_4^+]$ and $[\text{O}_2]$ profiles. Methane concentrations at the bottom of the model domain can also exceed the saturation concentration $[\text{CH}_4]^* = 14$ mM (estimated according to the value reported in Dale et al. (2008a)) to include the possibility of methane in gaseous form.

2.3 Modeling strategy

2.3.1 Steady state sensitivity analysis:

To evaluate the main physical and biogeochemical controls on the efficiency of the AOM biofilter and its impact on non-turbulent methane emission from deep methane sources such as dissociating permafrost and/or disintegrating methane gas hydrates in ESAS sediments, we conduct a comprehensive, steady state sensitivity study. For this purpose, we design a set of two baseline scenarios that are broadly representative for environmental conditions encountered on the shallow ESAS:

1. a passive case, *i.e.* $v_{up} = 0$ cm yr⁻¹;
2. an active case, *i.e.* with $v_{up} = 1$ cm yr⁻¹, a value which falls within the range of fluid flow velocities $v_{up} = 0.005 - 30$ cm yr⁻¹ observed across a wide range of different active environments (Regnier et al., 2011).

For both baseline scenarios, we assume a water depth of 30 m, which is similar to slightly shallower than the average water depth of the ESAS ~ 45 m (James et al., 2016), since we are here interested in the shallow, near-coastal part of the shelf that potentially hosts large subsea permafrost reservoirs and is most affected by the warming. Temperature is set equal to 0°C, and thus similar to the yearly average of -0.79°C observed in the Laptev Sea at a depth of about 30 m (Dmitrenko et al., 2011). The bioturbation coefficients D_b^0 and bioirrigation coefficients α_0 (Thullner et al., 2009) are then derived from global empirical relationships according to Middelburg et al. (1997) and Thullner et al. (2009), respectively. The methane saturation concentration $[\text{CH}_4]^*$ is calculated on the basis of the relationship proposed by Dale et al. (2008a) assuming a soil matrix density of 2.8 g cm⁻³. Values of φ_0 and c_0 (see eq. 6) are determined based on LaRowe et al. (2017). Boundary conditions are reported in Table S6-S7 and informed by observations. They are chosen to be broadly representative of the wider Siberian shelf environment.

Each sensitivity study run is forced with a range of different dissolved $[\text{CH}_4]$ concentrations at the lower model boundary, mimicking different methane fluxes from thawing permafrost-subsea permafrost and/or disintegrating methane gas hydrates at depth. The applied set of methane concentrations at the lower boundary range from zero to the methane gas saturation concentration $[\text{CH}_4]_- = 0 - 20 - 100 - 330 - 1169 - 5455$ μM and also include the highest methane concentration that has been to date observed in ESAS cores observed by Overduin et al. (2015) (Overduin et al., 2015) ($[\text{CH}_4]_- = 1.169$ mM).

Table 1 and Table S5-S6 summarize the parameters applied in the baseline simulation and Table S6-S7 provides an overview of the applied upper boundary conditions.

Table 1. Model parameters changed in the “one-at-time” sensitivity studies. Reported values are for the baseline simulations.

Quantity	Meaning	Value	Units	Reference
ω	Sedimentation rate	0.123	cm yr ⁻¹	Burwicz et al. (2011)
a	Average lifetime of reactive OM	10	yr	This study
v_{up}	Upward water velocity	0, 1	cm yr ⁻¹	This study
α_0	Bioirrigation coefficient	99.5	yr ⁻¹	Thullner et al. (2009)
k_{AOM}	AOM rate constant	$5.0 \cdot 10^3$	M ⁻¹ yr ⁻¹	Regnier et al. (2011)
$[CH_4]_-$	CH ₄ lower boundary condition	0 – 5.455	mM	This study

A To assess the influence of environmental conditions on the efficiency of the AOM biofilter and its influence on non-turbulent methane emission from dissociating permafrost and/or disintegrating methane gas hydrates in ESAS sediments a set of five “one-at-time” parameter variation experiments , encompassing is designed. It encompasses the most important controls on benthic methane cycling (Regnier et al., 2011; Meister et al., 2013; Egger et al., 2018) is and parameter variation experiments are performed for both the passive as well as active baseline scenario:

1. Sedimentation rate ω . The sedimentation rate is varied over two orders of magnitude (0.03 – 0.123 – 0.17 – 1.5 cm yr⁻¹). Maximum values are comparable to terrestrial sediment accumulation rates in the Lena river delta (Bolshiyarov et al., 2015), fast marine sedimentation rates during the early Holocene sea transgression (Bauch et al., 2001) and marine accumulation on subsea permafrost deposit in Buor Khaya Bay (~ 1.1 cm yr⁻¹, inferred from Overduin et al. (2015)), while minimum values are representative of sedimentation rates found in the East Siberian Arctic Sea (Stein et al. (2001) in Levitan and Lavrushin (2009)). The baseline value of ω is calculated based on the empirical global relationship proposed by Burwicz et al. (2011).
2. Active fluid flow v_{up} . Buoyancy-induced motion (Baker and Osterkamp, 1988), water streams channeled through fault lines or groundwater discharge (Charkin et al., 2017) can cause active fluid flow in Arctic shelf sediments underlain by subsea permafrost or gas hydrates (Judd and Hovland, 2009; Semenov et al., 2019). Therefore, v_{up} is varied from 0 – 0.3 – 0.5 – 1 – 3 – 7 – 10 cm yr⁻¹. This interval falls in the range of reported upward advective water velocities in marine sediments 0.005 – 30 cm yr⁻¹ (Regnier et al., 2011).
3. AOM constant k_{AOM} . Rate constants implicitly account for factors that are not explicitly described in the model and thus tend to show a strong variability between sites. A comprehensive compilation of published model AOM rate constants (Regnier et al., 2011) reveals a variability of over 6 order of magnitudes (10 – 10⁷ M⁻¹ yr⁻¹). The AOM rate constant k_{AOM} (eq. 7) is thus varied over the range $k_{AOM} = 5 \cdot 10^2 - 5 \cdot 10^3 - 5 \cdot 10^4 - 5 \cdot 10^5 - 5 \cdot 10^6 - 5 \cdot 10^7$ M⁻¹ yr⁻¹.
4. Organic matter reactivity (i.e. RCM parameter). Although the apparent OM reactivity is controlled by a combination of two parameters (a and ν), previous studies indicate a less pronounced variability in ν (Arndt et al., 2013; Sales de Freitas,

2018), as well as a strong control of a on the SMTZ depth (Regnier et al., 2011; Meister et al., 2013). Thus, ν was kept constant, while a was varied over the entire range of previously published values $a = 0.1 - 1 - 10 - 100 - 500 - 1000$ yr (Arndt et al., 2013). Studies about ESAS organic matter degradation shows a reactivity of deposited organic matter which is compatible with the RCM parameter we explored. For instance, Bröder et al. (2016) found an half life for the organic carbon in the East Siberian Arctic Shelf of 19 – 27 yr, which would correspond to an $a = 3.4 - 4.8$ yr, with $\nu = 0.125$.

5

10

5. Bioirrigation coefficient α_0 . Bioirrigation activity remains largely unconstrained on the Siberian shelf due to the scarcity of observational data (Teal et al., 2008). However, environmental stressors, such as ice scouring (*e.g.* Shakhova et al. (2017) and references therein) and trawling, which can dig furrows up to few meters (Shakhova et al., 2017) are detrimental to the local fauna, thus suggesting a low bioirrigation intensity. Yet, observations from other polar sites indicate that although biological diversity and activity is often low, it might be locally enhanced (Clough et al., 1997). In addition, ice scouring might also enhance non-local transport seasonally. We therefore, varied α_0 over the entire range of plausible values : $0 - 33 - 66 - 99.5 - 120 - 240 \text{ yr}^{-1}$ (Thullner et al., 2009).

2.3.2 Transient Sensitivity Study

15

20

Dale et al. (2008c) showed that temporally varying environmental conditions may reduce the efficiency of the benthic AOM filter and facilitate methane escape due to the delayed response of the microbial community to changing conditions. Therefore, in addition to the steady state sensitivity study, we also perform a series of transient simulations to explore the impacts of seasonal and projected climate change on benthic methane effluxes on the ESAS in rresponse to changing upward methane fluxes from dissociating permafrost and/or disintegrating methane gas hydrates. Transient simulations are run with a bioenergetic rate law for AOM (eq. 8) and an explicit description of AOM biomass ~~to explore the impacts of seasonal and climate change driven environmental activity on methane escape from the ESAS~~. Simulation results from the passive steady state baseline run with $[\text{CH}_4]_- = 0 \text{ mM}$ are used as initial conditions for the transient experiments. Four different transient environmental perturbation scenarios that reflect seasonal (1, 2), as well as idealized future (3, 4) environmental variability on the ESAS are run with three different values of $v_{up} = 0 - 1 - 5 \text{ cm yr}^{-1}$ over a period of 200 years:

25

30

1. *Seasonal* CH_4 : seasonal change of methane supply from permafrost thaw and/or hydrate destabilization. CH_4 concentration at the bottom of the sediment column: null for 6 months, then increasing up to a peak of $[\text{CH}_4]_-$ ($20 - 100 - 330 - 1169 - 5455 \mu\text{M}$) for the remaining 6 months of the year and again back to null concentration.
2. *Seasonal* $\text{CH}_4 + \text{SO}_4^{2-}$: seasonal freshening of waters due to riverine discharge and sea ice melt. During winter, higher bottom salinity (Dmitrenko et al., 2011) results in higher sulfate concentration (Dickson and Goyet, 1994), while lower salinities and thus sulphate concentrations characterise the melt season. The bottom boundary condition for methane $[\text{CH}_4]_-$ follows an opposite trend: it is set to zero during the winter months and increases in Arctic summer.
3. *Linear* CH_4 : slow increase in methane supply from permafrost thaw and/or hydrate destabilization. A linear increase of the bottom boundary methane concentration $[\text{CH}_4]_-$ (from 0 up to the peak) over 200 years is applied.

4. *Sudden* CH₄: abrupt increase of methane supply from permafrost thaw and/or hydrate destabilization. An instantaneous change of bottom boundary methane concentration - from 0 to one of the peak value [CH₄]₋ - is applied.

2.3.3 Analyzed output

For each simulation we evaluate the effect of the respective parameter change on:

- 5 1. the non-turbulent (i.e. not-ebullition driven) flux of methane from the sediments into the water column;
2. the depth of the SMTZ;
3. the efficiency (η) of the AOM biofilter (see Appendix A for the exact definition of AOM applied here).

In addition, fluxes of SO₄²⁻ and CH₄ at the SMTZ, the maximum and integrated AOM rate and the Damköhler number (D_a) for AOM and methanogenesis are also calculated. Damköhler number is defined as eq. B4 (see Appendix B) and sets the ratio
10 between the typical transport time-scale and the typical reaction time-scale. If $D_a < 1$, the reaction time-scale is longer than transport time-scale (i.e. the reaction is slower) and the process is reaction-limited. If $D_a > 1$ the process is transport-limited. Finally, for transient simulations, the integrated AOM-performing biomass (ΣB) was also analyzed.

3 Results and discussion

3.1 Case ~~studies~~study: sediment core on the Laptev Sea shelf

15 3.1.1 ~~Case study: Cold seep off Vesterålen, Norway~~

Fig. ??

Fig. 1 compares simulated and observed depth profiles for site ~~GC-51-14-3~~. Cores were retrieved during the SWERUS-C3 campaign (Miller et al., 2017; Brüchert et al., 2018; Brüchert, 2020). Simulation results show an overall ~~satisfactory good~~ agreement with measurements. ~~The general shape of the downward diffusing SO₄²⁻ and upward diffusing CH₄ depth profiles is similar to the profiles that are typically observed in passive sediments. In addition, the model reproduces the observed SMTZ depth, located at about 100 cm, but also reveal a slight overestimation of NH₄⁺. Above the SMTZ Data-model fitting reveals that, reconciling simulated and observed CH₄ and SO₄²⁻ depth profiles, the simulated requires a diffusive flux of CH₄ concentrations closely agree with measurements, but simulated and observed depth profiles diverge significantly below the SMTZ. Such a discrepancy is common (e.g. Dale et al. (2008a); Sauer et al. (2016)) and likely results from degassing during~~
20 ~~core extraction and recovery (Dickens et al., 2003). Yet, the simulated CH₄ concentration close to the lower model boundary (35 mM) is consistent with the values reported in Sauer et al. (2016) (30 mM) and is lower than the in-situ methane saturation concentration at that depth (39 mM). through the lower model boundary (i.e. a bottom boundary concentration of [CH₄]₋ = 16 mM). Neither higher marine OM contents in sediment layers below the first 22 cm for which observations are available, nor higher reactivities result can satisfactorily reproduce the observed sulfate depletion and observed gradients. Model-data fitting~~
25

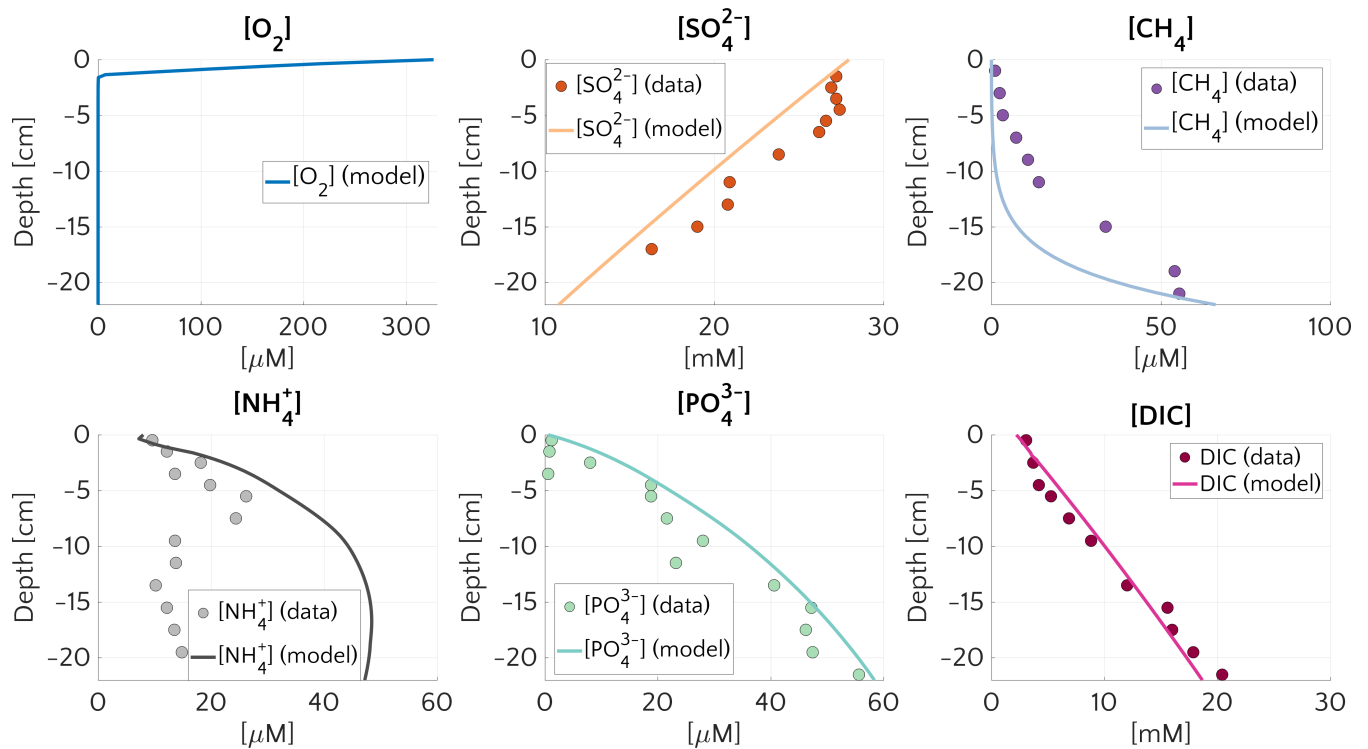


Figure 1. Pore water concentration profiles for CH_4 , O_2 , SO_4^{2-} (a) and CH_4 , NH_4^+ (b), PO_4^{3-} and DIC at site GC-51 of HOLA TROUGH 14-3 on the Laptev Sea (76.171°N, 129.333°E, 56 m water depth). Dots represent the measurements and continuous lines the simulated results. The boundary conditions and model parameters employed in the model are reported in table S4, the measured organic carbon content in table S5. For O_2 no measured profile is available.

thus not only highlights the important role of AOM in controlling the sulfate-methane transition zone (SMTZ), but also indicates that upward migrating methane from deep, pre-Holocene sources, such as subsea permafrost in the sediment might be an ubiquitous feature on the Siberian shelf.

Furthermore, The simulated PO_4^{3-} and DIC profiles are in good agreement with data, suggesting that the degradation dynamics of marine organic matter and adsorption are well captured by the model- although the maximum concentration of PO_4^{3-} at depth is mostly controlled by the saturation value of $[\text{PO}_4^{3-}]$. The largest discrepancy between data and modeling results are observed for NH_4^+ . Observed NH_4^+ concentrations first increase to a maximum at about 6 cm depth and the slightly decrease in the lower sediment layers, whereas simulated NH_4^+ show an asymptotic increase in NH_4^+ concentrations. The observed NH_4^+ profile is also well reproduced, suggesting that the model captures OM degradation dynamics well. Model derived organic matter degradation rate parameters of $a = 1100 \text{ yr}$, $\nu = 0.100$ indicate a generally low reactivity of OM depositing at this site, which is in agreement with observations and low NH_4^+ concentrations might either indicate changes in

OM reactivity and/or characteristics or spatially heterogeneous adsorption/desorption dynamics. Such downcore heterogeneity is not incorporated in the model and accounting for such a heterogeneity would require additional information.

3.2 Main physical and biogeochemical controls on potential non-turbulent methane flux from ESAS sediments

3.2.1 General patterns of methane and sulfate cycling on the ESAS

5 The comprehensive ensemble of all sensitivity experiments allows exploring the general patterns of methane and sulfate cycling under a range of environmental conditions that is broadly representative for conditions encountered on the ESAS at present (Fig. 2). Model results confirm that AOM is an efficient sink for the diffusive CH₄ supply from below. For most of the investigated environmental conditions (95% of the runs), 95-99.9% of the upward diffusing CH₄ is consumed within the SMTZ, resulting in very small or negligible methane effluxes ($\leq 10^{-2} \mu\text{molCH}_4 \text{ cm}^{-2} \text{ yr}^{-1}$) from the sediment. If upscaled to the total area
10 of the ESAS ($\sim 1.485 \cdot 10^6 \text{ km}^2$, Wegener et al. (2015)), for which methane outgassing estimates have been published, the smallest simulated non-turbulent methane flux (*i.e.* $1.4 \cdot 10^{-13} \mu\text{mol cm}^{-2} \text{ yr}^{-1}$, Fig. 2.b) would sum up to a total flux of 2.1 mmolCH₄ yr⁻¹, resulting in a negligible role of non-turbulent, benthic methane fluxes to the Arctic methane budget.

Yet, model results also show that, under a specific set of environmental conditions that lower the efficiency of the AOM biofilter (see detailed discussion below), non-turbulent CH₄ escape from ESAS sediments can reach values of up to 27 μmolCH_4
15 $\text{cm}^{-2} \text{ yr}^{-1}$. Simulation results show that these high effluxes and, thus, low AOM biofilter efficiencies are generally simulated for environmental conditions that cause a shallow location of the SMTZ (< 18 cm) and that they are very sensitive to changes in environmental conditions that would cause a deepening of the SMTZ. For instance, a deepening of the SMTZ from 18 to 26 cm results in a rapid increase in AOM efficiency from 1% to 98% (Fig. 2.a). Furthermore, results indicate that, for SMTZ depths larger than 26 cm, AOM remains an efficient barrier across the full spectrum of investigated environmental conditions (Fig. 2).
20 The observed link between AOM filter efficiency and SMTZ is reflected in the strong (semilog) linear relationship between methane flux at the SWI and the SMTZ depth (Fig.2.b). Such a relationship reveals the pivotal connections between these two quantities and mirrors the empirically found linear log-log relationship between measured CH₄ fluxes at the SMTZ and the SMTZ depths (Fig. S4) by Egger et al. (2018). Maximum simulated CH₄ effluxes are thus comparable in magnitude to fluxes reported from mud-volcanos other settings potentially sensible for CH₄ emissions. These include mud-volcanoes, e.g. in the Gulf
25 of Cadiz: 2.1-40.7 $\mu\text{molCH}_4 \text{ cm}^{-2} \text{ yr}^{-1}$ (Niemann et al., 2006a) or; Mosby mud-volcano in the Barents Sea: 0.03 $\mu\text{molCH}_4 \text{ cm}^{-2} \text{ yr}^{-1}$ (Niemann et al., 2006b) ; other coastal settings (and coastal settings, e.g. a Dutch coastal reservoir (20-80 $\mu\text{molCH}_4 \text{ cm}^{-2} \text{ yr}^{-1}$, Egger et al. (2016)) or tidal flats (4-800 $\mu\text{molCH}_4 \text{ cm}^{-2} \text{ yr}^{-1}$,Dale et al. (2008b) Borges and Abril (2011)). Upscaling the highest simulated non-turbulent flux (27.48 $\mu\text{molCH}_4 \text{ cm}^{-2} \text{ yr}^{-1}$) to the ESAS results in a total efflux of 0.408 TmolCH₄ yr⁻¹ = 6.52 TgCH₄ yr⁻¹ a value that. This value represents an estimated upper limit which, for comparison, equals
30 ~ 10% of global marine seepage at seabed level (Saunio et al., 2016) and similar in magnitude is in magnitude similar to the global methane efflux that has been estimated for upper continental slope sediments on a centennial timescale (4.73 TgCH₄ yr⁻¹, Kretschmer et al. (2015)).

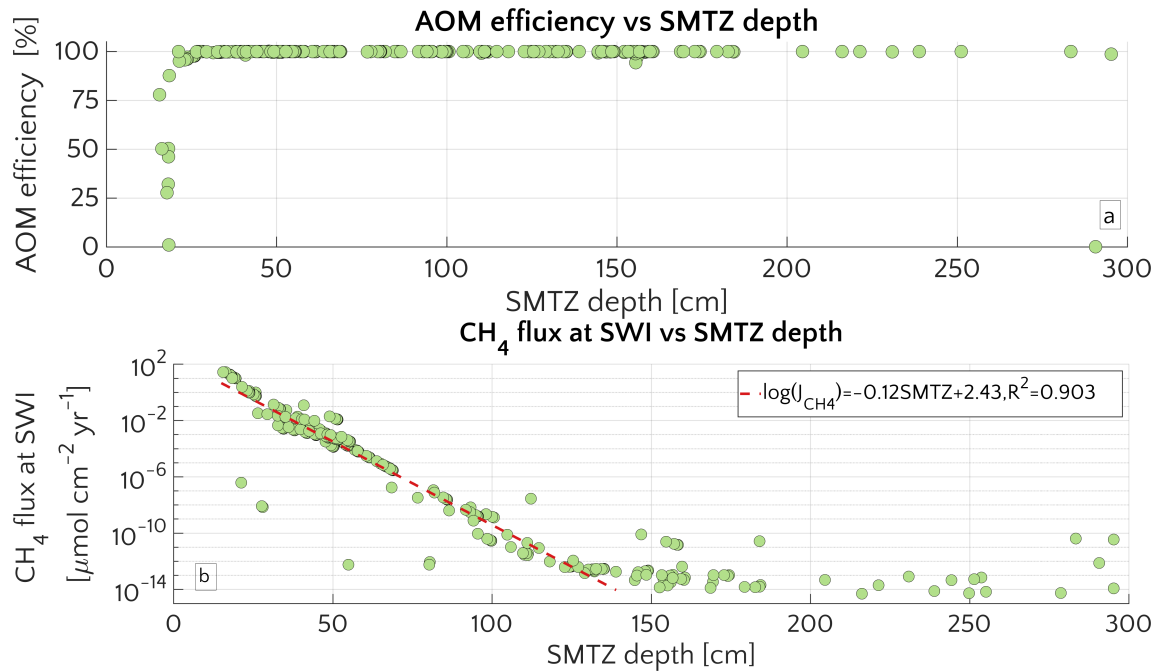


Figure 2. Aggregation of all the simulation performed for the “one-at-time” sensitivity study. *a.* AOM efficiency versus the depth of the SMTZ. *b.* Scatter plot and semi-log fit of the methane flux (J_{CH_4}) at the SWI versus SMTZ depth.

Further insights into the general drivers that control methane dynamics in ESAS sediments are provided by Damköhler numbers. Damköhler numbers for simulated methanogenesis ($D_{a_{MG}}$) and AOM ($D_{a_{AOM}}$) are reported in Fig. S2. $D_{a_{MG}}$ (purple circles) are < 1 , span a range of $\sim 0.0021 - 0.43$ and are thus comparable to previously reported $D_{a_{MG}}$ of 0.22 for methane gas hydrate bearing sites, such as Hydrate Ridge and Kithley Canyon (Chatterjee et al., 2011). They reveal that methanogenesis is always slower than methane transport and that CH_4 dynamics driven by methanogenesis are thus reaction-limited. This result is consistent with the fact that methanogenesis rates are merely supported by the slow influx and transport of OM by burial and bioturbation.

In contrast, high $D_{a_{AOM}}$ values ($D_{a_{AOM}} = 32-2.78 \cdot 10^5$ - Fig. S2, orange circles), show that AOM is transport-limited, suggesting a sensitive role of transport parameters in determining AOM efficiency and in controlling methane flux across the SMTZ and subsequently the SWI.

3.2.2 Environmental controls and mechanisms of methane escape from ESAS sediments

The simulated general patterns of methane and sulfate cycling on the ESAS thus broadly corroborate previous findings regarding the dominant environmental controls on AOM biofilter efficiency and SMTZ depth (Regnier et al., 2011; Egger et al., 2018; Meister et al., 2013; Winkel et al., 2018). Yet, they also challenge traditional-intuitive views on the factors that favour high CH_4 escape through the SWI. In particular, they highlight the essential link between AOM efficiency and SMTZ depth -and

as a consequence and the central importance of environmental conditions that control the depth of the SMTZ. In addition, they suggest that transport processes play a dominant role for non-turbulent methane effluxes from ESAS sediments. The following sections explore the role of each of the investigated environmental conditions on methane efflux in more detail. They also shed light on the mechanisms behind non-turbulent methane escape from ESAS sediments.

5 3.2.3 Role of advective transport

Fig. 3.a illustrates the effects of sedimentation rate ω on the flux of methane across the SWI. For both active ($v_{up} = 1$ cm yr^{-1}) and passive ($v_{up} = 0$ cm yr^{-1}) settings, simulated CH_4 effluxes increase exponentially with sedimentation rate (log-log linear, see fig. 3.c) from $5.5 \cdot 10^{-15}$ μmolCH_4 cm^{-2} yr^{-1} for low sedimentation rates ($\omega = 0.03$ cm yr^{-1}) to values as high as 27.5 μmolCH_4 cm^{-2} yr^{-1} for high sedimentation rates ($\omega = 1.5$ cm yr^{-1}). Accordingly AOM acts as an efficient filter for upward diffusing methane (with $\eta \sim 100\%$, see Fig. S3), in slowly accumulating sediments. Integrated AOM rates (ΣAOM), for both active and passive settings, are in agreement with these findings. They range from $0.04 - 3.7$ mol m^{-2} yr^{-1} and are, thus, comparable to values that are typically observed in sediments characterised by an efficient AOM biofilter (e.g. Albert et al. (1998); Martens et al. (1998); Regnier et al. (2011)). In contrast, the efficiency of the AOM biofilter drops to $50 - 0\%$ for high sedimentation rates. The main driver behind the simulated high CH_4 fluxes and low AOM efficiencies in these rapidly accumulating sediments, are enhanced methanogenesis rates. High sedimentation rates facilitate not only the supply of organic matter to the methanogenic zone of the sediment, but also reduce residence times in the upper sediment layer, resulting in a lower OM age (see eq. S13, S15)/degradation state (see eq. S11) within the methanogenic zone. The enhanced supply of reactive OM to anoxic sediment layers supports higher methanogenesis rates, resulting in higher methane porewater concentrations and an upward shift of the SMTZ.

In addition, the presence of active fluid flow further enhances methane efflux. The CH_4 fluxes from below adds complexity to the overall methane dynamics and this effect is investigated further by contrasting Damköhler numbers for passive and active margins settings on the shelf. Table 2 shows that for low to intermediate sedimentation rates, $D_{a_{AOM}}$ values significantly decrease with v_{up} , indicating that less and less methane consumption occurs within the typical transport time scale τ_T , thus, leading to a reduction in AOM biofilter efficiency. For instance, for $\omega = 0.123$ cm yr^{-1} , τ_T is about three orders of magnitude slower than τ_R without the presence of active fluid flow, while for $v_{up} = 10$ cm yr^{-1} τ_T accelerates and is only one order of magnitude slower than τ_R , resulting in a reduced consumption within the SMTZ. Accordingly, the decrease in $D_{a_{AOM}}$ coincides with an increase in CH_4 effluxes (Fig. 3. The trend in $D_{a_{AOM}}$ is reversed for high sedimentation rates ($\omega > 1.5$ cm yr^{-1} , i.e. $D_{a_{AOM}}$ increases with increasing v_{up} , while CH_4 efflux remains constant. This increase in $D_{a_{AOM}}$ can be explained with a simple increase in AOM rates due to the build-up of methane gas in deeper sediment layers and its partial re-dissolution with in the AOM zone where porewater methane concentrations decrease (also see Fig. 4 below).

Maximum simulated flux differences between active and passive settings can reach up to 10 orders of magnitude. Yet, flux differences quickly decrease with increasing sedimentation rates. Rapidly accumulating sediments show almost no difference in efflux between active and passive sites (Fig. 3.a). In contrast to sedimentation rates, the mechanism behind the control of v_{up} on non-turbulent methane efflux is straightforward and self-evident. Active flow enhances the upcore transport of

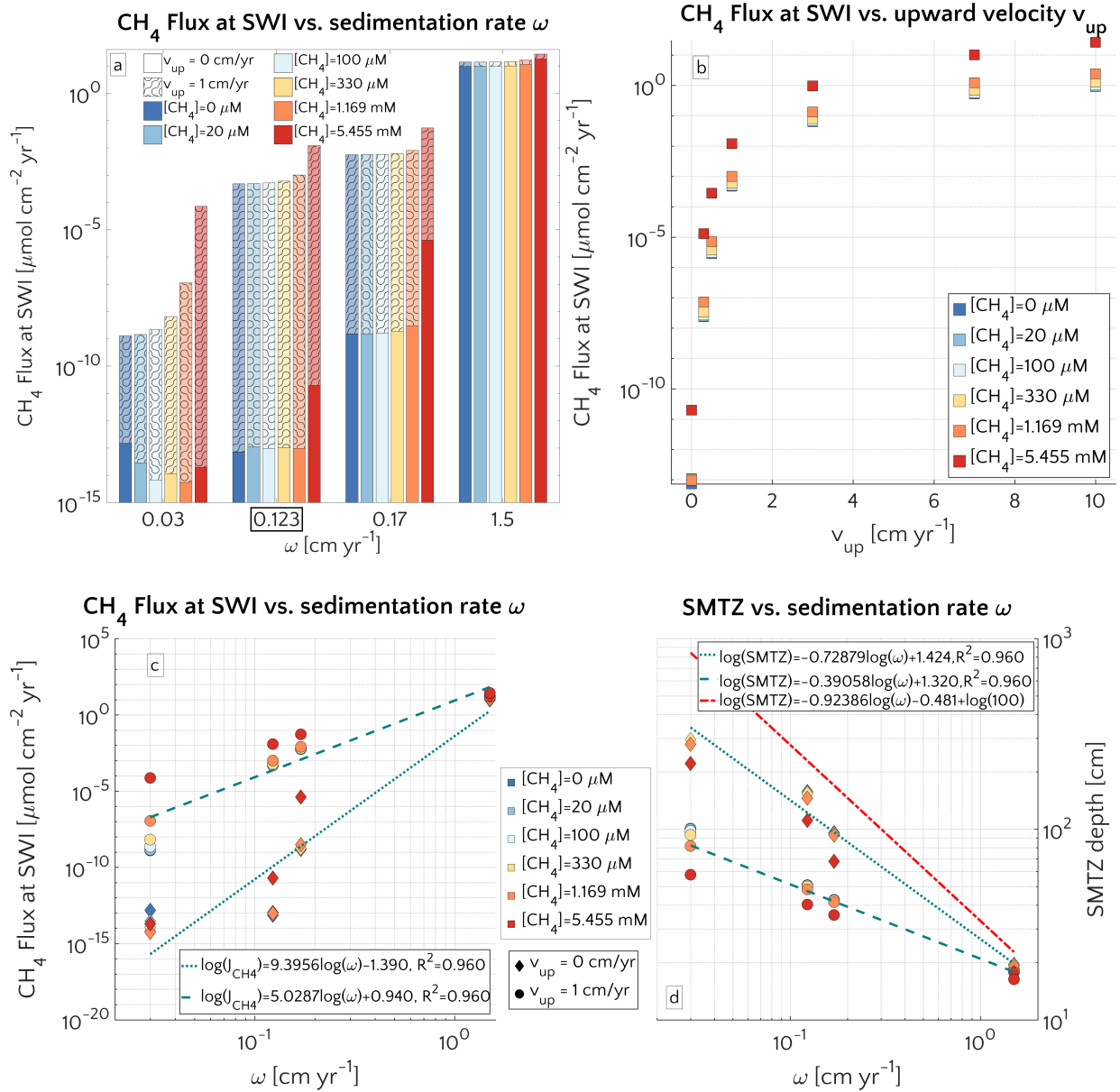


Figure 3. *a.* Barplot of the methane flux at the SWI versus ω for passive case (plain style) and active case (pattern style) and the $[\text{CH}_4]_0$ –reported in the text. The squared value of ω is the reference value. *b.* Semilog plot of methane flux at SWI versus v_{up} for the different $[\text{CH}_4]_0$ –reported in the text. *c.* Log-log plot of methane efflux at SWI versus ω for passive case (diamonds) and active case (circle). The log-log fit is also displayed. *d.* Log-log plot of SMTZ depth versus ω for passive case (diamonds) and active case (circle) with log-log fit. The red line is the trend found by Egger et al, 2018 (the term $\log(100)$ is to take into account unit conversion).

Table 2. AOM Damköhler number for $\omega = 0.123 \text{ cm yr}^{-1}$ and $\omega = 1.5 \text{ cm yr}^{-1}$. The two values are for the maximum and minimum values among the simulations with different bottom methane concentration. Missing values are because simulations were not run with the corresponding pair of parameters.

		$v_{up} \text{ [cm yr}^{-1}\text{]}$						
		0	0.3	0.5	1	3	7	10
ω	0.123	1206	1124	683	327	120	52	32
	[cm yr ⁻¹]	1521	1473	772	409	139	57	42
	1.5	470	-	-	1408	-	-	-
		518			1630			

CH₄, shifting the SMTZ upcore and, thus, increasing CH₄ concentrations at shallow sediment depths (see Fig. 3.d). The apparent paradox of the CH₄ efflux insensitive to fluid flow in fast accumulating sediments can be resolved by examining the dissolved CH₄ depth profiles (Fig. 4). Simulated depth profiles are nearly identical and reveal CH₄ concentrations at or near the saturation concentration. In fast accumulating sediments, high methanogenesis rates result in an over-saturation of porewaters directly below the generally shallow SMTZ. High methanogenesis rates thus support the build up of methane gas. Methane gas formation also explains why, in for these cases, integrated methanogenesis exceed no-turbulent CH₄ fluxes by up to 6 times. In rapidly accumulating, active and passive sediments, non-turbulent CH₄ fluxes are thus essentially identical. However, active settings will be characterised by the additional build-up of gaseous CH₄ and its potential escape through the sediment-water interface- a process not simulated in the present study.

Model results thus show that the dominant mechanism behind the observed transport-control on non-turbulent CH₄ efflux is an overall increase in CH₄ concentration and an upcore shift of the SMTZ rather than an increasing relative contribution of advective transport processes to the total efflux. In fact, a comparison of the different methane transport processes across the SWI (Fig. 5) shows that the relative contribution of both the advection and molecular diffusion flux to the total flux is small and further decreases with increasing v_{up} . High non-turbulent methane effluxes in rapidly accumulating and/or active settings are thus largely driven by the non-local irrigation flux (see section 3.2.5 for more details on the role of irrigation). With increasing ω or v_{up} , the SMTZ shifts upcore, resulting in higher methane concentrations at shallow sediment depths and thereby reinforcing the relative contribution of non-local transport for CH₄ fluxes, as well as lowering the efficiency of the AOM barrier from $\eta \sim 100\%$ to $\eta \sim 78\%$. The important role of the SMTZ location as a key control on CH₄ efflux is further confirmed by the observed exponential relationship between the location of the SMTZ and ω (Fig. 3.d). This result is qualitatively in agreement with the global compilation of empirical data by Egger et al. (2018), which reveals the same log-log decreasing trend between SMTZ and sedimentation rate. Our results are also consistent with observations from brackish sediments that show that sedimentation rates $> 10 \text{ cm yr}^{-1}$ give rise to high non-turbulent CH₄ fluxes ($20 - 80 \mu\text{molCH}_4 \text{ cm}^{-2} \text{ yr}^{-1}$) and a high OM burial efficiency ($\sim 78\%$, Egger et al. (2016)). Egger and co-workers explained these findings by the slow growth of AOM microorganisms and the resulting inability of the microbial community to consume all of the CH₄

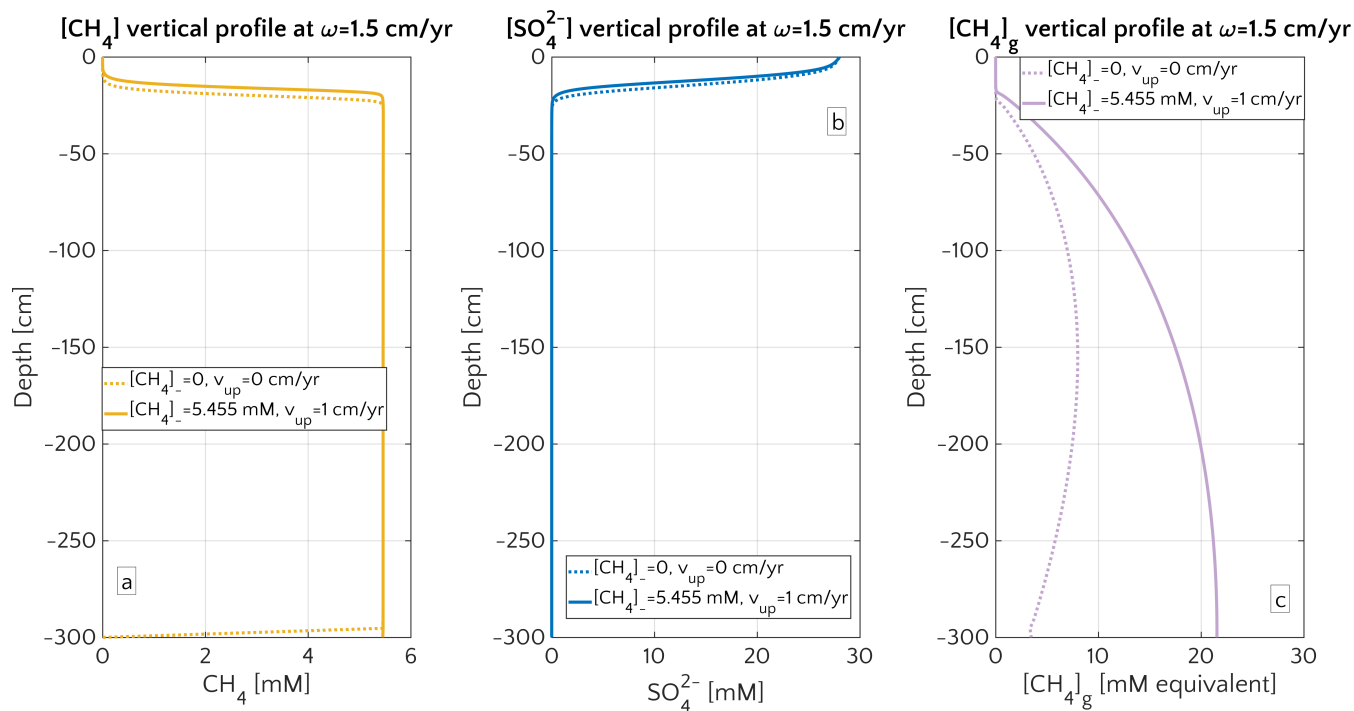


Figure 4. Porewater profiles in case of $\omega = 1.5 \text{ cm yr}^{-1}$ for CH_4 (a), SO_4^{2-} (b) and gaseous CH_4 (c). Dashed lines are simulation in passive scenario with $[\text{CH}_4]_- = 0 \text{ mM}$, while continuous lines simulations display active scenario with $[\text{CH}_4]_- = 5.455 \text{ mM}$, corresponding to the saturation concentration in the environmental conditions considered for the representative profile.

produced. Yet, our results show that the same pattern can be observed without having to invoke a low AOM efficiency. Our simulations thus indicate that the rapid burial of reactive organic matter to deeper sediment layers in rapidly accumulating sediments is sufficient to explain high CH_4 effluxes.

3.2.4 Role of organic matter quality

- 5 The quality of organic matter deposited onto the sediment exerts an additional control on CH_4 efflux. Fig. 6 illustrates the influence of organic matter quality (as a function of OM degradation model parameter a , see eq. S11) and sedimentation rate ω on non-turbulent methane efflux for both active and passive settings, as well as different methane fluxes from below. Results corroborate the dominant influence of sedimentation rates on methane efflux, while organic matter quality exerts a secondary control. [This also means that, in order to assess the main features of possible \$\text{CH}_4\$ efflux in terms of modeling, capturing the details of organic matter quality is not fundamental.](#)
- 10 Maximum fluxes are generally simulated for rapidly accumulating sediments $\omega > 0.5 \text{ cm yr}^{-1}$ that receive organic matter of intermediate quality ($a = 10 - 100 \text{ yr}$).

These findings are in agreement with previously published studies (Regnier et al., 2011; Meister et al., 2013) and can be explained with the fact that high methanogenesis rates require a supply of reactive OM to the methanogenic zone. If organic

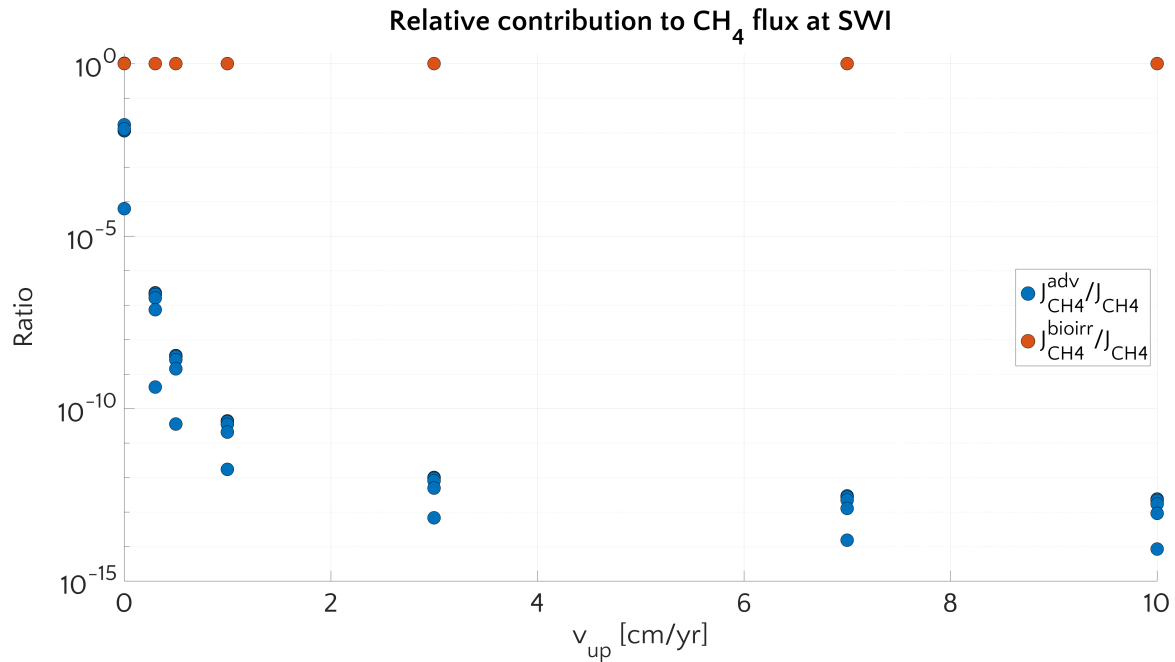


Figure 5. Relative contribution of transport process to the methane flux at the SWI: the advective component (blue) and the bioirrigation component (red). ω is set to the baseline value of 0.123 cm yr^{-1} . For each value of v_{up} and a specific flux component each dot corresponds to a simulation with a different value of bottom CH_4 concentration. Diffusive component of the flux is always $< 10^{-10}$.

matter quality is high ($a < 10 \text{ yr}$), methanogenesis becomes substrate limited due to the rapid degradation of organic matter through energetically more favourable degradation pathways in the shallow sediments. In turn, if organic matter quality is low ($a > 100 \text{ yr}$), methanogenesis becomes reactivity limited. The ideal combinations of organic matter reactivity and sedimentation rate that result in maximum methane effluxes correspond to conditions characterised by OM that is i) sufficiently

5 reactive to support enhanced methanogenesis rates and thus an accumulation of CH_4 at depth, but ii) sufficiently unreactive (in comparison to the burial rate) to escape the complete degradation in non-methanogenic sediments. Model results show that the onset of active fluid flow and an enhanced methane supply from below (i.e. higher CH_4 concentration at the lower boundary) increase the CH_4 efflux through the SWI without altering the overall patterns.

3.2.5 Role of non-local transport

- 10 Fig. 7 further investigates the influence of bioirrigation on non-turbulent CH_4 efflux from the ESAS. It enhances methane efflux in sediments that are characterised by a shallow SMTZ, for instance, due to high sedimentation rates, active fluid flow and/or methane flux from below. Yet, bioirrigation exerts a limited effect under a range of environmental conditions that favour a deep or shallow SMTZ location respectively.

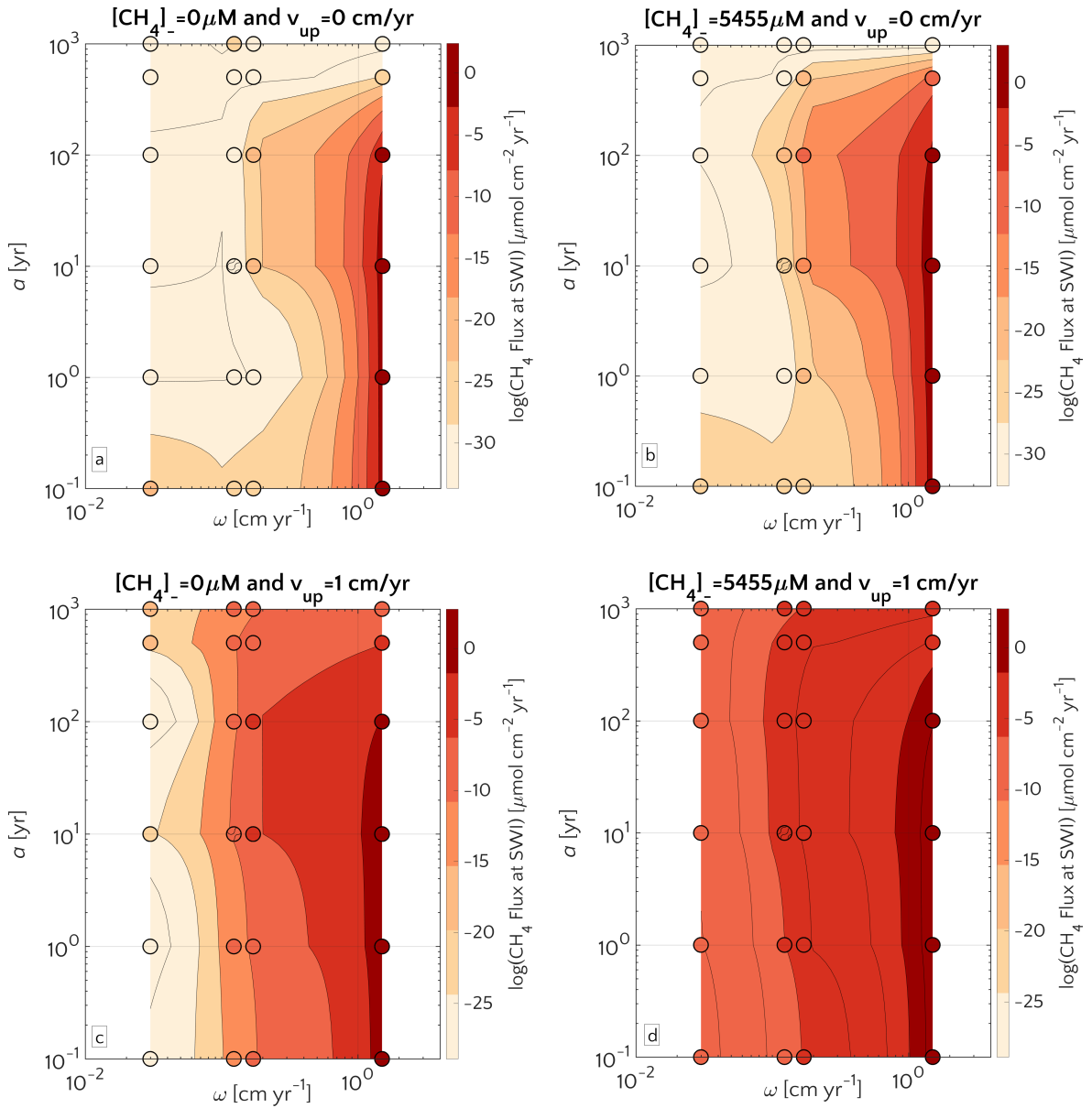


Figure 6. Flux of methane at the SWI as dependent on α and ω . For $[\text{CH}_4]_0 = 0 \text{ mM}$ (left) and $[\text{CH}_4]_0 = 5.455 \text{ mM}$ (right), and passive (top) and active (bottom) case. The circle with pattern corresponds to the baseline simulation.

In passive settings, changes in bioirrigation coefficient, α_0 , exert a limited influence on CH_4 effluxes. For most model scenarios, the SMTZ is located well below the sediment layer affected by bioirrigation ($z_{irr} = 3.5 \text{ cm}$, hence bioirrigation is strongly suppressed below 15 cm) and, thus, changes in α_0 have no effect on methane efflux. Changes in bioirrigation intensity only exert a noticeable effect on methane efflux when methane concentrations at the lower boundary exceed $[\text{CH}_4]_0 = 5.455$

mM. Under these conditions, a decrease in methane efflux is observed with increasing α_0 , because the increasing bioirrigation activity supports an enhanced downcore transport of SO_4^{2-} , leading to a deepening of the SMTZ and a reduction in methane efflux. Model results thus partly support previously published findings by Cordes et al. (2005) and Niemann et al. (2006a), who argued that bioirrigation increases methane consumption due to the enhanced downcore electron acceptors transport. However, model results also show that this effect is only observed under environmental conditions that result in a shallow SMTZ and that methane consumption and efflux remain largely unaffected by changes in bioirrigation intensity if the SMTZ is located deeper in the sediment.

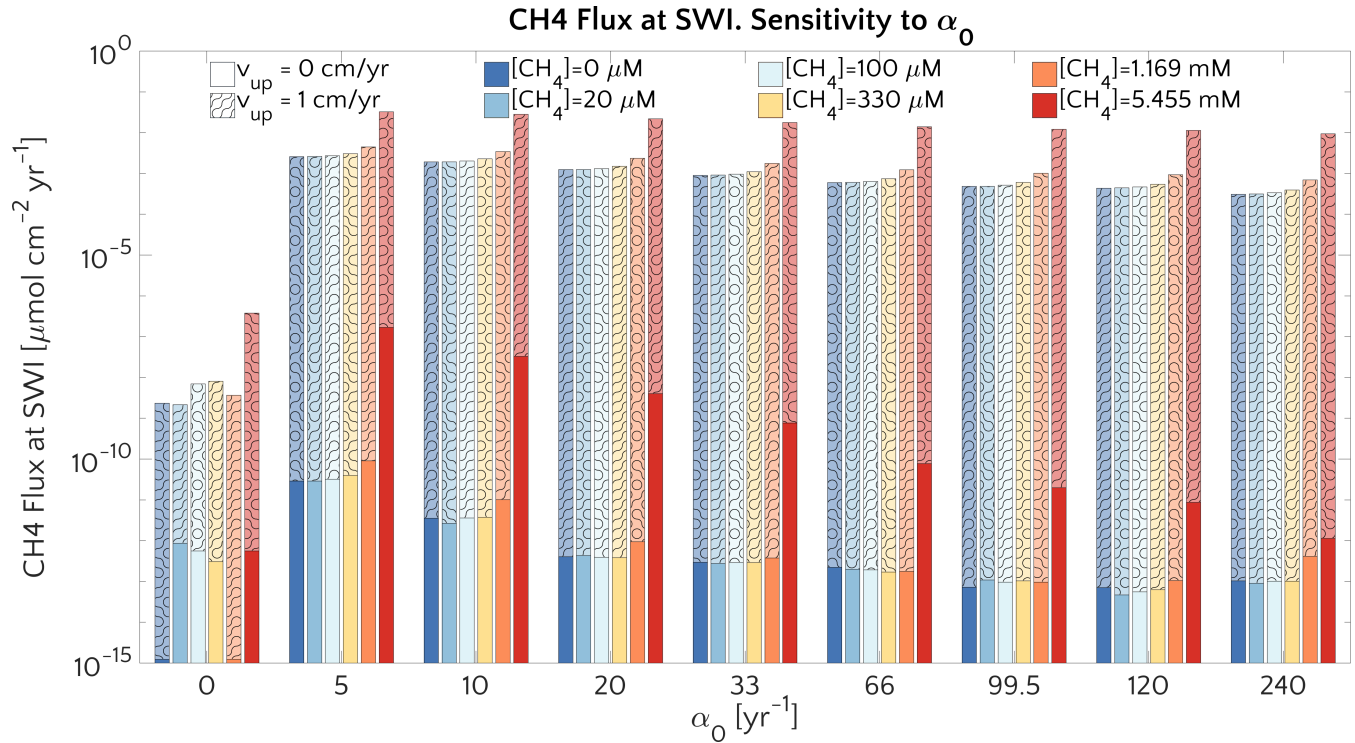


Figure 7. Barplot of the methane flux at the SWI versus α_0 for passive case (plain style) and active case (pattern style) and the $[\text{CH}_4]$ – reported in the text.

In contrast to passive settings, active settings reveal a rapid increase in methane efflux with the onset of bioirrigation activity. Methane effluxes first increase by up to 5 orders of magnitude from $\alpha_0=0 \text{ yr}^{-1}$ to $\alpha_0=5 \text{ yr}^{-1}$, reaching maximum effluxes of $\sim 0.02 \mu\text{molCH}_4 \text{ cm}^{-2} \text{ yr}^{-1}$, before remaining almost constant with a further increase in bioirrigation coefficients (up to 240 yr^{-1}). The simulated increase in methane efflux is a direct effect of the transport process itself, which enhances the upcore transport of methane accumulating in the upper sediment layers, including layers below the generally shallow SMTZ. The subsequently simulated constant methane effluxes with increasing bioirrigation intensity in combination with the fact that

bioirrigation represents the largest flux term at SWI (Fig.8) suggest that concentration differences close the the sediment-water interface remain broadly similar for all $\alpha_0 > 5 \text{ yr}^{-1}$.

These results are corroborated by the concomitant analysis of CH_4 dynamics over the 3-dimensional transport coefficient ω , v_{up} and α_0 space shown in Fig.8.

5 A comparison between simulations with $\alpha_0 = 0 \text{ yr}^{-1}$ and $\alpha_0 \neq 0 \text{ yr}^{-1}$ ($\alpha_0 = 5 \text{ yr}^{-1}$, $\alpha_0 = 10 \text{ yr}^{-1}$ and $\alpha_0 = 33 \text{ yr}^{-1}$) shows that irrigation increases the CH_4 efflux at low to intermediate sedimentation rates and/or high v_{up} (lower-left corner of the phase space in both plots). Yet, maximum methane effluxes that are simulated for high sedimentation rates or v_{up} are almost identical between bioirrigated and non-irrigated sites despite the differences in dominant transport mechanism (diffusion when $\alpha_0 = 0 \text{ yr}^{-1}$; irrigation when $\alpha_0 \neq 0 \text{ yr}^{-1}$). Under these conditions (i.e. high v_{up} and/or high ω), the SMTZ is located close
10 to the SWI. Under these conditions, non-local transport becomes the dominant transport process in bioirrigated sediments (see section 3.2.3) because it weakens concentration gradients near the SWI and, thus, contributes to a substantial reduction in the gradient-driven, diffusive transport terms. As a consequence, simulated CH_4 efflux at the SWI are broadly similar for all of the investigated $\alpha_0 \neq 0 \text{ yr}^{-1}$ (Fig. 8.b,c,d). It is worth noticing that, independently on the α_0 , CH_4 efflux for $\omega = 0.03 \text{ cm yr}^{-1}$ and $v_{up} = 10 \text{ cm yr}^{-1}$ is $\sim 1 \mu\text{molCH}_4 \text{ cm}^{-2} \text{ yr}^{-1}$ - a value almost identical to the one reported in Luff and Wallmann
15 (2003) - $1.4 \mu\text{molCH}_4 \text{ cm}^{-2} \text{ yr}^{-1}$ - for a sediments characterised by $v_{up} = 10 \text{ cm yr}^{-1}$ and $\omega = 0.0275 \text{ cm yr}^{-1}$.

3.2.6 AOM rate constant

Given its crucial role in AOM biogeochemistry, one would expect a pronounced influence of the kinetic rates constant, k_{AOM} , on non-turbulent methane effluxes. However, simulation results reveal that k_{AOM} only plays a minor role for non-turbulent methane fluxes across the SWI (see Fig. S11, S12). An increase in k_{AOM} can reduce methane effluxes from passive shelf
20 sediments by up to 5 order of magnitude. Still, its effect remains small compared, for instance, to the response to variations in sedimentation rate, which can change methane efflux by up to 14 orders of magnitude. The most important effect of increasing k_{AOM} is the increasing linearity of the $[\text{CH}_4]$ and $[\text{SO}_4^{2-}]$ profiles around the SMTZ and the concurrent narrowing and down-core movement of the SMTZ, which can result in a reduction in methane efflux. Model results thus show that the AOM biofilter and, as a consequence, non-turbulent methane effluxes from sediments are not affected by the exact value of the kinetic rate
25 constant, at least in the range we analyzed. This is in disagreement with results by Dale et al. (2008c), which show that, in dynamic settings subject to large methane fluxes, an increase of 3 orders of magnitude in k_{AOM} (from $10^2 \text{ M}^{-1} \text{ yr}^{-1}$ to $10^5 \text{ M}^{-1} \text{ yr}^{-1}$) leads to a reduction in steady state methane fluxes below $10^{-2} \mu\text{molCH}_4 \text{ cm}^{-2} \text{ yr}^{-1}$. However this discrepancy might be ascribable to the high water flow velocity employed in their simulation ($v_{up} = 10 \text{ cm yr}^{-1}$), ten times higher than the one we considered in our active simulations. Finally, on the ESAS, dissolved methane concentrations are limited by the comparably low
30 gas saturation concentration, resulting in ~~lower-a minor influence of k_{AOM} on methane fluxes (fig-S11) limiting the influence as the AOM rate is proportional to the CH_4 concentration). An indirect support to our findings regarding the secondary role of k_{AOM} .In addition, Luff and Wallmann (2003) already on the AOM itself comes from Luff and Wallmann (2003). They showed that, as long as not null, the actual value of k_{AOM} plays-only-a-secondary-role-is-unimportant for the precipitation of authigenic carbonate. Since this-the authigenic carbonate precipitation is largely driven by alkalinity produced during AOM (e.g.~~

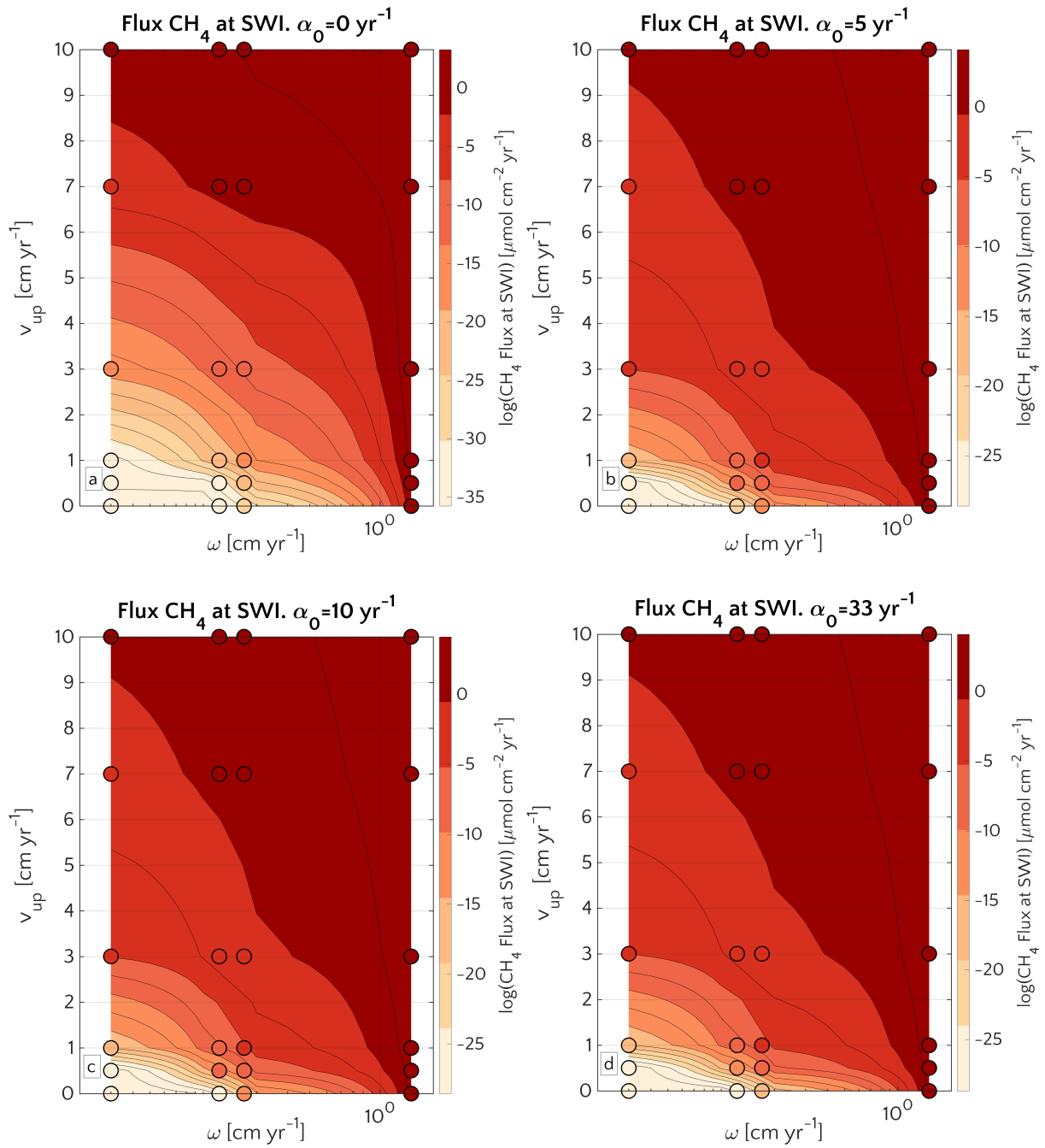


Figure 8. Efflux of methane at the SWI as dependent on v_{up} and ω for $\alpha_0 = 0 \text{ yr}^{-1}$ (a), $\alpha_0 = 5 \text{ yr}^{-1}$ (b), $\alpha_0 = 10 \text{ yr}^{-1}$ (c) and $\alpha_0 = 33 \text{ yr}^{-1}$ (d). Circles represent simulations outcomes. Results for $\alpha_0 \neq 0 \text{ yr}^{-1}$ are almost the same. The lower boundary condition for methane is $[\text{CH}_4]_- = 1.169 \text{ mM}$.

Aloisi et al. (2004); Luff et al. (2005); Karaca et al. (2010); Pierre et al. (2012); Crémière et al. (2016b, a); Meister et al. (2018)), the observed independence of precipitation rates from k_{AOM} ~~supports our findings~~ bolsters our conclusion.

3.2.7 Summary of steady state experiments

~~Succinctly, the~~ The results of the steady state sensitivity study indicate that, under environmental conditions that are broadly representative for the ESAS, low AOM efficiencies and thus high non-turbulent CH_4 effluxes from thawing subsea permafrost and/or dissociating methane gas hydrates (larger than $4 \mu\text{molCH}_4 \text{ cm}^{-2} \text{ yr}^{-1}$) are promoted by intense advective transport (sedimentation rate $\omega > 1 \text{ cm yr}^{-1}$, active fluid flow $v_{up} > 7 \text{ cm yr}^{-1}$). Under these conditions, CH_4 efflux can be further enhanced by moderate OM reactivity ($a = 10 - 10^2 \text{ yr}$) and intense non-local transport processes, such as bioirrigation (irrigation constant $\alpha_0 > 0 \text{ yr}^{-1}$). Overall, non-turbulent benthic escape of CH_4 fluxes appear from deep sources appears to be mainly controlled by the concurrent effects of ω , v_{up} and α_0 . In contrast, maximum AOM rates, k_{AOM} , exert no influence on the AOM filter efficiency.

3.2.8 Geographic pattern and potential for non-turbulent methane emissions from Laptev Sea sediments

~~The results of the model sensitivity study provide a~~ One strength of models is that they can provide the explorative means to assess dynamics at spatial/temporal scales that cannot easily be assessed by observations alone. In particular, transfer functions, simple look-up tables and neural networks that are derived from, or trained on, a large ensemble of individual model simulations over a broad range of plausible boundary conditions have been frequently and successfully used to investigate regional and even global dynamics (Gypens et al., 2008; Marquardt et al., 2010; Dale et al., 2015; Capet et al., 2016; Dale et al., 2017; Bowles et al., 2014). Such a quantitative framework in which first-order estimates of potential non-turbulent methane escape from ESAS sediments can ~~be derived. For instance, the~~ also be derived from the results of the model sensitivity study.

Model results indicate that sedimentation rate exerts the dominant control on benthic escape of methane from thawing subsea permafrost and/or dissociating methane gas hydrates on the ESAS. The functional relationship between sedimentation rate and methane flux across the SWI reported in Fig. 3.c thus allows estimating a potential non-turbulent ~~methane efflux,~~ benthic methane efflux derived from deep sources for a given sedimentation rate. Thus, if the spatial distributions of these environmental controls on methane efflux are known, a first-order geographical distribution of potential non-turbulent methane escape from the Siberian Shelf can be derived. However, the availability of observational data from the Siberian Shelf is extremely scarce. Therefore, we here focus on the Laptev Sea - a comparable well studied part of the Siberian Shelf. The Laptev Sea is well-known for its subsea permafrost and gas hydrate content and subject to large riverine inputs from the Lena river. To derive a map of sedimentation rates for Laptev Sea shelf sediments, we use published linear sedimentation rates (Table ~~S7S8~~) and extrapolate these values to the entire region by applying a simple 3D kriging method (see Fig. 9.a), using the International Bathymetric Chart of Arctic Ocean (IBCAO) (Jakobsson et al., 2012) and employing longitude, latitude and water depth as predictors for ω .

Observations indicate that sedimentation rates are highest (~~$\omega=0.45$~~ $\omega = 0.45$ cm yr^{-1}) close to the mouth of the Lena river and Moustakh Island in the Buor-Khaya Gulf. As a consequence, the vicinity of the river mouth, as well as the area

along the shallow bathymetric profile towards the NE of the Lena delta are characterized by comparably high sedimentation rates ($\omega = 0.27 - 0.42 \text{ cm yr}^{-1}$). The relatively shallow areas ($\sim 10 \sim 10 \text{ m}$ deep) around the New Siberian islands reveal intermediate values ($\omega = 0.06 - 0.12$), while minimum sedimentation rates ($\sim 0.002 - 0.03 \text{ cm yr}^{-1}$) roughly follow the ~~55~~ 55 m isobath down to the continental slope at ~~100m~~ 100 m. Deeper shelf areas are characterized by a more homogeneous distribution of sedimentation rates with values around $0.03 - 0.06 \text{ cm yr}^{-1}$.

Table 3. Estimated flux of CH_4 at SWI in mol yr^{-1} for different depth regions of Laptev Sea in a passive ($v_{up} = 0 \text{ cm yr}^{-1}$) and active ($v_{up} = 1 \text{ cm yr}^{-1}$) case.

Region (water depth, area)	v_{up}	
	0	1
0 – 10 m, $7.7 \cdot 10^4 \text{ km}^2$	6.5	$8.9 \cdot 10^5$
10 – 80 m, $4.5 \cdot 10^5 \text{ km}^2$	296.2	$8.5 \cdot 10^6$

Estimated non-turbulent methane effluxes corresponding to the highest measured sedimentation rates close to the Lena mouth do not exceed $1.57 \cdot 10^{-1} \mu\text{molCH}_4 \text{ cm}^{-2} \text{ yr}^{-1}$ assuming the presence of active fluid flow and $2.25 \cdot 10^{-5} \mu\text{molCH}_4 \text{ cm}^{-2} \text{ yr}^{-1}$ for passive settings. These findings are not surprising as steady state sensitivity results indicate that high CH_4 efflux requires sedimentation rates of $\omega > 1 \text{ cm yr}^{-1}$. The regional non-turbulent CH_4 efflux budget for different depth sections of the Laptev Sea assuming the absence of active fluid flow in Laptev Sea shelf sediments (see Table 3) thus indicates that non-turbulent CH_4 efflux is negligible. Even if we assume the omnipresence of an active fluid flow of $v_{up} = 1 \text{ cm yr}^{-1}$, the estimated non-turbulent methane efflux merely sums up to $9.39 \cdot 10^6 \text{ molCH}_4/\text{yr}$ ($\sim 0.1 \text{ GgCH}_4/\text{yr}$) over the entire Laptev Sea area of $527.4 \cdot 10^3 \text{ km}^2$. Such small effluxes would most likely be subject to further oxidation in the water column, thus limiting any potential impact on atmospheric methane concentrations and climate.

Higher advective fluid flow velocities, intermediate organic matter reactivity and/or a more intense macrobenthic biological activity could increase these estimates of non-turbulent methane escape from the Laptev Sea shelf. Higher advective fluid flow velocities (i.e. $v_{up} > 1 \text{ cm yr}^{-1}$), possibly in connection with active seepages, groundwater discharges and fault lines (the latter follow parallel pattern in Laptev Sea ~~Drachev et al. (1998)~~ (Drachev et al., 1998) on the direction SW-NE from the west of Lena delta up to the little Lyakhovsky and Kotelny island), could result in methane effluxes of up to $10 - 10^{1.3} \mu\text{molCH}_4 \text{ cm}^{-2} \text{ yr}^{-1}$ (see Fig. 6 and Fig. 8). However, such high fluid flow velocities would be only found locally and would thus merely give rise to a number of methane emission hot spots that would not change the overall non-turbulent methane flux budget. In addition, intermediate organic matter reactivity, in particular in the fast accumulating sediments close to the coastline and the Lena River Delta that receive more reactive organic matter from thawing terrestrial permafrost (Wild, 2019) could result in a higher estimated non-turbulent methane escape. However, our sensitivity study results show that OM reactivity merely plays a secondary role, suggesting that changes in OM reactivity would only change efflux by less than an order of magnitude assuming both $a = 100 \text{ yr}$ or $a = 1 \text{ yr}$. Changes in bioirrigation intensity would exert merely a limited effect on efflux estimates, as bioirrigation has already been included in the estimate calculations. ~~Additional physical reworking such as ice scouring or~~

Sedimentation rate across Laptev Sea

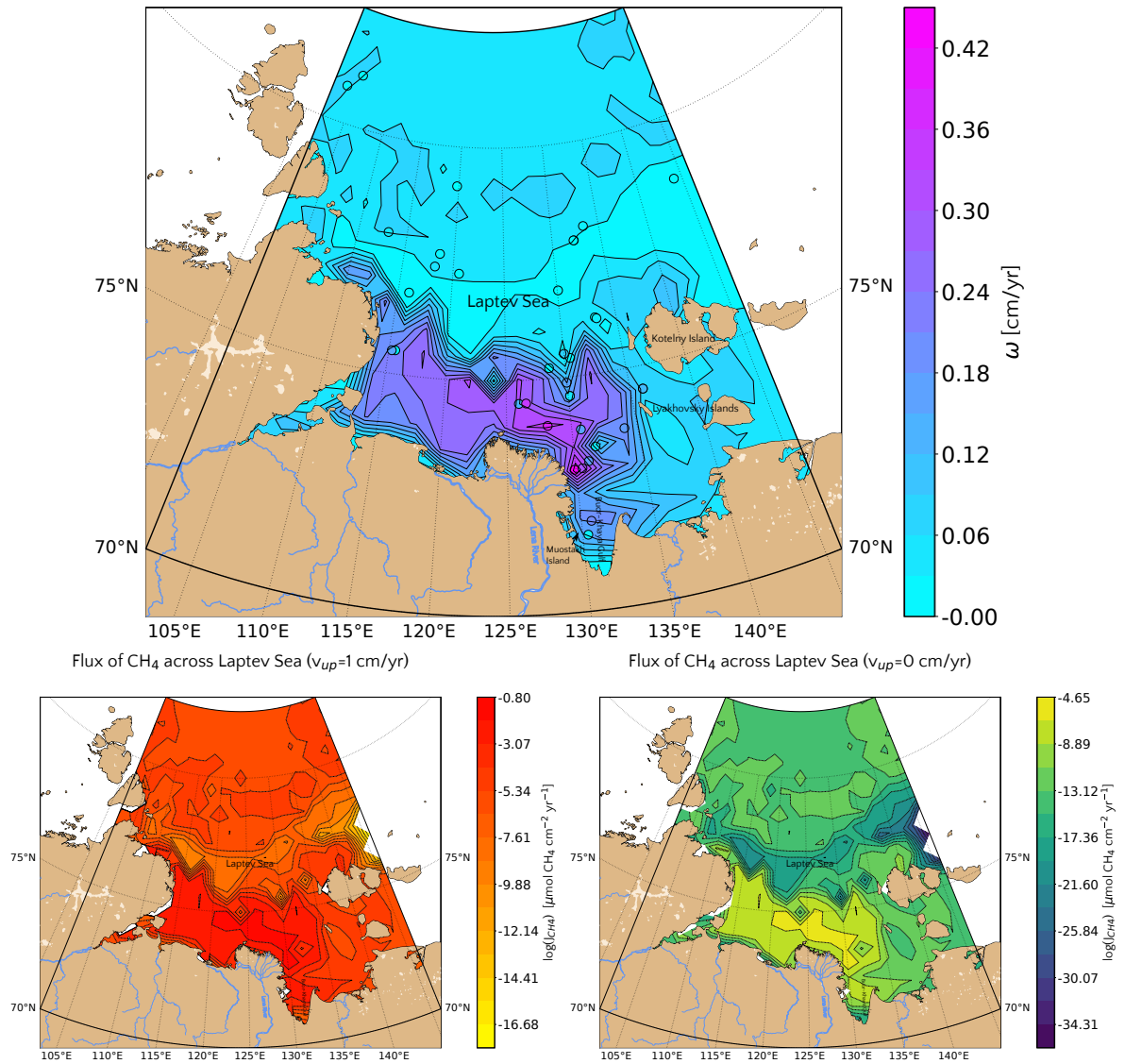


Figure 9. *a.* values of the sedimentation rate extrapolated for the whole Laptev Sea via a simple kriging method. The reference values (circles) are the ones reported in Table S7S8. *Bottom* (Log) Values of the potential methane emissions at the SWI considering the relationship presented in Fig. 3.c for passive (*b*) and active (*c*) cases.

~~dredging, or the~~ The absence of bioirrigation, which is known to be patchy in Arctic sediments ~~could even further reduce~~ estimated, could act both in the direction of further reducing (limiting the bioirrigated flux from the sediments) or increasing (by limiting the flux of TEAs from the seawater and therefore oxidation) the estimated non-turbulent methane efflux. Additional

physical reworking, such as ice scouring or dredging, may also have such an opposite effect: it could reduce the methane efflux (by enhancing the flux of TEAs into the sediments) but it could also intensify it (by removal of the upper sediment layer).

Model results thus show that, under present-day, steady state environmental conditions, AOM acts as an efficient biofilter for potential non-turbulent methane fluxes in Laptev Sea sediments. The estimated non-turbulent methane escape from Laptev Sea shelf sediments cannot support previously estimated methane outgassing fluxes of few teragrams of $\text{CH}_4 \text{ yr}^{-1}$ (Berchet et al., 2016) or even tens of teragrams of $\text{CH}_4 \text{ yr}^{-1}$ (Shakhova et al., 2014). If such outgassing were to be supported by methane efflux from Laptev Sea sediments, it would require the build-up of CH_4 gas reservoirs in Laptev Sea sediments of at least similar or larger size than the evaded amount, as well as the preferential and rapid transport of this CH_4 gas to the atmosphere. Nevertheless, model results also suggest that projected trends of terrestrial permafrost thawing and coastal permafrost degradation (Vonk et al., 2012) might increase the importance of non-turbulent methane escape for the Arctic's methane budget by potentially increasing sedimentation rates through coastal erosion and (vast amount of debris and terrigenous material) and increased riverine inputs (Guo et al., 2007); active fluid flow through permafrost and methane gas hydrate degradation (James et al., 2016; Ruppel and Kessler, 2017); organic matter reactivity through an enhanced delivery of more reactive permafrost organic matter (Wild et al., 2019) and/or an enhanced macrobenthic activity through warming and Atlantification. However, the magnitude of these projected environmental changes and thus there-their effect on non-turbulent methane escape from ESAS sediments is difficult to assess.

3.3 Methane efflux dynamics in response to seasonal and long term environmental variability

Although-The steady state sensitivity results revealed-that reveal that, under steady state conditions, AOM represents an efficient biofilter for upward migrating methane from thawing permafrost and/or dissociating methane gas hydrates on the ESAS. Yet, transient dynamics induced by, for instance, seasonal-variability, seasonally or climate change driven variability in environmental conditions, may weaken the efficiency of the AOM biofilter. Therefore, we also-additionally explore the potential for non-turbulent methane escape from thawing subsea permafrost and/or dissociating methane gas hydrate in ESAS sediments under transient conditions. Table 4 summarizes maximum-simulated, the maximum simulated non-turbulent methane escape for two seasonal fluxes for two kinds of environmental change scenarios, as well as two longterm environmental change scenarios: seasonal and long-term. With the former, we explore seasonal changes in deep methane flux and seasonal freshening of bottom waters. With the latter instead, we investigate the impacts of a slow linear increase and a sudden maximum increase in deep methane flux (see Section 2.3.2).

Interestingly, model results-Results reveal that the temporal-dynamics-of-simulated-, transient response of simulated non-turbulent methane fluxes does not depend on the specific environmental scenario (i.e. fluxes respond in a similar way to all methane forcing scenarios), but is rather controlled by the presence/absence of active fluid flow (Table 4). In passive settings, methane efflux is similar for all environmental scenarios, but instead significantly differs for passive and active sites. In general, passive settings do not allow for significant methane escape (Fig. S14). Although transient methane efflux monotonously increases to low, maximum fluxes over the simulated period, it only reaches a maximum value of 0.03-0.05 $\mu\text{molCH}_4 \text{ cm}^{-2} \text{ yr}^{-1}$. At the same time, the SMTZ (Fig. S14). Similarly, the simulated SMTZ depth merely migrates 11.5 – 29 cm upcore

Table 4. Maximum of methane fluxes (in $\mu\text{mol cm}^{-2} \text{ yr}^{-1}$) at SWI for [the 4 analyzed transient simulation scenarios](#). Values in round parenthesis indicate the year after the beginning of simulation corresponding to the reported maximum.

		[1. Seasonal CH ₄]			[2. Seasonal CH ₄ + SO ₄ ²⁻]		
		v_{up} (cm yr ⁻¹)			v_{up} (cm yr ⁻¹)		
		0	1	5	0	1	5
CH ₄ (μM)	20	0.030 (200)	0.550 (50)	12.7 (17.5)	0.059 (200)	0.772 (51)	13.7 (18)
	100	0.029 (200)	0.550 (50)	12.7 (17.5)	0.058 (200)	0.753 (51)	13.7 (18)
	330	0.030 (200)	0.552 (49.5)	12.8 (18)	0.058 (200)	0.775 (51)	13.8 (18)
	1169	0.031 (200)	0.558 (49.5)	12.9 (18)	0.059 (200)	0.783 (51)	14.0 (18)
	5455	0.034 (200)	0.577 (49)	14.0 (19)	0.062 (200)	0.832 (50)	15.2 (19)
		[3. Linear CH ₄]			[4. Sudden CH ₄]		
		v_{up} (cm yr ⁻¹)			v_{up} (cm yr ⁻¹)		
		0	1	5	0	1	5
CH ₄ (μM)	20	0.029 (200)	0.550 (50)	11.7 (20)	0.029 (200)	0.550 (50)	12.7 (18)
	100	0.030 (200)	0.550 (50)	11.7 (20)	0.030 (200)	0.552 (50)	12.7 (18)
	330	0.030 (200)	0.550 (50)	11.7 (20)	0.031 (200)	0.557 (50)	12.9 (18)
	1169	0.032 (200)	0.550 (50)	11.7 (20)	0.033 (200)	0.565 (49.5)	13.4 (18)
	5455	0.036 (200)	0.560 (50)	11.8 (20)	0.040 (200)	0.639 (47)	18.8 (23)

(Fig. S15). Over a period of the simulated 200 years, the [integrated](#) non-turbulent methane escape from passive settings [merely for all environmental change scenarios barely](#) reaches 3-4 $\mu\text{molCH}_4 \text{ cm}^{-2}$. [Even under transient environmental conditions on both seasonal and longterm scales, passive settings thus generally allow for little methane escape \(Fig.S14\).](#) Active settings, in turn, are characterised by-

- 5 [In contrast, active settings \(i.e. \$v_{up} = 1 \text{ cm yr}^{-1}\$ \) exhibit](#) an initial increase in CH₄ fluxes to maxima of 0.55-0.83 $\mu\text{molCH}_4 \text{ cm}^{-2} \text{ yr}^{-1}$ [ea. over the first 50 years into the simulation \(assuming a flow velocity of \$v_{up} = 1 \text{ cm yr}^{-1}\$ \).](#) [During this initial time period, the SMTZ rapidly shifts upcore. This growth coincides with a rapid upward shift of the SMTZ by 100 cm. While the SMTZ subsequently remains located in shallow sediment layers for the remaining simulation period, methane escape temporarily decreases. Methane escape then temporarily drops](#) by 17-20% until year 70-75, [followed by a monotonous increase](#)
- 10 [when it begins to increase again](#) until the end of the simulation [at year 200.](#) [For \$v_{up} = 1 \text{ cm yr}^{-1}\$, the temporarily. During this second phase \(i.e. after the first 50 years\), the SMTZ remains stationary. Temporally integrated methane efflux \(over 200 years\) falls within the range increases with active fluid flow rate rate from 66-121 \$\mu\text{molCH}_4 \text{ cm}^{-2}\$. For \$v_{up} = 5\$ for \$v_{up} = 1 \text{ cm yr}^{-1}\$, the integrated efflux is 10- to 14-fold larger \(i.e. to \$\sim 0.95 - 1.154 \text{ mmolCH}_4 \text{ cm}^{-2}\$ \). For \$v_{up} = 1\$ for \$v_{up} = 5 \text{ cm yr}^{-1}\$;](#)

almost 30%. A large fraction of these emissions (30% and 48-87%, respectively) occurs in the first century-100 years after the perturbation. This fraction increases to 48-87% for $v_{up} = 5 \text{ cm yr}^{-1}$.

The similarity of the CH_4 efflux dynamics in response to different environmental scenarios (*i.e.* seasonal CH_4 , seasonal $\text{CH}_4 + \text{SO}_4^{2-}$, linear CH_4 and sudden CH_4) as well as the smooth, continuous upcore movement of the SMTZ thus indicates that the Model results thus indicate that the exact temporal character of environmental changes does not exert an important influence on non-turbulent methane efflux. Conversely, both microbial growth dynamics and the presence/absence of active fluid flow (Table 4) largely control the transient response to environmental change. The reasons for this are twofold. First, the response time of the biogeochemical process network that controls CH_4 dynamics and efflux (*i.e.* biomass growth, AOM rate, methanogenesis) is slower resident AOM community is longer than the characteristic timescales of the investigated environmental variability. In addition, results show that notable methane escape from sediments in response to environmental variability on both seasonal as well as long timescales requires environmental conditions that allow for the creation of a "window of opportunity" during which the efficiency of the AOM biofilter is temporarily weakened, under investigation, thus smoothing out the impact of environmental perturbations. Second, active fluid flow enhances the impact of the perturbation by triggering a significant upcore shift of the SMTZ. In particular, the initial movement of the SMTZ prevents the establishment of an efficient AOM community at the SMTZ: this creates a "window of opportunity" for methane escape. In contrast, the comparably slow and limited movements of the SMTZ in passive settings (Fig. S15) enables the efficient establishment of an AOM community that acts as an efficient biofilter for upward migrating methane.

The following sections explore the factors that control the creation of such a window of opportunity and discusses the mechanisms behind the simulated methane escape.

3.3.1 Window of opportunity

Given the broadly similar behaviour of Given the overall similar transient response of non-turbulent methane fluxes to the range of environmental scenarios, we will focus different environmental scenarios (Fig. S14, S15), we will base the following discussion on scenario 4 (*i.e.*, namely a step-like CH_4 forcing) with $v_{up} = 1 \text{ cm yr}^{-1}$ and a specific bottom concentration (*e.g.* $[\text{CH}_4]_- = 1.169 \text{ mM}$). The reason for selecting this scenario is simple. In contrast to the other scenarios that are characterized by transient CH_4 supply from below, scenario 4 allows for a straightforward definition of the initial and final state, which allows attributing a typical system response timescale facilitates the attribution of a typical response time-scale for the system.

3.3.1 Window of opportunity

Fig. 10 illustrates the temporal evolution of the simulated (a) filter efficiency and AOM rate (a), CH_4 flux, (b) SMTZ depth CH_4 efflux, (c) and AOM biomass SMTZ depth and (d) for AOM biomass for the scenario 4 (in case of $v_{up} = 1 \text{ cm yr}^{-1}$ and $[\text{CH}_4]_- = 1.169 \text{ mM}$). During the initial. The onset of a sudden methane flux from thawing permafrost and/or dissociating methane gas hydrates below the sediment column triggers the rapid movement of the SMTZ. Simulation outputs show that velocity at which the SMTZ moves upward (v_{SMTZ}) is solely controlled by v_{up} , as evident from the constant $v_{SMTZ} \sim 2.46 \text{ cm yr}^{-1}$ for all the transient scenarios with $v_{up} = 1 \text{ cm yr}^{-1}$ (Fig. S15). The initial upwards movement of the SMTZ delays the

microbial response since the transient dynamics inhibits the establishment of a resident AOM community sufficiently large to consume upward migrating methane. The AOM rate, and thus the filter efficiency, is controlled by the AOM biomass dynamics (Eq. 8), which in turn is determined by the kinetic (F_K , eq. 9) and thermodynamic (F_T , eq. 10) constraints. Fig. 12 illustrates the depth profiles of the thermodynamic and kinetic terms in the bioenergetic AOM formulation (eq. 8), as well as their evolution in response to the onset of a sudden methane flux from below. Initially, although kinetically possible (i.e. $F_K \neq 0$), AOM is inhibited by thermodynamic constraints (i.e. $F_T = 0$). During the first 23 years, AOM biomass is constant and thus, thus remains largely constant (Fig. S18.a) and, as a consequence, AOM rate and filter efficiency are zero. In addition this period, aerobic methane oxidation represents a weak barrier as oxygen is merely present in the upper few centimetres and aerobic methane oxidation competes the only barrier to upward diffusing methane. However, this barrier is weak due to the limited availability of oxygen and the competition with aerobic organic matter degradation, as well as a number of additional secondary redox reactions that also consume oxygen (see Table S3). As a consequence, *in situ* produced, as well as externally supplied methane diffuses upward and mostly escapes, leading to an increase in CH_4 fluxes. A large fraction of this efflux increases. The initial methane efflux is produced largely supported by *in situ* since the average advective velocity of methane in the sediment ($\bar{v} = v_{up} - \omega = 0.877$ in situ methanogenesis since the advective transport of methane (occurring at $v_{up} - \omega = 0.877$ cm yr⁻¹) merely covers 20.2 cm in 24 years. It is hence, corresponding to 20.17 cm in 23 years) is too slow to allow methane from deep sources below 3 m to reach the sediment-water interface.

Transient model results thus reveal that the temporary perturbation of AOM and, thus, the creation of a “window of opportunity” for methane escape from sediments requires a significant shift of the SMTZ, which has to be rapid enough to prevent the establishment of an AOM community within the SMTZ. In the passive settings, all investigated environmental scenarios trigger a limited and comparably slow movement of the SMTZ (Fig. S15) thus allowing for the establishment of an AOM community and preventing the creation of such a window of opportunity. In contrast, active settings show a rapid and significant shift of the SMTZ in response to methane supply from below, which creates a window of opportunity for methane escape, whose onset and duration is controlled by advective velocity v_{up} of the active fluid flow and the AOM biomass growth. Assuming After the first 23 years, thermodynamic constraints ease and AOM begins to efficiently consume upward migrating methane at the SMTZ by 40% (Fig. 10.a). However, as consumption occurs at the SMTZ (for the specific case at a sediment depth of 100.4 cm), it does not immediately affect the methane efflux at the SWI. The time required for the consumption signal to propagate to the SWI with velocity $\bar{v} = v_{SMTZ} + v_{up} - \omega = 3.337$ cm yr⁻¹ is therefore $\frac{100.4 \text{ cm}}{3.337 \text{ cm yr}^{-1}} = 30.1$ yr. Consequently, methane efflux further increases. This methane efflux is now also supported from deep sources such as thawing permafrost and/or dissociating methane gas hydrates, which have started to contribute to methane efflux between years 7 and 20 (assuming typical values of v_{up} reported for active marine sediments (of 0.5-5 cm yr⁻¹), we show that methane from deep sources (ca. 3 m) reaches the sediment-water interface within 7 to 20 years. Maximum CH_4 effluxes are typically simulated. Methane efflux typically peaks 2-3 decades after the onset of methane supply. Furthermore, simulation results reveal that the maximum magnitude of methane effluxes Maximum methane efflux increases with v_{up} from 0.5-0.6: from 0.5 – 0.6 μmolCH_4 cm⁻² yr⁻¹ for $v_{up} = 1$ cm yr⁻¹ to 11 – 15 – 11 – 19 μmolCH_4 cm⁻² yr⁻¹ for $v_{up} = 5$ cm yr⁻¹. In parallel Yet, the duration of the this initial “window of opportunity” for methane escape in turn decreases with increasing v_{up} . Values of methane fluxes for

the maximum and for the new steady state fall in In general, simulated maximum methane fluxes fall within the range of other previous model results previous models applied to different environments (Sommer et al., 2006; Dale et al., 2008c) but do not reach the high values measured in other settings (Linke et al., 2005; Regnier et al., 2011).

An insight into the mechanism that drive the creation of this After the initial " window of opportunity and control non-turbulent methane efflux under these conditions can be inferred by evaluating methane migration time scales within the sediments. After the first 23 years, AOM begins to efficiently consume upward migrating methane (see Fig. 10.a) and reduces the methane flux by 40%. Because consumption occurs at SMTZ, it does not immediately affect the methane efflux through the SWI. The effect of this consumption on methane concentration first has to propagate upwards through the sediments till it reaches the SWI, resulting in a delayed efflux response to the onset of AOM. The velocity of this propagation is given by $\bar{v} = v_{SMTZ} + v_{up} - \omega$, where v_{SMTZ} denotes the velocity at which the SMTZ (where consumption happens) moves upward. From Fig. 10.c and fig. S15 we can infer that, initially, the SMTZ moves with a fairly constant velocity of about 2.46 cm yr^{-1} and, hence, $\bar{v} = 2.46 + 1 - 0.123 = 3.337 \text{ cm yr}^{-1}$. At the onset of an efficient AOM barrier (" (i.e. after $23 + 30.1 = 53.1$ years), the SMTZ is located at a sediment depth of 100.4 cm and the time required for the consumption signal to propagate to the SWI thus amounts to $\frac{100.4 \text{ cm}}{3.337 \text{ cm yr}^{-1}} = 30.1 \text{ yr}$. After this initial period of 53.1 years, effect of an efficient methane consumption at the SMTZ starts to reduce the non-turbulent methane efflux at the SWI (Fig. 10.b).

Time evolution over 200 years for the case of an active setup with $v_{up} = 1 \text{ cm yr}^{-1}$ and a step-like methane forcing from below from 0 to $[\text{CH}_4]_- = 1.169 \text{ mM}$. a. AOM vertically integrated rate (blue) and AOM efficiency (red). b. CH_4 flux at SWI. c. SMTZ depth. d. Vertically integrated biomass (number of cells).

Simulations show that v_{SMTZ} is solely controlled by v_{up} and does not depend on additional environmental conditions, as revealed by the constant velocity with which the SMTZ moves upwards ($\sim 11.4 \text{ cm yr}^{-1}$). This indicates that the methane efflux is initially controlled by the velocity of the SMTZ movement, which is in turn is determined by the upward velocity v_{up} . The reduction in methane efflux after the onset an efficient AOM barrier This reduction lasts until the upward movement of the SMTZ slows down. At this point, the AOM filter efficiency reaches a quasi-stationary level of $\sim 85\%$ (as Fig. 10.a). Meanwhile, in-situ methane production in situ methanogenesis continues to produce methane, which is not entirely consumed by the AOM community that already reached its full capacity. As a consequence, methane fluxes at SWI increase again and until a new steady state is reached. This simulated pattern arises even more clearly in simulations with $v_{up} = 5 \text{ cm yr}^{-1}$ (see Fig.

3.3.2 Final new steady state

The final new steady state value of methane efflux (Fig. 10.b, S14 and S16) . Here, the onset of a new steady state occurs earlier and AOM suppresses the non-turbulent methane efflux to the value of about 7 is generally in good agreement with Dale et al. (2008c), who reported an efflux of the same order of magnitude ($3 \mu\text{molCH}_4 \text{ cm}^{-2} \text{ yr}^{-1}$) (Fig. S16). The comparison of such value with simulated steady state efflux under identical environmental conditions (i. e.) for the new steady state at the end of a transient run with $v_{up} = 10 \text{ cm yr}^{-1}$ and $[\text{CH}_4]_- = 70 \text{ mM}$. Simulations with $v_{up} = 5 \text{ cm yr}^{-1}$, $\omega = 0.123 \text{ cm yr}^{-1}$ and $[\text{CH}_4]_- = 1.169 \text{ mM}$; inferred from Fig. 8) indicates that the final steady state flux observed in transient simulations

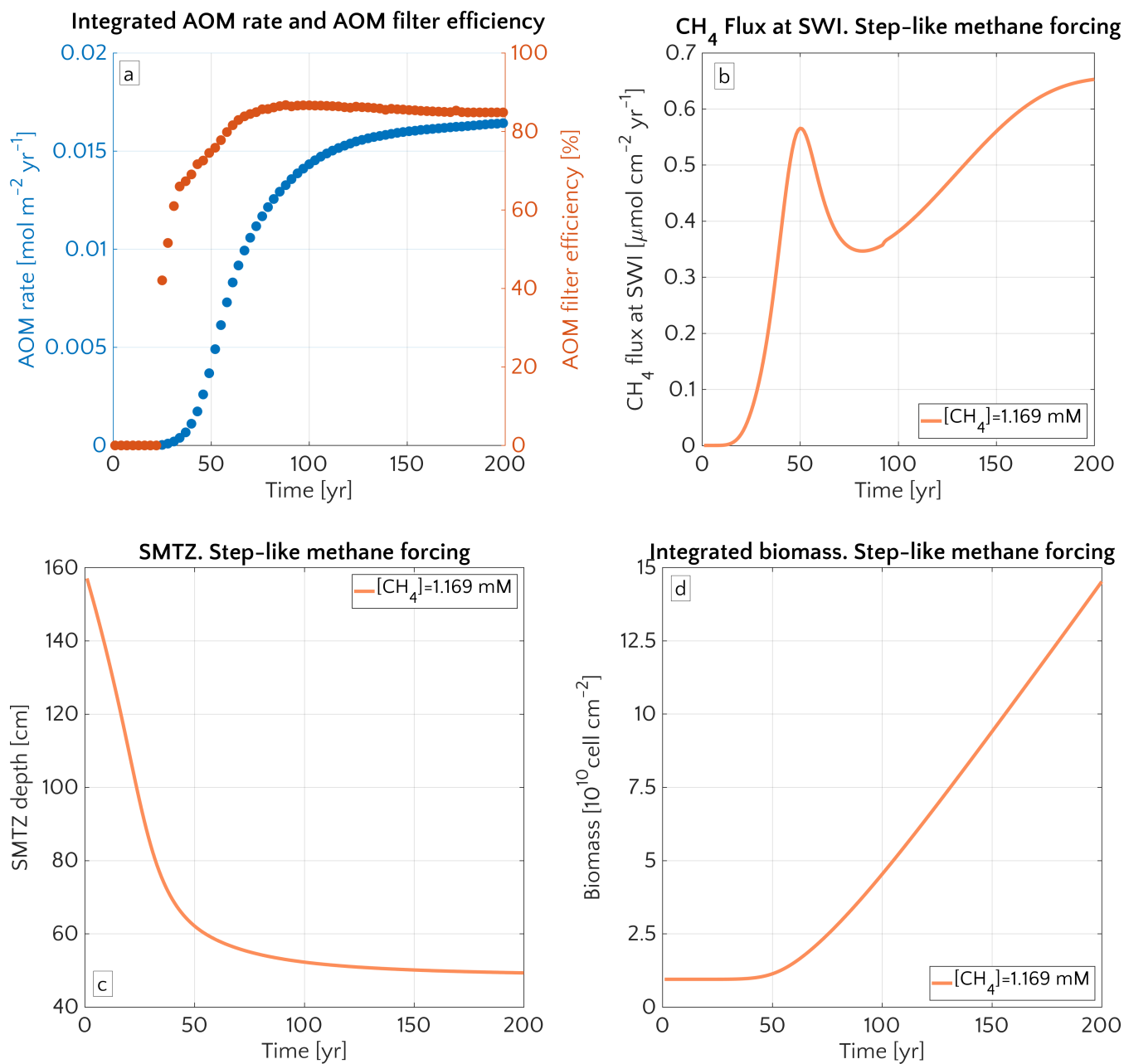


Figure 10. Time evolution over 200 years for the case of an active setup with $v_{vp} = 1 \text{ cm yr}^{-1}$ and a step-like methane forcing from below from 0 to $[\text{CH}_4]_+ = 1.169 \text{ mM}$. *a.* AOM vertically integrated rate (blue) and AOM efficiency (red). *b.* CH_4 flux at SWI. *c.* SMTZ depth. *d.* Vertically integrated biomass (number of cells).

(bioenergetic AOM formulation) is roughly two orders (Fig. S16) offer a better understanding of the model. In this case, the final new steady state is about two orders of magnitude larger than the flux-efflux of $\sim 0.1 \mu\text{molCH}_4 \text{ cm}^{-2} \text{ yr}^{-1}$ simulated

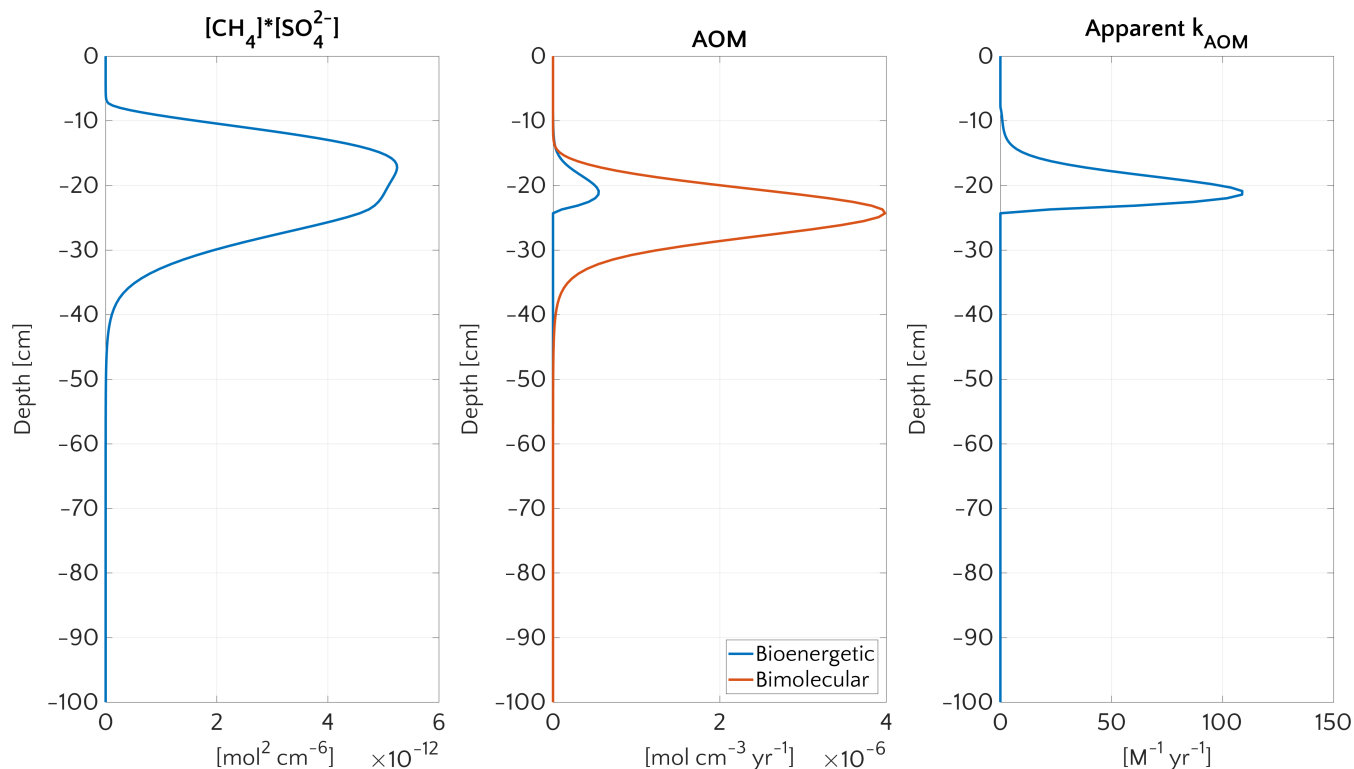


Figure 11. Vertical profiles at the end of transient simulation (after 200 years) with bioenergetic AOM fomulation for the case $[\text{CH}_4]_- = 1.169 \text{ mM}$ and $v_{up} = 5 \text{ cm yr}^{-1}$. *a.* Bimolecular product $[\text{CH}_4] \cdot [\text{SO}_4^{2-}]$. *b.* AOM rate according to the bioenergetic fomulation (blue) and, for comparison, according to bimolecular fomulation used for the steady-state simulations (red). *c.* Apparent k_{AOM} , estimated from eq. 7.

with a in the steady state simulations, with bimolecular rate law. These findings are in agreement with Dale et al. (2008e), who reported a new steady state efflux of similar magnitude ($3 \mu\text{molCH}_4 \text{ cm}^{-2} \text{ yr}^{-1}$) for $v_{up} = 10 \text{ cm yr}^{-1}$ and $[\text{CH}_4]_- = 70 \text{ mM}$. They also show that CH_4 efflux simulated with a bimolecular AOM rate law can vary from being higher to much smaller than the one estimated in the bioenergetic approach, depending on the value of k_{AOM} , under identical environmental conditions (inferred from Fig. 8).

Such a conclusion might sound in disagreement with what we showed in section 3.2.6, where we deflated the role of k_{AOM} . The reason for this discrepancy can be clarified by plotting the apparent k_{AOM} , but it has to be put into perspective. Firstly it is indeed expected that, also with the bimolecular AOM implementation, CH_4 flux increases if the k_{AOM} is increased. Such a value is calculated by computing an apparent bimolecular rate constant k_{AOM} were further reduced down, and it could not be otherwise, considered that it controls the AOM rate. But the employment of values for k_{AOM} smaller than the ones we explored is not supported by any other previous study and would have then therefore rather arbitrary. Finally some light should be shed on why the bimolecular and the bioenergetic AOM fomulation give such different methane effluxes, under the

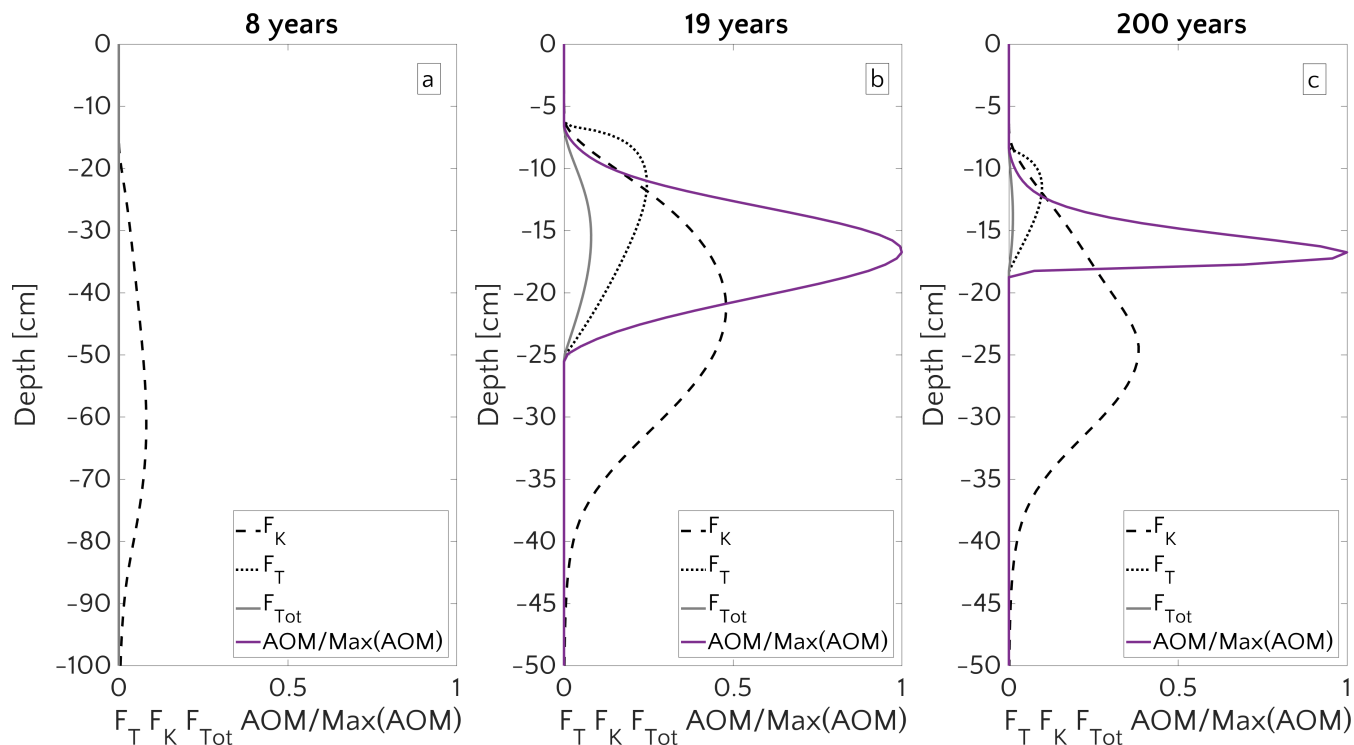


Figure 12. Vertical profile of F_T , F_K , $F_{Tot} = F_K \cdot F_T$ and the AOM (scaled to the maximum) for three instant in times. 8 years (a), 19 years (b) and 200 years (c) of simulation, for the case $[\text{CH}_4]_- = 1.169 \text{ mM}$ and $v_{up} = 5 \text{ cm yr}^{-1}$.

same conditions. Vertical profiles at the end of transient simulation (after 200 years) with bioenergetic AOM formulation for the case $[\text{CH}_4]_- = 1.169 \text{ mM}$ and $v_{up} = 5 \text{ cm yr}^{-1}$. a. Bimolecular product $[\text{CH}_4] \cdot [\text{SO}_4^{2-}]$. b. AOM rate. c. Apparent k_{AOM} , estimated from eq. 7. For this purpose we assessed an apparent k_{AOM} , i.e. what k_{AOM} would look like if we wanted to describe AOM rate we find at the end of the transient simulation by means of the bimolecular description of eq. 7. (as in eq. 7) from the transient bioenergetic simulations for the new final steady state. Results are shown in Fig. 11. Panel 11.a shows the the illustrates that the concentration product $[\text{CH}_4] \cdot [\text{SO}_4^{2-}]$ is broader wider than the AOM rate profile (panel 11.b), which results then being is strongly limited by the thermodynamic constraint, blue curve). Fig. 11.c also shows that the apparent k_{AOM} is not constant and never exceeds uniform: it reaches a maximum value of $109 \text{ M}^{-1} \text{ yr}^{-1}$, being for the most of the depths but remains well below $100 \text{ M}^{-1} \text{ yr}^{-1}$. It confirms that AOM resulting from bioenergetic formulation cannot be trivially described by a simple bimolecular expression of the rate with a constant value. This, combined to the low values of apparent k_{AOM} , gives reason of the difference in steady-state CH_4 effluxes.

The onset of an efficient AOM biofilter requires the establishment of an AOM community that is sufficiently large to consume upward migrating methane. Therefore, the onset of AOM and, consequently, the efficiency of the AOM filter are controlled by AOM biomass dynamics, which in turn are determined by kinetic and thermodynamic constraints. Fig. 12 illustrates the depth profiles of the thermodynamical and kinetic terms in the bioenergetic AOM formulation (eq. 8), as well as their evolution

in response to the onset of a sudden methane flux from below. Initially, although kinetically possible (i.e. $F_K \neq 0$, eq. 9), AOM is inhibited by thermodynamic constraints (i.e. $F_T = 0$, eq. 10). These thermodynamic constraints ease when the SMTZ becomes stationary after the initial decades. At that point, favourable conditions are encountered over a depth of about 20 cm (for methane scenario 4 and $v_{up} = 5 \text{ cm yr}^{-1}$ at most depths. Compared to the values typically applied for bimolecular rate laws (i.e. $k_{AOM} = 10^2 - 10^7 \text{ M}^{-1}$) and the increasing AOM filter efficiency reduces methane efflux (yr^{-1}), these values are rather low and reflect the ongoing thermodynamic limitation of AOM. F_T remains the main constraint on AOM throughout the simulation (Fig. 12.b). After 200 years (Fig. 12.c), a more uniform sulfide concentration in lower sediments together with the upward movement of the SMTZ pushes the maximum of F_T upwards, thus limiting the zone where AOM is thermodynamically favourable ($\sim 13 \text{ cm}$ deep). F_T remains the main constraint on AOM throughout the simulation.

Vertical profile of F_T , F_K , $F_{Tot} = F_K - F_T$ and the AOM (scaled to the maximum) for three instant in times: 8 years (a), 19 years (b) and 200 years (c) of simulation, for the case $[\text{CH}_4]_- = 1.169 \text{ mM}$ and $v_{up} = 5 \text{ cm yr}^{-1}$.

Integrated biomass ΣB ranges from $\sim 1.2 \cdot 10^{10}$ to $3.5 \cdot 10^{11} \text{ cells cm}^{-2}$ (except for simulation with $v_{up} = 5 \text{ cm yr}^{-1}$ and $[\text{CH}_4]_- = 5.455 \text{ mM}$, whose $\Sigma B = 1.2 \cdot 10^{12}$). These values are comparable with AOM biomass reported in Treude et al. (2003) ($1.5 - 1.8 \cdot 10^{10} \text{ cells cm}^{-2}$) or with values simulated in Dale et al. (2008c) ($3.7 \cdot 10^{11} \text{ cells cm}^{-2}$ for $v_{up} = 5 \text{ cm yr}^{-1}$). In addition, the maximum simulated biomass for active settings of ($0.5 - 2.5 \cdot 10^{10} \text{ cells cm}^{-3}$) agrees well with previously reported values, ranging from 0.27 to $7.4 \cdot 10^{10} \text{ cells cm}^{-3}$ (Dale et al., 2008c). However, integrated AOM rates, Integrated AOM rates (ΣAOM_r) are instead smaller than previously published rates for shallow, active sites above the shelf break (Boetius et al., 2000; Haese et al., 2003; Luff and Wallmann, 2003; Linke et al., 2005; Wallmann et al., 2006b; Dale et al., 2008c), but comparable to those observed in active sites below the shelf break (Aloisi et al., 2004; Wallmann et al., 2006a; Maher et al., 2006) or in passive settings (Borowski et al., 1996; Martens et al., 1998; Fossing et al., 2000; Jørgensen et al., 2001; Dale et al., 2008c). The discrepancy is likely may be due to different environmental conditions encountered at these sites. For instance, Dale et al. (2008c) applied an advective velocity of $v_{up} = 10 \text{ cm yr}^{-1}$ and $[\text{CH}_4]_- = 60 \text{ mM}$). While differences in v_{up} affect the ΣAOM , its effect on ΣB is negligible since an efficient AOM microbial filter is known has to account for at least $> 10^{10} \text{ cells cm}^{-3}$ (Lösekann et al., 2007; Knittel and Boetius, 2009).

Simulation results finally show that AOM biomass and, thus, AOM rate increase with an increase in methane supply from below (Fig. S17). The ratio between the flux of methane at the SWI and the advective methane flux at the bottom of the sediment column reflects this behaviour. It decrease from values > 1 to values < 1 with an increase in methane from below (Fig. S18.b). This does not only mean that *in situ* methanogenesis rather than methane supply from below drives methane efflux for low methane supply scenarios, but also that the influence of methanogenesis on efflux decreases with an increase in methane supply. This shift is accompanied by a shift in the a diffusion-driven to a advection-driven influx (not shown). In addition, although absolute methane efflux is higher for higher $[\text{CH}_4]_-$, the smaller values of the efflux/influx ratio show that the system becomes much more efficient in removing methane when it is forced with a higher methane flux. Simulation results show that the AOM biofilter efficiency increases by 17% (49% in passive settings) over the increase of $[\text{CH}_4]_-$ from 20 μM to 5.455 mM in agreement with observations (Treude et al., 2003; de Beer et al., 2006; Niemann et al., 2006a). However,

although AOM becomes more efficient, it cannot keep up with increasing fluxes, indicating that the inability of the AOM biomass to completely consume higher CH_4 flux does not exclusively depend on the presence of methane bubbles, as previously stated (James et al., 2016).

4 Conclusions

5 In this study, we evaluate the potential for non-turbulent, benthic methane escape from thawing subsea permafrost and/or dissociating methane gas hydrates in both passive as well as active settings and under a range of environmental conditions that are broadly representative for conditions encountered on the present and future East Siberian Arctic Shelf (ESAS) sediments that are affected by deep methane supply from, for instance, thawing subsea permafrost or methane gas hydrate dissociation. We identify the most important biogeochemical and physical controls on non-turbulent methane escape from those sediments under
10 steady state conditions, as well as in response to environmental variability on seasonal and centennial timescales. Finally Based on model results, we derive a first-simple transfer function that allows establishing a first-order regional estimate of (non-turbulent) methane benthic-pelagic flux-efflux and of potential methane consumption in the Laptev-Sea-Laptev Sea sediments.

Model results reveal that AOM is an efficient sink for upward migrating, dissolved methane in ESAS sediments. Simulated non-turbulent methane effluxes are negligible for a broad range of environmental conditions under both steady state and tran-
15 sient conditions. On the ESAS, Since AOM is a transport-limited process and transport parameters thus exert an important, transport parameters exert a dominant control on the efficiency of the AOM biofilter and, thus, on methane efflux ultimately, on the methane efflux at the SWI. Both steady state and transient model results confirm the key role of advective transport (mainly sedimentation and active fluid flow) in supporting methane escape from Arctic shelf sediments. Under steady state conditions, high methane effluxes (up to $27.5 \mu\text{mol cm}^{-2} \text{yr}^{-1}$) are generally found for sediments that are characterized by
20 high sedimentation rates and/or active fluid flow (sedimentation rate $\omega > 0.7 \text{ cm yr}^{-1}$, active fluid flow $v_{up} > 6 \text{ cm yr}^{-1}$). Under these conditions, methane efflux can be further enhanced by intermediate organic matter reactivity (RCM model parameter $a = 10 - 10^2 \text{ yr}$) and even though the control exerted by organic matter is only secondary with respect to the transport parameters. Finally intense local transport processes, such as bioirrigation (irrigation constant $\alpha_0 > 1 \text{ yr}^{-1}$), do also contribute to larger methane effluxes. Our results indicate therefore that present methane efflux from ESAS sediments can be supported
25 by methane gas escape and non-turbulent CH_4 efflux from rapidly accumulating and/or active sediments (*e.g.* coastal settings, portions close to river mouths or submarine slumps). In particular, active sites sediments may release methane in response to the onset or increase of permafrost thawing or CH_4 gas hydrate destabilization.

High methane escape (up to $11\text{-}19 \mu\text{molCH}_4 \text{ cm}^{-2} \text{ yr}^{-1}$ corresponding to $2.6\text{-}4.5 \text{ TgCH}_4 \text{ yr}^{-1}$ if upscaled to the ESAS) can occur during a transient period following the onset of methane flux from the deep sediments. Under these conditions,
30 substantial methane escape from sediments requires the presence of active fluid flow that supports a significant and rapid upward migration of the SMTZ in response to the onset of CH_4 flux from below. Such rapid and pronounced movements create a window of opportunity for non-turbulent methane escape by inhibiting the accumulation of AOM-performing biomass within the SMTZ - mainly through thermodynamic constraints - thereby perturbing the efficiency of the AOM biofilter. The

magnitude of methane effluxes, as well as the duration of this window of opportunity, is largely controlled by the active flow velocity. In addition, results of transient scenario runs indicated that the characteristic response time of the AOM biofilter is of the order of few decades (20-30 years), thus exceeding seasonal-interannual variability. Consequently, seasonal variation of bottom methane and sea water sulfates exert a negligible effect on methane escape through the sediment-water interface.

5 AOM generally acts as an efficient biofilter for upward migrating CH_4 under environmental conditions that are representative for the present-day ESAS with potentially important, yet unquantified implications for the Arctic ocean's alkalinity budget and, thus, CO_2 fluxes. Our results thus suggest that previously published fluxes estimated from ESAS waters to atmosphere cannot be supported by non-turbulent methane efflux alone.

A regional upscaling of non-turbulent methane efflux for the Laptev Sea Shelf using a model-derived transfer function
 10 that relates sedimentation rate and methane efflux merely sums up to $\sim 0.1 \text{ GgCH}_4 \text{ yr}^{-1}$. Nevertheless, it also suggests that the evaluation of methane efflux from Siberian Shelf sediments should pay particular attention to the dynamic and rapidly changing Arctic coastal areas close to big river mouths, as well as areas that may favor preferential methane gas release (*e.g.* rapidly eroding coastlines, fault lines or shallow sea floors, *i.e.* $<30 \text{ m}$). In addition, our findings call for more data concerning sedimentation and active fluid flow rates, as well as the reactivity of depositing organic matter and bioirrigation rates in Arctic
 15 shelf sediments.

In conclusion, we argue that the evaluation of projected subsea permafrost thaw and/or hydrate destabilization impacts on the Arctic environment requires models that include an explicit description of 1) methane gas, 2) AOM biomass, as well as 3) the entire network of the most pertinent biogeochemical reactions. Such approaches, valid globally for all the shelves underlain by methane reservoirs (*e.g.* continental slopes), are even more recommended in order to enable a robust quantification of methane
 20 escape from the Arctic shelf to the Arctic ocean, settings even more sensible to the rapidly changing environmental conditions. Finally such refined modeling will also help evaluate the impact of subsea permafrost thaw and methane destabilization on Arctic alkalinity and biogeochemical cycling.

Code and data availability. Primary data needed to reproduce the analyses presented in this study are archived by the MaxPlanck Institute for Meteorology are available upon request (publications@mpimet.mpg.de)

25 **Appendix A: AOM efficiency η**

If we identify the SMTZ region as the portion of the sediment column where the rate of AOM is 1% of the maximum, we can define the efficiency of the AOM filter η as

$$\eta(\%) = \left(1 - \frac{J_{\text{CH}_4}^+}{J_{\text{CH}_4}^-} \right) \cdot 100 \quad (\text{A1})$$

where $J_{\text{CH}_4}^+$ is the methane flux at the shallowest point where the AOM rate is 1% of the maximum (upper dashed line in Fig. A1), and $J_{\text{CH}_4}^-$ is methane flux at the deepest point where the AOM rate is 1% of the maximum (lower dashed line in Fig. A1).
 30

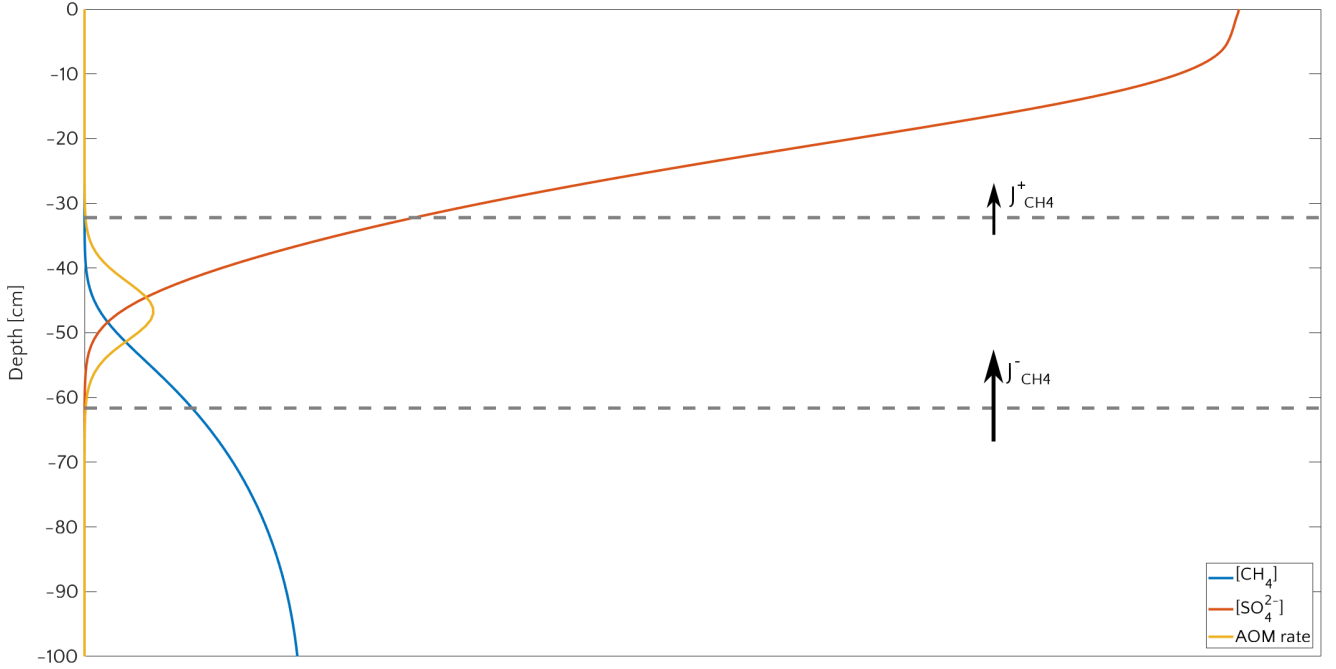


Figure A1. Typical sediment profile of $[\text{SO}_4^{2-}]$, $[\text{CH}_4]$ and AOM rate. Units are mM for concentration and mM yr^{-1} for rate. The region between the two dashed lines represents the zone where AOM rate is larger than 1% of its maximum and defines the Sulfate Methane Transition Zone (SMTZ). The fluxes $J_{\text{CH}_4}^-$ and $J_{\text{CH}_4}^+$ are the fluxes used in the definition of η of eq. (A1).

Appendix B: Damköhler number

The Damköhler number D_a is a dimensionless quantity which relates time scales typical of transport processes to time scales typical of chemical reactions. It compares the consumption/production rate with the advective transport and is defined as

$$D_a = \tau_T / \tau_R \quad (\text{B1})$$

- 5 where τ_T is the advective timescale and τ_R is the reaction timescale. τ_R is defined as $1/K_R$ where K_R is the reaction rate of AOM or methanogenesis. If we call R the reaction rate then K_R reads:

$$K_R = \frac{1}{\mathcal{L}} \int_{\mathcal{L}} \frac{R}{[\text{CH}_4]} dz \quad (\text{B2})$$

where \mathcal{L} is the width where the reaction rate is larger than 1% of the maximum rate. τ_T is instead defined as

$$\tau_T = \frac{\mathcal{L}}{|v_{up} - \omega|} \quad (\text{B3})$$

- 10 where $v_{up} - \omega$ is the effective advective velocity. D_a can be expressed by:

$$D_a = \frac{\tau_T}{\tau_R} = \frac{1}{|v_{up} - \omega|} \int_{\mathcal{L}} \frac{R}{[\text{CH}_4]} dz. \quad (\text{B4})$$

Competing interests. All contributing authors declare that no competing interests are present.

Acknowledgements. [We would like to thank Prof. Volker Brüchert \(Department of Geological Sciences at Stockholm University and Bolin Centre for Climate Research\) for his constructive criticism during the reviewing process and for having shared the data of Laptev Sea sediment cores.](#) The research leading to these results has received funding from the European Union's Horizon 2020 research and innovation programme under the Marie Skłodowska-Curie grant agreement No 643052 (C-CASCADES project).

References

- Aguilera, D., Jourabchi, P., Spiteri, C., and Regnier, P.: A knowledge-based reactive transport approach for the simulation of biogeochemical dynamics in Earth systems, *Geochemistry, Geophysics, Geosystems*, 6, 2005.
- Albert, D. B., Martens, C. S., and Alperin, M. J.: Biogeochemical processes controlling methane in gassy coastal sediments—part 2: Ground-
5 water flow control of acoustic turbidity in Eckernförde Bay Sediments, *Continental Shelf Research*, 18, 1771–1793, 1998.
- Aloisi, G., Wallmann, K., Haese, R., and Saliege, J.-F.: Chemical, biological and hydrological controls on the ^{14}C content of cold seep carbonate crusts: numerical modeling and implications for convection at cold seeps, *Chemical Geology*, 213, 359–383, 2004.
- Aris, R.: Prolegomena to the rational analysis of systems of chemical reactions II. Some addenda, *Archive for Rational Mechanics and Analysis*, 27, 356–364, 1968.
- 10 Arndt, S., Jørgensen, B. B., LaRowe, D. E., Middelburg, J., Pancost, R., and Regnier, P.: Quantifying the degradation of organic matter in marine sediments: a review and synthesis, *Earth-science reviews*, 123, 53–86, 2013.
- Athy, L. F.: Density, porosity, and compaction of sedimentary rocks, *AAPG Bulletin*, 14, 1–24, 1930.
- Baker, G. and Osterkamp, T.: Implications of salt fingering processes for salt movement in thawed coarse-grained subsea permafrost, *Cold regions science and technology*, 15, 45–52, 1988.
- 15 Barton, B. I., Lenn, Y.-D., and Lique, C.: Observed Atlantification of the Barents Sea causes the Polar Front to limit the expansion of winter sea ice, *Journal of Physical Oceanography*, 48, 1849–1866, 2018.
- Bauch, H. A., Mueller-Lupp, T., Taldenkova, E., Spielhagen, R. F., Kassens, H., Grootes, P. M., Thiede, J., Heinemeier, J., and Petryashov, V.: Chronology of the Holocene transgression at the North Siberian margin, *Global and Planetary Change*, 31, 125–139, 2001.
- Bekryaev, R. V., Polyakov, I. V., and Alexeev, V. A.: Role of polar amplification in long-term surface air temperature variations and modern
20 Arctic warming, *Journal of Climate*, 23, 3888–3906, 2010.
- Berchet, A., Bousquet, P., Pison, I., Locatelli, R., Chevallier, F., Paris, J.-D., Dlugokencky, E. J., Laurila, T., Hatakka, J., Viisanen, Y., et al.: Atmospheric constraints on the methane emissions from the East Siberian Shelf, *Atmospheric Chemistry and Physics*, 16, 4147–4157, 2016.
- Berner, R. A.: *Early diagenesis: a theoretical approach*, 1, Princeton University Press, 1980.
- 25 Biastoch, A., Treude, T., Rüpke, L. H., Riebesell, U., Roth, C., Burwicz, E. B., Park, W., Latif, M., Böning, C. W., Madec, G., et al.: Rising Arctic Ocean temperatures cause gas hydrate destabilization and ocean acidification, *Geophysical Research Letters*, 38, 2011.
- Boetius, A., Ravenschlag, K., Schubert, C. J., Rickert, D., Widdel, F., Gieseke, A., Amann, R., Jørgensen, B. B., Witte, U., and Pfannkuche, O.: A marine microbial consortium apparently mediating anaerobic oxidation of methane, *Nature*, 407, 623, 2000.
- Bolshiyarov, D., Makarov, A., and Savelieva, L.: Lena River delta formation during the Holocene, *Biogeosciences*, 12, 579–593, 2015.
- 30 Borges, A. and Abril, G.: 5.04-Carbon dioxide and methane dynamics in estuaries, *Treatise on Estuarine and Coastal Science, Volume 5: Biogeochemistry*, pp. 119–161, 2011.
- Borowski, W. S., Paull, C. K., and Ussler III, W.: Marine pore-water sulfate profiles indicate in situ methane flux from underlying gas hydrate, *Geology*, 24, 655–658, 1996.
- Boudreau, B. P.: Mathematics of tracer mixing in sediments: I. Spatially-dependent, diffusive mixing, *Am. J. Sci.*, 286, 161–198, 1986.
- 35 Boudreau, B. P.: *Diagenetic models and their implementation*, vol. 505, Springer Berlin, 1997.
- Boudreau, B. P.: Boudreau, Bernard P. "The physics of bubbles in surficial, soft, cohesive sediments, *Marine and Petroleum Geology*, 38, 1–18, 2012.

- Boudreau, B. P. and Ruddick, B. R.: On a reactive continuum representation of organic matter diagenesis, *American Journal of Science*, 291, 507–538, 1991.
- Boudreau, B. P., Algar, C., Johnson, B. D., Croudace, I., Reed, A., Furukawa, Y., Dorgan, K. M., Jumars, P. A., Grader, A. S., and Gardiner, B. S.: Bubble growth and rise in soft sediments, *Geology*, 33, 517–520, 2005.
- 5 Bowles, M. W., Mogollón, J. M., Kasten, S., Zabel, M., and Hinrichs, K.-U.: Global rates of marine sulfate reduction and implications for sub-sea-floor metabolic activities, *Science*, 344, 889–891, 2014.
- Bröder, L., Tesi, T., Andersson, A., Eglinton, T. I., Semiletov, I. P., Dudarev, O. V., Roos, P., and Gustafsson, Ö.: Historical records of organic matter supply and degradation status in the East Siberian Sea, *Organic Geochemistry*, 91, 16–30, 2016.
- Bruce, E. R. and Perry, L. M.: *Environmental biotechnology: principles and applications*, New York: McGrawHill, 400, 2001.
- 10 Brüchert, V.: Unpublished raw data, 2020.
- Brüchert, V., Bröder, L., Sawicka, J. E., Tesi, T., Joye, S. P., Sun, X., Semiletov, I. P., and Samarkin, V. A.: Carbon mineralization in Laptev and East Siberian sea shelf and slope sediment, *Biogeosciences*, 15, 471–490, 2018.
- Burwicz, E. B., Rüpke, L., and Wallmann, K.: Estimation of the global amount of submarine gas hydrates formed via microbial methane formation based on numerical reaction-transport modeling and a novel parameterization of Holocene sedimentation, *Geochimica et Cos-*
- 15 *mochimica Acta*, 75, 4562–4576, 2011.
- Capet, A., Meysman, F. J., Akoumianaki, I., Soetaert, K., and Grégoire, M.: Integrating sediment biogeochemistry into 3D oceanic models: a study of benthic-pelagic coupling in the Black Sea, *Ocean Modelling*, 101, 83–100, 2016.
- Carmack, E. C., Macdonald, R. W., Perkin, R. G., McLaughlin, F. A., and Pearson, R. J.: Evidence for warming of Atlantic water in the southern Canadian Basin of the Arctic Ocean: Results from the Larsen-93 expedition, *Geophysical Research Letters*, 22, 1061–1064,
- 20 1995.
- Centler, F., Shao, H., De Biase, C., Park, C.-H., Regnier, P., Kolditz, O., and Thullner, M.: GeoSysBRNS—A flexible multidimensional reactive transport model for simulating biogeochemical subsurface processes, *Computers & Geosciences*, 36, 397–405, 2010.
- Charkin, A. N., Rutgers van der Loeff, M., Shakhova, N. E., Gustafsson, Ö., Dudarev, O. V., Cherepnev, M. S., Salyuk, A. N., Koshurnikov, A. V., Spivak, E. A., Gunar, A. Y., et al.: Discovery and characterization of submarine groundwater discharge in the Siberian Arctic seas: a case study in the Buor-Khaya Gulf, Laptev Sea, *The Cryosphere*, 11, 2305–2327, 2017.
- 25 Chatterjee, S., Dickens, G. R., Bhatnagar, G., Chapman, W. G., Dugan, B., Snyder, G. T., and Hirasaki, G. J.: Pore water sulfate, alkalinity, and carbon isotope profiles in shallow sediment above marine gas hydrate systems: A numerical modeling perspective, *Journal of Geophysical Research: Solid Earth*, 116, 2011.
- Christensen, J., Krishna Kumar, K., Aldrian, E., An, S., Cavalcanti, I., de Castro, M., Dong, W., Goswami, A., Hall, A., Kanyanga, J., et al.: Climate change 2013: the physical scientific basis, Contribution of Working Group I to the Fifth Assessment Report of the Intergovernmental Panel on Climate Change, 2013.
- 30 Clough, L. M., Ambrose Jr, W. G., Cochran, J. K., Barnes, C., Renaud, P. E., and Aller, R. C.: Infaunal density, biomass and bioturbation in the sediments of the Arctic Ocean, *Deep Sea Research Part II: Topical Studies in Oceanography*, 44, 1683–1704, 1997.
- Cordes, E. E., Arthur, M. A., Shea, K., Arvidson, R. S., and Fisher, C. R.: Modeling the mutualistic interactions between tubeworms and microbial consortia, *PLoS Biology*, 3, e77, 2005.
- 35 Crémière, A., Lepland, A., Chand, S., Sahy, D., Condon, D. J., Noble, S. R., Martma, T., Thorsnes, T., Sauer, S., and Brunstad, H.: Timescales of methane seepage on the Norwegian margin following collapse of the Scandinavian Ice Sheet, *Nature communications*, 7, 11 509, 2016a.

- Crémière, A., Lepland, A., Chand, S., Sahy, D., Kirsimäe, K., Bau, M., Whitehouse, M. J., Noble, S. R., Martma, T., Thorsnes, T., et al.: Fluid source and methane-related diagenetic processes recorded in cold seep carbonates from the Alvheim channel, central North Sea, *Chemical Geology*, 432, 16–33, 2016b.
- 5 Dale, A. W., Regnier, P., and Van Cappellen, P.: Bioenergetic controls on anaerobic oxidation of methane (AOM) in coastal marine sediments: a theoretical analysis, *American Journal of Science*, 306, 246–294, 2006.
- Dale, A. W., Aguilera, D., Regnier, P., Fossing, H., Knab, N., and Jørgensen, B. B.: Seasonal dynamics of the depth and rate of anaerobic oxidation of methane in Aarhus Bay (Denmark) sediments, *Journal of Marine Research*, 66, 127–155, 2008a.
- Dale, A. W., Regnier, P., Knab, N., Jørgensen, B. B., and Van Cappellen, P.: Anaerobic oxidation of methane (AOM) in marine sediments from the Skagerrak (Denmark): II. Reaction-transport modeling, *Geochimica et Cosmochimica Acta*, 72, 2880–2894, 2008b.
- 10 Dale, A. W., Van Cappellen, P., Aguilera, D., and Regnier, P.: Methane efflux from marine sediments in passive and active margins: Estimations from bioenergetic reaction–transport simulations, *Earth and Planetary Science Letters*, 265, 329–344, 2008c.
- Dale, A. W., Brüchert, V., Alperin, M., and Regnier, P.: An integrated sulfur isotope model for Namibian shelf sediments, *Geochimica et Cosmochimica Acta*, 73, 1924–1944, 2009.
- Dale, A. W., Nickelsen, L., Scholz, F., Hensen, C., Oschlies, A., and Wallmann, K.: A revised global estimate of dissolved iron fluxes from 15 marine sediments, *Global Biogeochemical Cycles*, 29, 691–707, 2015.
- Dale, A. W., Graco, M., and Wallmann, K.: Strong and dynamic benthic-pelagic coupling and feedbacks in a coastal upwelling system (Peruvian shelf), *Frontiers in Marine Science*, 4, 29, 2017.
- de Beer, D., Sauter, E., Niemann, H., Kaul, N., Foucher, J.-P., Witte, U., Schlüter, M., and Boetius, A.: In situ fluxes and zonation of microbial activity in surface sediments of the Håkon Mosby Mud Volcano, *Limnology and Oceanography*, 51, 1315–1331, 2006.
- 20 Dean, J. F., Middelburg, J. J., Röckmann, T., Aerts, R., Blauw, L. G., Egger, M., Jetten, M. S., Jong, A. E., Meisel, O. H., Rasigraf, O., et al.: Methane feedbacks to the global climate system in a warmer world, *Reviews of Geophysics*, 2018.
- Dickens, G., Schroeder, D., Hinrichs, K., and Party, L. S.: The pressure core sampler (PCS) on Ocean Drilling Program Leg 201: general operations and gas release, in: *Proceedings ODP, Initial Reports 201*, pp. 1–22, Ocean Drilling Program College Station, TX, 2003.
- Dickson, A. G. and Goyet, C.: *Handbook of methods for the analysis of the various parameters of the carbon dioxide system in sea water*. 25 Version 2, Tech. rep., Oak Ridge National Lab., TN (United States), 1994.
- Dmitrenko, I. A., Kirillov, S. A., Tremblay, L. B., Kassens, H., Anisimov, O. A., Lavrov, S. A., Razumov, S. O., and Grigoriev, M. N.: Recent changes in shelf hydrography in the Siberian Arctic: Potential for subsea permafrost instability, *Journal of Geophysical Research: Oceans*, 116, 2011.
- Drachev, S. S., Savostin, L. A., Groshev, V. G., and Bruni, I. E.: Structure and geology of the continental shelf of the Laptev Sea, Eastern 30 Russian Arctic, *Tectonophysics*, 298, 357–393, 1998.
- Drake, T. W., Wickland, K. P., Spencer, R. G., McKnight, D. M., and Striegl, R. G.: Ancient low–molecular-weight organic acids in permafrost fuel rapid carbon dioxide production upon thaw, *Proceedings of the National Academy of Sciences*, 112, 13 946–13 951, 2015.
- Duan, Z., Møller, N., Greenberg, J., and Weare, J. H.: The prediction of methane solubility in natural waters to high ionic strength from 0 to 250 C and from 0 to 1600 bar, *Geochimica et Cosmochimica Acta*, 56, 1451–1460, 1992.
- 35 Egger, M., Lenstra, W., Jong, D., Meysman, F. J., Sapart, C. J., van der Veen, C., Röckmann, T., Gonzalez, S., and Slomp, C. P.: Rapid sediment accumulation results in high methane effluxes from coastal sediments, *PloS one*, 11, e0161 609, 2016.
- Egger, M., Riedinger, N., Mogollón, J. M., and Jørgensen, B. B.: Global diffusive fluxes of methane in marine sediments, *Nature Geoscience*, 11, 421, 2018.

- Fairbanks, R. G.: A 17,000-year glacio-eustatic sea level record: influence of glacial melting rates on the Younger Dryas event and deep-ocean circulation, *Nature*, 342, 637, 1989.
- Fossing, H., Ferdelman, T. G., and Berg, P.: Sulfate reduction and methane oxidation in continental margin sediments influenced by irrigation (South-East Atlantic off Namibia), *Geochimica et Cosmochimica Acta*, 64, 897–910, 2000.
- 5 Gramberg, I. S., Kulakov, Y. N., Pogrebitsky, Y. E., and Sorokov, D. S.: Arctic oil and gas super basin, X World Petroleum Congress., pp. 93–99, 1983.
- Graves, C. A., James, R. H., Sapart, C. J., Stott, A. W., Wright, I. C., Berndt, C., Westbrook, G. K., and Connelly, D. P.: Methane in shallow subsurface sediments at the landward limit of the gas hydrate stability zone offshore western Svalbard, *Geochimica et Cosmochimica Acta*, 198, 419–438, 2017.
- 10 Guo, L., Ping, C.-L., and Macdonald, R. W.: Mobilization pathways of organic carbon from permafrost to arctic rivers in a changing climate, *Geophysical Research Letters*, 34, 2007.
- Gypens, N., Lancelot, C., and Soetaert, K.: Simple parameterisations for describing N and P diagenetic processes: Application in the North Sea, *Progress in oceanography*, 76, 89–110, 2008.
- Haeckel, M., Suess, E., Wallmann, K., and Rickert, D.: Rising methane gas bubbles form massive hydrate layers at the seafloor, *Geochimica et Cosmochimica Acta*, 68, 4335–4345, 2004.
- 15 Haese, R. R., Meile, C., Van Cappellen, P., and De Lange, G. J.: Carbon geochemistry of cold seeps: methane fluxes and transformation in sediments from Kazan mud volcano, eastern Mediterranean Sea, *Earth and Planetary Science Letters*, 212, 361–375, 2003.
- Hensen, C. and Wallmann, K.: Methane formation at Costa Rica continental margin—constraints for gas hydrate inventories and cross-décollement fluid flow, *Earth and Planetary Science Letters*, 236, 41–60, 2005.
- 20 Hinrichs, K.-U. and Boetius, A.: The anaerobic oxidation of methane: new insights in microbial ecology and biogeochemistry, in: *Ocean margin systems*, pp. 457–477, Springer, 2002.
- Ho, T. and Aris, R.: On apparent second-order kinetics, *AIChE journal*, 33, 1050–1051, 1987.
- Hunter, S., Goldobin, D., Haywood, A., Ridgwell, A., and Rees, J.: Sensitivity of the global submarine hydrate inventory to scenarios of future climate change, *Earth and Planetary Science Letters*, 367, 105–115, 2013.
- 25 Iversen, N. and Jorgensen, B. B.: Anaerobic methane oxidation rates at the sulfate-methane transition in marine sediments from Kattegat and Skagerrak (Denmark) I, *Limnology and Oceanography*, 30, 944–955, 1985.
- Jakobsson, M., Mayer, L., Coakley, B., Dowdeswell, J. A., Forbes, S., Fridman, B., Hodnesdal, H., Noormets, R., Pedersen, R., Rebesco, M., et al.: The international bathymetric chart of the Arctic Ocean (IBCAO) version 3.0, *Geophysical Research Letters*, 39, 2012.
- James, R. H., Bousquet, P., Bussmann, I., Haeckel, M., Kipfer, R., Leifer, I., Niemann, H., Ostrovsky, I., Piskozub, J., Rehder, G., et al.: Effects of climate change on methane emissions from seafloor sediments in the Arctic Ocean: A review, *Limnology and oceanography*, 30, 61, 2016.
- 30 Janout, M., Hölemann, J., Juhls, B., Krumpen, T., Rabe, B., Bauch, D., Wegner, C., Kassens, H., and Timokhov, L.: Episodic warming of near-bottom waters under the Arctic sea ice on the central Laptev Sea shelf, *Geophysical Research Letters*, 43, 264–272, 2016.
- Jeffries, M. and Richter-Menge, J.: State of the climate in 2011: The Arctic, *Bull. Am. Meteorol. Soc.*, 93, S127–S148, 2012.
- 35 Jin, Q. and Bethke, C. M.: Predicting the rate of microbial respiration in geochemical environments, *Geochimica et Cosmochimica Acta*, 69, 1133–1143, 2005.
- Jørgensen, B. B., Weber, A., and Zopf, J.: Sulfate reduction and anaerobic methane oxidation in Black Sea sediments, *Deep Sea Research Part I: Oceanographic Research Papers*, 48, 2097–2120, 2001.

- Jourabchi, P., Van Cappellen, P., and Regnier, P.: Quantitative interpretation of pH distributions in aquatic sediments: A reaction-transport modeling approach, *American Journal of Science*, 305, 919–956, 2005.
- Judd, A. and Hovland, M.: *Seabed fluid flow: the impact on geology, biology and the marine environment*, Cambridge University Press, 2009.
- 5 Karaca, D., Hensen, C., and Wallmann, K.: Controls on authigenic carbonate precipitation at cold seeps along the convergent margin off Costa Rica, *Geochemistry, Geophysics, Geosystems*, 11, 2010.
- Knab, N., Cragg, B. A., Hornibrook, E., Holmkvist, L., Borowski, C., Parkes, R., and Jørgensen, B. B.: Regulation of anaerobic methane oxidation in sediments of the Black Sea, *Biogeosciences Discussions*, 5, 2305–2341, 2008.
- Knittel, K. and Boetius, A.: Anaerobic oxidation of methane: progress with an unknown process, *Annual review of microbiology*, 63, 311–
10 334, 2009.
- Kretschmer, K., Biastoch, A., Rüpke, L., and Burwicz, E.: Modeling the fate of methane hydrates under global warming, *Global Biogeochemical Cycles*, 29, 610–625, 2015.
- Krüger, M., Meyerdierks, A., Glöckner, F. O., Amann, R., Widdel, F., Kube, M., Reinhardt, R., Kahnt, J., Böcher, R., Thauer, R. K., et al.: A conspicuous nickel protein in microbial mats that oxidize methane anaerobically, *Nature*, 426, 878, 2003.
- 15 LaRowe, D., Dale, A. W., and Regnier, P.: A thermodynamic analysis of the anaerobic oxidation of methane in marine sediments, *Geobiology*, 6, 436–449, 2008.
- LaRowe, D. E., Burwicz, E., Arndt, S., Dale, A. W., and Amend, J. P.: Temperature and volume of global marine sediments, *Geology*, 45, 275–278, 2017.
- Leifer, I., Chernykh, D., Shakhova, N., and Semiletov, I.: Sonar gas flux estimation by bubble insonification: application to methane bubble
20 flux from seep areas in the outer Laptev Sea, *The Cryosphere*, 11, 1333–1350, 2017.
- Levitan, M. A. and Lavrushin, Y. A.: *Sedimentation history in the Arctic Ocean and Subarctic Seas for the last 130 kyr*, vol. 118, Springer Science & Business Media, 2009.
- Linke, P., Wallmann, K., Suess, E., Hensen, C., and Rehder, G.: In situ benthic fluxes from an intermittently active mud volcano at the Costa Rica convergent margin, *Earth and Planetary Science Letters*, 235, 79–95, 2005.
- 25 Lösekann, T., Knittel, K., Nadalig, T., Fuchs, B., Niemann, H., Boetius, A., and Amann, R.: Diversity and abundance of aerobic and anaerobic methane oxidizers at the Haakon Mosby Mud Volcano, Barents Sea, *Appl. Environ. Microbiol.*, 73, 3348–3362, 2007.
- Luff, R. and Wallmann, K.: Fluid flow, methane fluxes, carbonate precipitation and biogeochemical turnover in gas hydrate-bearing sediments at Hydrate Ridge, Cascadia Margin: numerical modeling and mass balances, *Geochimica et Cosmochimica Acta*, 67, 3403–3421, 2003.
- Luff, R., Greinert, J., Wallmann, K., Klauke, I., and Suess, E.: Simulation of long-term feedbacks from authigenic carbonate crust formation
30 at cold vent sites, *Chemical Geology*, 216, 157–174, 2005.
- Maher, K., Steefel, C. I., DePaolo, D. J., and Viani, B. E.: The mineral dissolution rate conundrum: Insights from reactive transport modeling of U isotopes and pore fluid chemistry in marine sediments, *Geochimica et Cosmochimica Acta*, 70, 337–363, 2006.
- Marquardt, M., Hensen, C., Pinero, E., Wallmann, K., and Haeckel, M.: A transfer function for the prediction of gas hydrate inventories in marine sediments, *Biogeosciences (BG)*, 7, 2925–2941, 2010.
- 35 Martens, C. S., Albert, D. B., and Alperin, M. J.: Biogeochemical processes controlling methane in gassy coastal sediments—Part I. A model coupling organic matter flux to gas production, oxidation and transport, *Continental Shelf Research*, 18, 1741–1770, 1998.
- Masson-Delmotte, V., Zhai, P., Pörtner, H. O., Roberts, D., Skea, J., Shukla, P., Pirani, A., Moufouma-Okia, W., Péan, C., Pidcock, R., Connors, S., Matthews, J. B. R., Chen, Y., Zhou, X., Gomis, M. I., Lonnoy, E., Maycock, T., Tignor, M., and Waterfield, T.: IPCC, 2018:

- Global warming of 1.5°C. An IPCC Special Report on the impacts of global warming of 1.5°C above pre-industrial levels and related global greenhouse gas emission pathways, in the context of strengthening the global response to the threat of climate change, sustainable development, and efforts to eradicate poverty, Tech. rep., 2018.
- 5 McGlynn, S. E., Chadwick, G. L., Kempes, C. P., and Orphan, V. J.: Single cell activity reveals direct electron transfer in methanotrophic consortia, *Nature*, 526, 531, 2015.
- McGuire, A. D., Anderson, L. G., Christensen, T. R., Dallimore, S., Guo, L., Hayes, D. J., Heimann, M., Lorenson, T. D., Macdonald, R. W., and Roulet, N.: Sensitivity of the carbon cycle in the Arctic to climate change, *Ecological Monographs*, 79, 523–555, 2009.
- Meister, P., Liu, B., Ferdelman, T. G., Jørgensen, B. B., and Khalili, A.: Control of sulphate and methane distributions in marine sediments by organic matter reactivity, *Geochimica et Cosmochimica Acta*, 104, 183–193, 2013.
- 10 Meister, P., Wiedling, J., Lott, C., Bach, W., Kuhfuß, H., Wegener, G., Böttcher, M. E., Deusner, C., Lichtschlag, A., Bernasconi, S. M., et al.: Anaerobic methane oxidation inducing carbonate precipitation at abiogenic methane seeps in the Tuscan archipelago (Italy), *PloS one*, 13, 2018.
- Middelburg, J. J., Soetaert, K., and Herman, P. M.: Empirical relationships for use in global diagenetic models, *Deep Sea Research Part I: Oceanographic Research Papers*, 44, 327–344, 1997.
- 15 Miller, C. M., Dickens, G. R., Jakobsson, M., Johansson, C., Koshurnikov, A., O’Regan, M., Muschitiello, F., Stranne, C., and Mörrh, C.-M.: Pore water geochemistry along continental slopes north of the East Siberian Sea: inference of low methane concentrations, *Biogeosciences*, 14, 2929–2953, 2017.
- Milucka, J., Ferdelman, T. G., Polerecky, L., Franzke, D., Wegener, G., Schmid, M., Lieberwirth, I., Wagner, M., Widdel, F., and Kuypers, M. M.: Zero-valent sulphur is a key intermediate in marine methane oxidation, *Nature*, 491, 541, 2012.
- 20 Mogollón, J. M., L’Heureux, I., Dale, A. W., and Regnier, P.: Methane gas-phase dynamics in marine sediments: A model study, *American Journal of Science*, 309, 189–220, 2009.
- Nauhaus, K., Albrecht, M., Elvert, M., Boetius, A., and Widdel, F.: In vitro cell growth of marine archaeal-bacterial consortia during anaerobic oxidation of methane with sulfate, *Environmental Microbiology*, 9, 187–196, 2007.
- Niemann, H., Duarte, J., Hensen, C., Omorigie, E., Magalhaes, V., Elvert, M., Pinheiro, L., Kopf, A., and Boetius, A.: Microbial methane 25 turnover at mud volcanoes of the Gulf of Cadiz, *Geochimica et Cosmochimica Acta*, 70, 5336–5355, 2006a.
- Niemann, H., Lösekann, T., De Beer, D., Elvert, M., Nadalig, T., Knittel, K., Amann, R., Sauter, E. J., Schlüter, M., Klages, M., et al.: Novel microbial communities of the Haakon Mosby mud volcano and their role as a methane sink, *Nature*, 443, 854, 2006b.
- O’Connor, F. M., Boucher, O., Gedney, N., Jones, C., Folberth, G., Coppel, R., Friedlingstein, P., Collins, W., Chappellaz, J., Ridley, J., et al.: Possible role of wetlands, permafrost, and methane hydrates in the methane cycle under future climate change: A review, *Reviews 30 of Geophysics*, 48, 2010.
- Overduin, P., Wetterich, S., Günther, F., Grigoriev, M. N., Grosse, G., Schirrmeister, L., Hubberten, H.-W., and Makarov, A. S.: Coastal dynamics and submarine permafrost in shallow water of the central Laptev Sea, East Siberia, *Cryosphere*, 10, 1449–1462, 2016.
- Overduin, P. P., Liebner, S., Knoblauch, C., Günther, F., Wetterich, S., Schirrmeister, L., Hubberten, H.-W., and Grigoriev, M. N.: Methane 35 oxidation following submarine permafrost degradation: Measurements from a central Laptev Sea shelf borehole, *Journal of Geophysical Research: Biogeosciences*, 120, 965–978, 2015.
- Piechura, J. and Walczowski, W.: The Arctic Front: structure and dynamics, *Oceanologia*, 37, 47–73, 1995.
- Pierre, C., Blanc-Valleron, M.-M., Demange, J., Boudouma, O., Foucher, J.-P., Pape, T., Himmler, T., Fekete, N., and Spiess, V.: Authigenic carbonates from active methane seeps offshore southwest Africa, *Geo-Marine Letters*, 32, 501–513, 2012.

- Piker, L., Schmaljohann, R., and Imhoff, J. F.: Dissimilatory sulfate reduction and methane production in Gotland Deep sediments (Baltic Sea) during a transition period from oxic to anoxic bottom water (1993-1996), *Aquatic Microbial Ecology*, 14, 183–193, 1998.
- Polyakov, I. V., Pnyushkov, A. V., Alkire, M. B., Ashik, I. M., Baumann, T. M., Carmack, E. C., Goszczko, I., Guthrie, J., Ivanov, V. V., Kanzow, T., et al.: Greater role for Atlantic inflows on sea-ice loss in the Eurasian Basin of the Arctic Ocean, *Science*, 356, 285–291, 2017.
- Reagan, M. T. and Moridis, G. J.: Large-scale simulation of methane hydrate dissociation along the West Spitsbergen Margin, *Geophysical research letters*, 36, 2009.
- Reeburgh, W. S.: Oceanic methane biogeochemistry, *Chemical reviews*, 107, 486–513, 2007.
- Regnier, P., O’kane, J., Steefel, C., and Vanderborght, J.-P.: Modeling complex multi-component reactive-transport systems: towards a simulation environment based on the concept of a Knowledge Base, *Applied Mathematical Modelling*, 26, 913–927, 2002.
- Regnier, P., Dale, A. W., Arndt, S., LaRowe, D., Mogollón, J., and Van Cappellen, P.: Quantitative analysis of anaerobic oxidation of methane (AOM) in marine sediments: a modeling perspective, *Earth-Science Reviews*, 106, 105–130, 2011.
- Rittmann, B. and VanBriesen, J. M.: Microbiological processes in reactive modeling, in: *Reactive Transport in Porous Media*, pp. 311–334, Walter de Gruyter GmbH, 2019.
- Rittmann, B. E. and McCarty, P. L.: *Environmental biotechnology: principles and applications*, Tata McGraw-Hill Education, 2012.
- Romanovskii, N., Hubberten, H.-W., Gavrilov, A., Tumskey, V., and Kholodov, A.: Permafrost of the east Siberian Arctic shelf and coastal lowlands, *Quaternary Science Reviews*, 23, 1359–1369, 2004.
- Romanovskii, N., Hubberten, H.-W., Gavrilov, A., Eliseeva, A., and Tipenko, G.: Offshore permafrost and gas hydrate stability zone on the shelf of East Siberian Seas, *Geo-marine letters*, 25, 167–182, 2005.
- Romanovskii, N. N. and Hubberten, H.-W.: Results of permafrost modelling of the lowlands and shelf of the Laptev Sea region, Russia, *Permafrost and periglacial processes*, 12, 191–202, 2001.
- Ruppel, C. D. and Kessler, J. D.: The interaction of climate change and methane hydrates, *Reviews of Geophysics*, 55, 126–168, 2017.
- Sales de Freitas, F.: Deciphering the relationships between reactivity and sources of organic matter in marine sediments: a coupled large-scale model and lipid biomarker analysis, Ph.D. thesis, School on Earth Sciences, University of Bristol, 2018.
- Sapart, C. J., Shakhova, N., Semiletov, I., Jansen, J., Szidat, S., Kosmach, D., Dudarev, O., Van Der Veen, C., Egger, M., Sergienko, V., et al.: The origin of methane in the East Siberian Arctic Shelf unraveled with triple isotope analysis, *Biogeosciences*, 14, 2283–2292, 2017.
- Sauer, S., Knies, J., Lepland, A., Chand, S., Eichinger, F., and Schubert, C. J.: Hydrocarbon sources of cold seeps off the Vesterålen coast, northern Norway, *Chemical Geology*, 417, 371–382, 2015.
- Sauer, S., Hong, W.-L., Knies, J., Lepland, A., Forwick, M., Klug, M., Eichinger, F., Baranwal, S., Crémière, A., Chand, S., et al.: Sources and turnover of organic carbon and methane in fjord and shelf sediments off northern Norway, *Geochemistry, Geophysics, Geosystems*, 17, 4011–4031, 2016.
- Saunio, M., Bousquet, P., Poulter, B., Peregón, A., Ciais, P., Canadell, J. G., Dlugokencky, E. J., Etiope, G., Bastviken, D., Houweling, S., et al.: The global methane budget 2000–2012, *Earth System Science Data*, 8, 697–751, 2016.
- Semenov, P., Portnov, A., Krylov, A., Egorov, A., and Vanshtein, B.: Geochemical evidence for seabed fluid flow linked to the subsea permafrost outer border in the South Kara Sea, *Geochemistry*, 2019.
- Shakhova, N., Semiletov, I., Leifer, I., Salyuk, A., Rekant, P., and Kosmach, D.: Geochemical and geophysical evidence of methane release over the East Siberian Arctic Shelf, *Journal of Geophysical Research: Oceans*, 115, 2010a.

- Shakhova, N., Semiletov, I., Salyuk, A., Yusupov, V., Kosmach, D., and Gustafsson, Ö.: Extensive methane venting to the atmosphere from sediments of the East Siberian Arctic Shelf, *Science*, 327, 1246–1250, 2010b.
- Shakhova, N., Semiletov, I., Leifer, I., Sergienko, V., Salyuk, A., Kosmach, D., Chernykh, D., Stubbs, C., Nicolsky, D., Tumskey, V., et al.: Ebullition and storm-induced methane release from the East Siberian Arctic Shelf, *Nature Geoscience*, 7, 64, 2014.
- 5 Shakhova, N., Semiletov, I., Sergienko, V., Lobkovsky, L., Yusupov, V., Salyuk, A., Salomatin, A., Chernykh, D., Kosmach, D., Panteleev, G., et al.: The East Siberian Arctic Shelf: towards further assessment of permafrost-related methane fluxes and role of sea ice, *Philosophical Transactions of the Royal Society A: Mathematical, Physical and Engineering Sciences*, 373, 20140451, 2015.
- Shakhova, N., Semiletov, I., Gustafsson, O., Sergienko, V., Lobkovsky, L., Dudarev, O., Tumskey, V., Grigoriev, M., Mazurov, A., Salyuk, A., et al.: Current rates and mechanisms of subsea permafrost degradation in the East Siberian Arctic Shelf, *Nature communications*, 8, 15 872, 2017.
- Shakhova, N., Semiletov, I., and Chuvilin, E.: Understanding the permafrost–hydrate system and associated methane releases in the east Siberian Arctic Shelf, *Geosciences*, 9, 251, 2019.
- Sloan Jr, E. D. and Koh, C.: *Clathrate hydrates of natural gases*, CRC press, 2007.
- Sommer, S., Pfannkuche, O., Linke, P., Luff, R., Greinert, J., Drews, M., Gubsch, S., Pieper, M., Poser, M., and Viergutz, T.: Efficiency of the benthic filter: Biological control of the emission of dissolved methane from sediments containing shallow gas hydrates at Hydrate Ridge, *Global Biogeochemical Cycles*, 20, 2006.
- 15 Sparrow, K. J., Kessler, J. D., Southon, J. R., Garcia-Tigueros, F., Schreiner, K. M., Ruppel, C. D., Miller, J. B., Lehman, S. J., and Xu, X.: Limited contribution of ancient methane to surface waters of the US Beaufort Sea shelf, *Science advances*, 4, eaao4842, 2018.
- Stein, R., Boucsein, B., Fahl, K., de Oteyza, T. G., Knies, J., and Niessen, F.: Accumulation of particulate organic carbon at the Eurasian continental margin during late Quaternary times: controlling mechanisms and paleoenvironmental significance, *Global and Planetary Change*, 31, 87–104, 2001.
- 20 Teal, L., Bulling, M. T., Parker, E., and Solan, M.: Global patterns of bioturbation intensity and mixed depth of marine soft sediments, *Aquatic Biology*, 2, 207–218, 2008.
- Tesi, T., Semiletov, I., Hugelius, G., Dudarev, O., Kuhry, P., and Gustafsson, Ö.: Composition and fate of terrigenous organic matter along the Arctic land–ocean continuum in East Siberia: Insights from biomarkers and carbon isotopes, *Geochimica et Cosmochimica Acta*, 133, 235–256, 2014.
- Thang, N. M., Brüchert, V., Formolo, M., Wegener, G., Ginters, L., Jørgensen, B. B., and Ferdelman, T. G.: The impact of sediment and carbon fluxes on the biogeochemistry of methane and sulfur in littoral Baltic Sea sediments (Himmerfjärden, Sweden), *Estuaries and Coasts*, 36, 98–115, 2013.
- 30 Thornton, B. F., Geibel, M. C., Crill, P. M., Humborg, C., and Mörh, C.-M.: Methane fluxes from the sea to the atmosphere across the Siberian shelf seas, *Geophysical Research Letters*, 43, 5869–5877, 2016.
- Thullner, M., Van Cappellen, P., and Regnier, P.: Modeling the impact of microbial activity on redox dynamics in porous media, *Geochimica et Cosmochimica Acta*, 69, 5005–5019, 2005.
- Thullner, M., Dale, A. W., and Regnier, P.: Global-scale quantification of mineralization pathways in marine sediments: A reaction-transport modeling approach, *Geochemistry, geophysics, geosystems*, 10, 2009.
- 35 Tishchenko, P., Hensen, C., Wallmann, K., and Wong, C. S.: Calculation of the stability and solubility of methane hydrate in seawater, *Chemical geology*, 219, 37–52, 2005.

- Trenberth, K., Jones, P., Ambenje, P., Bojariu, R., Easterling, D., Klein Tank, A., Parker, D., Rahimzadeh, F., Renwick, J., Rusticucci, M., et al.: Observations: surface and atmospheric climate change. Chapter 3, Climate change, pp. 235–336, 2007.
- Treude, T., Boetius, A., Knittel, K., Wallmann, K., and Jørgensen, B. B.: Anaerobic oxidation of methane above gas hydrates at Hydrate Ridge, NE Pacific Ocean, *Marine Ecology Progress Series*, 264, 1–14, 2003.
- 5 Treude, T., Krüger, M., Boetius, A., and Jørgensen, B. B.: Environmental control on anaerobic oxidation of methane in the gassy sediments of Eckernförde Bay (German Baltic), *Limnology and oceanography*, 50, 1771–1786, 2005.
- Vonk, J. E., Sánchez-García, L., Van Dongen, B., Alling, V., Kosmach, D., Charkin, A., Semiletov, I. P., Dudarev, O. V., Shakhova, N., Roos, P., et al.: Activation of old carbon by erosion of coastal and subsea permafrost in Arctic Siberia, *Nature*, 489, 137, 2012.
- Wallmann, K., Aloisi, G., Haeckel, M., Obzhairov, A., Pavlova, G., and Tishchenko, P.: Kinetics of organic matter degradation, microbial methane generation, and gas hydrate formation in anoxic marine sediments, *Geochimica et Cosmochimica Acta*, 70, 3905–3927, 2006a.
- 10 Wallmann, K., Drews, M., Aloisi, G., and Bohrmann, G.: Methane discharge into the Black Sea and the global ocean via fluid flow through submarine mud volcanoes, *Earth and Planetary Science Letters*, 248, 545–560, 2006b.
- Wang, Y. and Van Cappellen, P.: A multicomponent reactive transport model of early diagenesis: Application to redox cycling in coastal marine sediments, *Geochimica et Cosmochimica Acta*, 60, 2993–3014, 1996.
- 15 Wegener, G., Krukenberg, V., Riedel, D., Tegetmeyer, H. E., and Boetius, A.: Intercellular wiring enables electron transfer between methanotrophic archaea and bacteria, *Nature*, 526, 587, 2015.
- Wegner, C., Bennett, K. E., de Vernal, A., Forwick, M., Fritz, M., Heikkilä, M., Łacka, M., Lantuit, H., Laska, M., Moskalik, M., et al.: Variability in transport of terrigenous material on the shelves and the deep Arctic Ocean during the Holocene, *Polar Research*, 34, 24964, 2015.
- 20 Westbrook, G. K., Thatcher, K. E., Rohling, E. J., Piotrowski, A. M., Pälike, H., Osborne, A. H., Nisbet, E. G., Minshull, T. A., Lanoisellé, M., James, R. H., et al.: Escape of methane gas from the seabed along the West Spitsbergen continental margin, *Geophysical Research Letters*, 36, 2009.
- Wild, B., Andersson, A., Bröder, L., Vonk, J., Hugelius, G., McClelland, J. W., Song, W., Raymond, P. A., and Gustafsson, Ö.: Rivers across the Siberian Arctic unearth the patterns of carbon release from thawing permafrost, *Proceedings of the National Academy of Sciences*, p. 201811797, 2019.
- 25 Winkel, M., Mitzscherling, J., Overduin, P. P., Horn, F., Winterfeld, M., Rijkers, R., Grigoriev, M. N., Knoblauch, C., Mangelsdorf, K., Wagner, D., et al.: Anaerobic methanotrophic communities thrive in deep submarine permafrost, *Scientific reports*, 8, 1291, 2018.
- Wright, J., Taylor, A., and Dallimore, S.: Thermal Impact of Holocene Lakes on a Permafrost Landscape, Mackenzie Delta, Canada, in: *Proceedings of the Ninth international conference on Permafrost*, Fairbanks, AK, 2008.
- 30 Yakushev, V. S.: Gas hydrates in cryolithozone, 11, 100–105, 1989.
- Yao, H., Hong, W.-L., Panieri, G., Sauer, S., Torres, M. E., Lehmann, M. F., Gründger, F., and Niemann, H.: Fracture-controlled fluid transport supports microbial methane-oxidizing communities at Vestnesa Ridge, *Biogeosciences*, 16, 2221–2232, 2019.
- Zhang, J., Rothrock, D. A., and Steele, M.: Warming of the Arctic Ocean by a strengthened Atlantic inflow: Model results, *Geophysical Research Letters*, 25, 1745–1748, 1998.

Supplementary material

Matteo Puglini^{1,2}, Victor Brovkin¹, Pierre Regnier², and Sandra Arndt²

¹Land in the Earth System, Max Planck Institute for Meteorology, Hamburg, Germany

²BGeosys, Department Geoscience, Environment & Society (DGES), Université Libre de Bruxelles, Brussels, Belgium

Correspondence: Matteo Puglini (matteo.puglini@mpimet.mpg.de)

S1 From continuity equation to advection-diffusion-reaction equation

Each equation (one per species i) is a specific generalization of a continuity equation with fluxes \mathcal{F}_i , related to the the transport processes, and sources/sinks \mathcal{S}_i related to the biogeochemical reactions. It reads:

$$\frac{\partial \xi(z)C_i(z,t)}{\partial t} = -\frac{\partial \mathcal{F}_i(z,t)}{\partial z} + \mathcal{S}_i(z,t). \quad (\text{S1})$$

- 5 Where $C_i(z,t)$ is the concentration of the species i (referred to porewater volume if it is a dissolved species or solid matrix volume if it is a solid species) and $\xi(z)$ is the term accounting for this, *i.e.* the porosity $\xi = \varphi$ in case of a dissolved species or the solid fraction $\xi = \varphi_s = 1 - \varphi$ in case of a solid species. The fluxes $\mathcal{F}_i(z,t)$ consist of several components:

- $\mathcal{F}_{D,i}(z,t)$: the molecular diffusive flux (only for dissolved species) is given by the Fick's law

$$\mathcal{F}_{D,i}(z,t) = -D_i(z,t)\varphi(z)\frac{\partial C_i(z,t)}{\partial z} \quad (\text{S2})$$

- 10 where $D_i(z,t)$ is the effective diffusion coefficient. D_i is usually modelled as a time-independent variable and considered constant for each species at a given salinity and temperature and locally only affected by sediment tortuosity $\theta(z)$. The relation between diffusion coefficient and salinity and temperature is provided in Table S6. Tortuosity has been considered strictly linked to porosity $\varphi(z)$ according to $\theta(z) = 1 - \ln \varphi^2(z)$. And porosity follows an exponential decay with depth (Athy, 1930):

$$15 \quad \varphi(z) = \varphi_0 e^{-c_0 z} \quad (\text{S3})$$

with φ_0 porosity at the Sediment-Water Interface (SWI) and c_0 typical length scale for compaction (Table S6).

- $\mathcal{F}_{D_b,i}(z,t)$: the bioturbation flux, described as a diffusive flux (to be considered also for solid species), reads

$$\mathcal{F}_{D_b,i}(z,t) = -D_{b,i}(z,t)\xi(z)\frac{\partial C_i(z,t)}{\partial z} \quad (\text{S4})$$

with $D_b(z,t)$ bioturbation coefficient. Considering no time dependency, the latter is assumed to follow an exponential trend below 5 cm depth, *i.e.* :

$$20 \quad \begin{cases} D_b(z) = D_b^0, & 0 \leq z \leq 5 \text{ cm} \\ D_b(z) = D_b^0 e^{-(z-5)}, & 5 < z < 300 \text{ cm} \end{cases} \quad (\text{S5})$$

and D_b^0 given in Table S6.

– $\mathcal{F}_{v,i}(z,t)$: the advective flux is given by

$$\mathcal{F}_{v,i}(z,t) = v(z,t)\xi(z)C_i(z,t) \quad (\text{S6})$$

5 where $v(z,t)$ is the sedimentation rate $v(z,t) = \omega(z,t)$ for solid species and the sum of sedimentation rate and possible advective flow velocity $v_{up}(z,t)$ for dissolved species, *i.e.* $v(z,t) = \omega(z,t) + v_{up}(z,t)$. If we assume steady state compaction then burial velocity reads (Berner (1980)):

$$\omega(z) = \left(\frac{1 - \varphi_0}{1 - \varphi(z)} \right) \omega_0 \quad (\text{S7})$$

with ω_0 sedimentation rate at the SWI. A site where $v_{up} \neq 0$ is denominated as *active* while a site with null upward water velocity is defined as *passive*.

10 – $\mathcal{F}_{NL,i}(z,t)$ represent any form of non-local transport. In its more classical form (Boudreau (1997)) it is given by bioirrigation provided by irrigated furrows digged by benthic fauna and it reads

$$\mathcal{F}_{irr}(z,t) = - \int_0^z \alpha_i(y)\xi(y)[C_i(0,t) - C_i(y,t)]dy \quad (\text{S8})$$

where $\alpha_i(z)$ is the bioirrigation coefficient, $C_i(0,t)$ is the concentration of the species i at the SWI. Bioirrigation parameter α is modelled as (Thullner et al. (2009)):

$$15 \quad \alpha(z) = \alpha_0 e^{-z/z_{irr}} \quad (\text{S9})$$

where α_0 is the bioirrigation coefficient and z_{irr} the bioirrigation attenuation depth (see Table S6). Yet other forms of non-local transport may be considered in the Arctic shelf scenario, such as ice scouring or bubble migration in sediments rich of free gas. These processes are even more difficult to be modelled and are not included in current BRNS version.

20 With the fluxes described above eq. S1 takes the form of the standard advection-diffusion-reaction equation (see eq. 4) usually implemented in reactive-transport diagenetic models (Berner (1980); Boudreau (1997))

$$\frac{\partial \xi C_i}{\partial t} = \frac{\partial}{\partial z} \left[(D_i + D_{b,i})\xi \frac{\partial C_i}{\partial z} \right] - \frac{\partial}{\partial z} (v\xi C_i) + \alpha_i \xi (C_i(0) - C_i) + \mathcal{S}_i.$$

S2 Primary redox reactions

25 Organic matter (OM) decomposition is a complex multi-step process (Arndt et al. (2013)) carried out by micro-organism along a chain of enzyme-mediated biochemical redox reactions which exploits electronic cascades to provide energy. Carbon in organic matter plays the role of electron donor, getting oxidized, and energy yield of the full redox reaction ultimately depends on the terminal electron acceptor (TEA) which overall acts as an oxidant, getting reduced. This entails a preferential sequence

of how OM gets mineralized by microorganism along different metabolic pathways with different TEAs according to energy gain ladder.

It determines the typical vertical zonation of the TEAs and byproducts of organic matter decomposition throughout the sediment column according to the redox sequence (Claypool and Kaplan (1974); Froelich et al. (1979); Stumm and Morgan (1996)). The chained reactions involving OM mineralization are reported in Table S2. OM degradation is modeled by a generalized first order kinetic equation, namely decomposition rate is faster the more OM is present. The proportionality between organic carbon decay rate and organic carbon content is set by a degradability rate k which not necessarily has to be constant. We employed reactive continuum model (RCM) to model this degradability rate k as a continuous variable, whose distribution reads:

$$g(k) = \frac{g_0 k^{\nu-1} e^{-ak}}{\Gamma(\nu)} \quad (\text{S10})$$

where g_0 is a scale parameter, ν and a determine the shape of the distribution of k and $\Gamma(\nu)$ is the Gamma function. The quantity a represents the average lifetime of the more reactive organic matter components in a reactive-continuum model (Boudreau and Ruddick (1991)) and the mean degradation constant \bar{k} of the OM spectrum is given by $\bar{k} = \nu/a$. The choice of RCM relies on the fact that it is considered more suitable for marine sediments than a discrete model (Aller and Blair (2004); Arndt et al. (2013)). It manages to encompass all the information about OM degradability in only two parameters, carriers of a theoretical meanings, instead that in as many degradation constants as carbon pools considered in a discrete model. Moreover RCM is more flexible to account for the whole range of degradability that Arctic OM shows, shifting its peak just by tweaking the parameters instead of the initial carbon content of each pool. Another peculiarity of this formulation of RCM is that, assuming distribution in eq. (S10), OM degradation can actually be rewritten as a first-order kinetic with the a degradability $K(t)$ dependent on sediment age t (Boudreau and Ruddick (1991)), *i.e.*

$$\mathcal{S}_{POC} = \frac{dPOC(t)}{dt} = -K(t)POC(t) = -\frac{\nu}{a+t}POC(t) \quad (\text{S11})$$

where $POC(t)$ is the particulate organic carbon, which in turns reads

$$POC(t) = POC(0) \left(\frac{a}{a+t} \right)^\nu \quad (\text{S12})$$

$POC(0)$ being the initial organic carbon concentration. This features allows to estimate sediment age and POC vertical profile just coupling RCM and a discrete model

25 S3 Estimate of sediment age t and POC content

POC age and vertical profile are critical quantity to be evaluated. One approach would be performing *ab initio* simulations, but they are difficult since a complete knowledge of past boundary conditions and how they evolved over time would be needed. Even when this knowledge is enough, simulation times are usually rather long and hence a different approach is generally used.

Using eq. (S7 and S3), in an unperturbed sediment setting, we find that the age at a certain depth z is provided by

$$t(z) = \int_0^z \frac{1}{\omega(z)} = \frac{z + \frac{\varphi_0}{c_0} (e^{-c_0 z} - 1)}{\omega_0 (1 - \varphi_0)}. \quad (\text{S13})$$

If another formulation for the porosity is employed, for instance:

$$\varphi(z) = \varphi_\infty + (\varphi_0 - \varphi_\infty) e^{-c_0 z} \quad (\text{S14})$$

where φ_∞ specifies the asymptotic value of the porosity, then the expression for the age $t(z)$ modifies as:

$$5 \quad t(z) = \int_0^z \frac{1}{\omega(z)} = \frac{(1 - \varphi_\infty)z + \frac{\varphi_0 - \varphi_\infty}{c_0} (e^{-c_0 z} - 1)}{\omega_0 (1 - \varphi_0)}. \quad (\text{S15})$$

If the sediment column were not bioturbated, plugging results (S13) into eq. (S12) would give the steady state profile of the organic matter throughout the whole sediments, with $POC(0)$ POC concentration at the SWI (because considerations above legitimize a *space for time* substitution and initial time corresponds to the uppermost concentration).

The column is instead divided in bioturbated (the upper part) and not-bioturbated (below a certain depth). Because of
10 bioturbation the upper layers are mixed, *i.e.* POC of different ages coexist at the same depth (Meile and Van Cappellen (2005)). This is actually the most difficult problem to be tackled to assign age to a certain sediment level. In order to deal with issue, similarly to **Dale et al 2015**, the POC in the bioturbated zone was modelled resorting to multi-G approximation of the RCM. It means that, within the bioturbated region, the POC is represented by 500 distinct OM fractions, whose reactivity covers the spectrum $k = [k_{min} : 10^{-15}, k_{max} : -\log(a) + 2] \text{ yr}^{-1}$ plus two extra fractions accounting for the reactivity $[0, k_{min}]$ and
15 $[k_{max}, \infty]$. With these considerations and considering constant porosity and sedimentation rate eq. (??) reads:

$$\varphi_s \frac{\partial POC(z,t)}{\partial t} = D_b \varphi_s \frac{\partial^2 POC(z,t)}{\partial z^2} - \omega \varphi_s \frac{\partial POC(z,t)}{\partial z} - \varphi_s k_i POC(z,t) \quad (\text{S16})$$

where $\varphi_s = 1 - \varphi$ and k_i is the reactivity of the i -th fraction of POC considered. Eq. (S16) is an advective-diffusive-reactive equation which in steady state can be analytically solved for each fraction i , once boundary conditions are provided. The general solution is:

$$20 \quad POC(z) = A e^{\lambda_1 z} + B e^{\lambda_2 z} \quad \text{where} \quad \begin{cases} \lambda_1 = \frac{\omega - \sqrt{\omega^2 + 4D_b k_i}}{2D_b} \\ \lambda_2 = \frac{\omega + \sqrt{\omega^2 + 4D_b k_i}}{2D_b} \end{cases} \quad (\text{S17})$$

In this case boundary conditions are given by

$$\begin{cases} POC(0) = POC_0 \cdot F_i & \text{at } z = 0 \\ D_b \frac{\partial POC}{\partial z} = 0 & \text{at } z = z_{bio} \end{cases} \quad (\text{S18})$$

where F_i is the fraction of initial POC_0 whose reactivity lies around k_i and z_{bio} is the depth of bioturbated zone where we impose that bioturbated flux shall be null. Bearing in mind eq. (S11) and (S12), the distribution of the POC_0 lying around a

25 certain value of $k = k_i$ can be written as:

$$f(k_i) = \frac{g(k_i)}{POC_0} = \frac{a^\nu k_i^{\nu-1} e^{-ak_i}}{\Gamma(\nu)}. \quad (S19)$$

The initial fraction of POC_0 whose reactivity is within $[0, k_i]$, *i.e.* $F(k_i)$, can be obtained via integration of eq. (S19) and this allows to find finally the fraction F_i of POC_0 whose reactivity is in $[k_{i-1}, k_i]$ as

$$F_i = F(k_i) - F(k_{i-1}). \quad (S20)$$

Enforcing boundary conditions (S18) for each of 502 fractions and summing up their solutions we find an approximate solution of the RCM in the bioturbated layer. A comparison between the solution obtained in this way and what should be the RCM solution (eq. (S12)) allows to find the apparent age $t(z)$ of the sediments at each depth within the bioturbated zone and also at its bottom, *i.e.* $t(z_{bio})$. Below the bioturbated zone the apparent age is then found simply adding $t(z_{bio})$ and results of eq. (S13).

The age profile and the POC profile found in this way is then calculated from BRNS at the very beginning and imposed throughout the whole steady-state simulation.

S4 Biogeochemical network: tables

Table S1. The 6 inhibition factors ruling the onset of metabolic pathways according to the succession of the redox ladder.

f_{O_2}	$\begin{cases} 1 & \text{if } [O_2] > K_{O_2} \\ \frac{[O_2]}{K_{O_2}} & \text{if } [O_2] < K_{O_2} \end{cases}$
$f_{NO_3^-}$	$\begin{cases} 0 & \text{if } [O_2] > K_{O_2} \\ \left(1 - \frac{[O_2]}{K_{O_2}}\right) \frac{NO_3^-}{K_{NO_3^-}} & \text{if } [O_2] < K_{O_2} \end{cases}$
f_{MnO_2}	$\begin{cases} 0 & \text{if } [NO_3^-] > K_{NO_3^-} \\ \left(1 - \frac{[O_2]}{K_{O_2}} - \frac{[NO_3^-]}{K_{NO_3^-}}\right) \frac{MnO_2}{K_{MnO_2}} & \text{if } [NO_3^-] < K_{NO_3^-} \end{cases}$
$f_{Fe(OH)_3}$	$\begin{cases} 0 & \text{if } [MnO_2] > K_{MnO_2} \\ \left(1 - \frac{[O_2]}{K_{O_2}} - \frac{[NO_3^-]}{K_{NO_3^-}} - \frac{[MnO_2]}{K_{MnO_2}}\right) \frac{Fe(OH)_3}{K_{Fe(OH)_3}} & \text{if } [MnO_2] < K_{MnO_2} \end{cases}$
$f_{SO_4^{2-}}$	$\begin{cases} 0 & \text{if } [Fe(OH)_3] > K_{Fe(OH)_3} \\ \left(1 - \frac{[O_2]}{K_{O_2}} - \frac{[NO_3^-]}{K_{NO_3^-}} - \frac{[MnO_2]}{K_{MnO_2}} - \frac{[Fe(OH)_3]}{K_{Fe(OH)_3}}\right) \frac{SO_4^{2-}}{K_{SO_4^{2-}}} & \text{if } [Fe(OH)_3] < K_{Fe(OH)_3} \end{cases}$
f_{CH_4}	$\begin{cases} 0 & \text{if } [SO_4^{2-}] > K_{SO_4^{2-}} \\ \left(1 - \frac{[O_2]}{K_{O_2}} - \frac{[NO_3^-]}{K_{NO_3^-}} - \frac{[MnO_2]}{K_{MnO_2}} - \frac{[Fe(OH)_3]}{K_{Fe(OH)_3}} - \frac{[SO_4^{2-}]}{K_{SO_4^{2-}}}\right) \frac{CH_4}{K_{CH_4}} & \text{if } [SO_4^{2-}] < K_{SO_4^{2-}} \end{cases}$

Table S2. The 6 primary redox reactions involved in the degradation of OM. The coefficients x , y and z , enforce Redfield ratio ($x = 106$, $y = 16$ and $z = 1$). SD stands for the conversion factor between solid and liquid volume, *i.e.* $SD = \varphi_s / \varphi$. For the expression of the inhibition factors f see Table S1. $[\text{CH}_2\text{O}]$ is a shortcut for $(\text{CH}_2\text{O})(\text{NH}_3)_y(\text{H}_3\text{PO}_4)_z$, to take into account nutrients.

#	Reaction	Rate expression
R1	$[\text{CH}_2\text{O}] + \left(\frac{x+2y}{x}\right) SD \cdot \text{O}_2 + \left(\frac{y+2z}{x}\right) SD \cdot \text{HCO}_3^- \longrightarrow \left(\frac{x+y+2z}{x}\right) SD \cdot \text{CO}_2 + \left(\frac{y}{x}\right) SD \cdot \text{NO}_3^- + \left(\frac{z}{x}\right) SD \cdot \text{HPO}_4^{2-} + \left(\frac{x+2y+2z}{x}\right) SD \cdot \text{H}_2\text{O}$	$\frac{\nu}{a+t} [\text{CH}_2\text{O}] \cdot f_{\text{O}_2}$
R2	$[\text{CH}_2\text{O}] + \left(\frac{4x+3y}{5x}\right) SD \cdot \text{NO}_3^- \longrightarrow \left(\frac{x-3y+10z}{5x}\right) SD \cdot \text{CO}_2 + \left(\frac{4x+3y-10z}{5x}\right) SD \cdot \text{HCO}_3^- + \left(\frac{z}{x}\right) SD \cdot \text{HPO}_4^{2-} + \left(\frac{3x+6y+10z}{5x}\right) \text{H}_2\text{O} + \left(\frac{2x+4y}{5x}\right) \text{N}_2$	$\frac{\nu}{a+t} [\text{CH}_2\text{O}] \cdot f_{\text{NO}_3^-}$
R3	$[\text{CH}_2\text{O}] + 2\text{MnO}_2 + \left(\frac{3x+y-2z}{x}\right) SD \cdot \text{CO}_2 + \left(\frac{x+y-2z}{x}\right) SD \cdot \text{H}_2\text{O} \longrightarrow 2SD \cdot \text{Mn}^{2+} + \left(\frac{y}{x}\right) SD \cdot \text{NH}_4^+ + \left(\frac{4x+y-2z}{x}\right) SD \cdot \text{HCO}_3^- + \left(\frac{z}{x}\right) SD \cdot \text{HPO}_4^{2-}$	$\frac{\nu}{a+t} \cdot [\text{CH}_2\text{O}] \cdot f_{\text{MnO}_2}$
R4	$[\text{CH}_2\text{O}] + 4\text{Fe}(\text{OH})_3 + \left(\frac{7x+y-2z}{x}\right) SD \cdot \text{CO}_2 \longrightarrow 4SD \cdot \text{Fe}^{2+} + \left(\frac{8x+y-2z}{x}\right) SD \cdot \text{HCO}_3^- + \left(\frac{y}{x}\right) SD \cdot \text{NH}_4^+ + \left(\frac{z}{x}\right) SD \cdot \text{HPO}_4^{2-} + \left(\frac{3x-y+2z}{x}\right) \text{H}_2\text{O}$	$\frac{\nu}{a+t} \cdot [\text{CH}_2\text{O}] \cdot f_{\text{Fe}(\text{OH})_3}$
R5	$[\text{CH}_2\text{O}] + \frac{1}{2} SD \cdot \text{SO}_4^{2-} + \left(\frac{y-2z}{x}\right) SD \cdot \text{CO}_2 + \left(\frac{y-2z}{x}\right) SD \cdot \text{H}_2\text{O} \longrightarrow \left(\frac{x+y-2z}{x}\right) SD \cdot \text{HCO}_3^- + \left(\frac{y}{x}\right) SD \cdot \text{NH}_4^+ + \frac{1}{2} SD \cdot \text{H}_2\text{S} + \left(\frac{z}{x}\right) SD \cdot \text{HPO}_4^{2-}$	$\frac{\nu}{a+t} \cdot [\text{CH}_2\text{O}] \cdot f_{\text{SO}_4^{2-}}$
R6	$[\text{CH}_2\text{O}] \longrightarrow \left(\frac{x-2y+4z}{2x}\right) SD \cdot \text{CO}_2 + \left(\frac{y-2z}{x}\right) SD \cdot \text{HCO}_3^- + \left(\frac{y}{x}\right) SD \cdot \text{NH}_4^+ + \frac{1}{2} SD \cdot \text{CH}_4 + \left(\frac{z}{x}\right) SD \cdot \text{HPO}_4^{2-}$	$\frac{\nu}{a+t} \cdot [\text{CH}_2\text{O}] \cdot f_{\text{CH}_4}$

Table S3. The secondary redox, precipitation, absorption and equilibrium reactions

#	Reaction	Rate expression
R7	$2\text{O}_2 + \text{NH}_4^+ + 2\text{HCO}_3^- \longrightarrow \text{NO}_3^- + 2\text{CO}_2 + 3\text{H}_2\text{O}$	$k_7[\text{O}_2][\text{NH}_4^+]$
R8	$\frac{1}{2}\text{O}_2 + \text{Mn}^{2+} + 2\text{HCO}_3^- \longrightarrow \frac{\text{MnO}_2}{SD} + 2\text{CO}_2 + \text{H}_2\text{O}$	$k_8[\text{O}_2][\text{Mn}^{2+}]$
R9	$\text{MnO}_2 + 2\text{SD} \cdot \text{Fe}^{2+} + 2\text{SD} \cdot \text{HCO}_3^- + 2\text{SD} \cdot \text{H}_2\text{O} \longrightarrow$ $2\text{Fe}(\text{OH})_3 + \text{SD} \cdot \text{Mn}^{2+} + 2\text{SD} \cdot \text{CO}_2$	$k_9[\text{Fe}^{2+}][\text{MnO}_2]$
R10	$\frac{1}{4}\text{O}_2 + \text{Fe}^{2+} + 2\text{HCO}_3^- + \frac{1}{2}\text{H}_2\text{O} \longrightarrow \frac{\text{Fe}(\text{OH})_3}{SD} + 2\text{CO}_2$	$k_{10}[\text{O}_2][\text{Fe}^{2+}]$
R11	$2\text{O}_2 + \text{H}_2\text{S} + 2\text{HCO}_3^- \longrightarrow \text{SO}_4^{2-} + 2\text{CO}_2 + 2\text{H}_2\text{O}$	$k_{11}[\text{O}_2]([\text{H}_2\text{S}] + [\text{HS}^-])$
R12	$\text{MnO}_2 + \text{SD} \cdot \text{H}_2\text{S} + 2\text{SD} \cdot \text{CO}_2 \longrightarrow$ $\text{S}^0 + \text{SD} \cdot \text{Mn}^{2+} + 2\text{SD} \cdot \text{HCO}_3^-$	$k_{12}[\text{MnO}_2]([\text{H}_2\text{S}] + [\text{HS}^-])$
R13	$2\text{Fe}(\text{OH})_3 + \text{SD} \cdot \text{H}_2\text{S} + 4\text{SD} \cdot \text{CO}_2 \longrightarrow$ $\text{S}^0 + 2\text{SD} \cdot \text{Fe}^{2+} + 4\text{SD} \cdot \text{HCO}_3^-$	$k_{13}[\text{Fe}(\text{OH})_3]([\text{H}_2\text{S}] + [\text{HS}^-])$
R14	$\text{CH}_4 + 2\text{O}_2 \longrightarrow \text{CO}_2 + 2\text{H}_2\text{O}$	$k_{14}[\text{CH}_4][\text{O}_2]$
R15	$\text{FeS} + \text{SD} \cdot \text{O}_2 \longrightarrow \text{S}^0 + \text{SD} \cdot \text{Fe}^{2+} + \text{SD} \cdot \text{SO}_4^{2-}$	$k_{15}[\text{FeS}][\text{O}_2]$
R16	$\text{Mn}^{2+} + 2\text{HCO}_3^- \longrightarrow \frac{\text{MnCO}_3}{SD} + \text{CO}_2 + \text{H}_2\text{O}$	$\begin{cases} k_{16} \left(\frac{[\text{Mn}^{2+}][\text{CO}_3^{2-}]}{K_{s,\text{MnCO}_3}} - 1 \right) & \text{if } [\text{Mn}^{2+}][\text{CO}_3^{2-}] > K_{s,\text{MnCO}_3} \\ 0 & \text{if } [\text{Mn}^{2+}][\text{CO}_3^{2-}] < K_{s,\text{MnCO}_3} \end{cases}$
R17	$\text{Fe}^{2+} + \text{H}_2\text{S} + 2\text{HCO}_3^- \longrightarrow \frac{\text{FeS}}{SD} + 2\text{CO}_2 + 2\text{H}_2\text{O}$	$\begin{cases} k_{17} \left(\frac{[\text{Fe}^{2+}][\text{HS}^-]}{[\text{H}^+]K_{s,\text{FeS}}} - 1 \right) & \text{if } \frac{[\text{Fe}^{2+}][\text{HS}^-]}{[\text{H}^+]} > K_{s,\text{FeS}} \\ 0 & \text{if } \frac{[\text{Fe}^{2+}][\text{HS}^-]}{[\text{H}^+]} < K_{s,\text{FeS}} \end{cases}$

R18	$\frac{FeS}{SD} + 2CO_2 + 2H_2O \longrightarrow Fe^{2+} + H_2S + 2HCO_3^-$	$\begin{cases} k_{18} \left(1 - \frac{[Fe^{2+}][HS^-]}{[H^+][K_sFeS]} \right) & \text{if } \frac{[Fe^{2+}][H_2S]}{[H^+]} < K_sFeS \\ 0 & \text{if } \frac{[Fe^{2+}][H_2S]}{[H^+]} > K_sFeS \end{cases}$
R19	$Fe^{2+} + 2HCO_3^- \longrightarrow FeCO_3 + CO_2 + H_2O$	$\begin{cases} k_{19} \left(\frac{[Fe^{2+}][CO_3^{2-}]}{K_sFeCO_3} - 1 \right) & \text{if } [Fe^{2+}][CO_3^{2-}] > K_sFeCO_3 \\ 0 & \text{if } [Fe^{2+}][CO_3^{2-}] < K_sFeCO_3 \end{cases}$
R20	$FeS + SD \cdot H_2S \longrightarrow FeS_2$	$k_{20}[FeS]([H_2S] + [HS^-])$
R21	$3FeS + SD \cdot S^0 \longrightarrow Fe_3S_4$	$k_{21}[FeS][S^0]$
R22	$PO_4^{3-} \longrightarrow CFA$	$\begin{cases} k_{22} ([PO_4^{3-}] - [PO_4^{3-}]^*) & \text{if } [PO_4^{3-}] > [PO_4^{3-}]^* \\ 0 & \text{if } [PO_4^{3-}] < [PO_4^{3-}]^* \end{cases}$
R23	$CaCO_3 + SD \cdot H^+ \longrightarrow SD \cdot Ca^{2+} + SD \cdot HCO_3^-$	$\begin{cases} k_{23} \left(1 - \frac{[Ca^{2+}][CO_3^{2-}]}{K_sCaCO_3} \right) & \text{if } [Ca^{2+}][CO_3^{2-}] < K_sCaCO_3 \\ 0 & \text{if } [Ca^{2+}][CO_3^{2-}] > K_sCaCO_3 \end{cases}$
R24	$Ca^{2+} + HCO_3^- \longrightarrow \frac{CaCO_3}{SD} + H^+$	$\begin{cases} k_{24} \left(\frac{[Ca^{2+}][CO_3^{2-}]}{K_sCaCO_3} - 4.5 \right) & \text{if } \frac{[Ca^{2+}][CO_3^{2-}]}{K_sCaCO_3} > 4.5 \\ 0 & \text{if } \frac{[Ca^{2+}][CO_3^{2-}]}{K_sCaCO_3} < 4.5 \end{cases}$
R25	$CH_4(g) \longrightarrow CH_4(aq)$	$\begin{cases} k_{25}[CH_4(g)]([CH_4]^* - [CH_4]) & \text{if } [CH_4] < [CH_4]^* \\ 0 & \text{if } [CH_4] > [CH_4]^* \end{cases}$
R26	$CH_4(aq) \longrightarrow CH_4(g)$	$\begin{cases} k_{26}([CH_4] - [CH_4]^*) & \text{if } [CH_4] > [CH_4]^* \\ 0 & \text{if } [CH_4] < [CH_4]^* \end{cases}$
R27	$4S^0 + 4H_2O \longrightarrow SO_4^{2-} + 3H_2S + 2H^+$	$k_{27}[S^0]$
R28	$NH_4^+(aq) \longrightarrow NH_4^+(ads)$	$k_{28}^f[NH_4^+(aq)]\varphi - k_{28}^b[NH_4^+(ads)]\varphi_s$
R29	$PO_4^{3-}(aq) \longrightarrow PO_4^{3-}(ads)$	$k_{29}^f[PO_4^{3-}(aq)]\varphi - k_{29}^b[PO_4^{3-}(ads)]\varphi_s$
R30	$Fe^{2+}(aq) \longrightarrow Fe^{2+}(ads)$	$k_{30}^f[Fe^{2+}(aq)]\varphi - k_{30}^b[Fe^{2+}(ads)]\varphi_s$

R31	$\text{FeOH}_3 + \text{PO}_4^{-3} \longrightarrow \text{PO}_4(\text{ads}_{\text{Fe}(\text{OH})_3})$	$k_{31}^f [\text{PO}_4^{3-}] [\text{Fe}(\text{OH})_3] - k_{31}^b [\text{PO}_4(\text{ads}_{\text{Fe}(\text{OH})_3})]$
R32	$\text{CO}_2 + \text{H}_2\text{O} \longrightarrow \text{H}^+ + \text{HCO}_3^-$	k_{32} thermodynamic equilibrium
R33	$\text{HCO}_3^- \longrightarrow \text{H}^+ + \text{CO}_3^{2-}$	k_{33} thermodynamic equilibrium
R34	$\text{H}_2\text{S} \longrightarrow \text{H}^+ + \text{HS}^-$	k_{34} thermodynamic equilibrium
R35	$\text{B}(\text{OH})_3 \longrightarrow \text{B}(\text{OH})_4^- + \text{H}^+$	k_{35} thermodynamic equilibrium

S5 Model validations

5 S5.1 Sediment core offshore ~~Vesterålen Archipelago~~ the Laptev Sea

Table S4. Model boundary parameters and boundary conditions for the case study of a site offshore the Laptev Sea, Russia (core 14-3). Values with (!) are set for this study. All the other variables are as in Brüchert et al. (2018) and Brüchert (2020). $[-]$ stands for lower boundary conditions (at 3 m depth), while $[+]_+$ stand for upper boundary conditions. “Extrapolation” means that the value has been extrapolated from data.

Quantity	Value	Units
$\alpha \cdot a(!)$	1100 <u>10</u>	yr
$\nu \cdot \nu(!)$	100 <u>0.200</u>	-
v_{up}	0 <u>0.0</u>	cm yr ⁻¹
$C/N \cdot 14.8 \cdot [SO_4^{2-}]_+$	28.3 <u>27.95</u>	mM
$[SO_4^{2-}]_- = [O_2]_+$	0.0 <u>326.61</u>	mM <u>μM</u>
$[CH_4]_+$	42 <u>0.0</u>	nM
$[CH_4]_- = [CH_4]_-(!)$	35 <u>16.0</u>	mM
$[CH_4]^*$	<u>14.0</u>	<u>mM</u>
$[NH_4^+]_+$	9.1 <u>8.0</u>	μ M (extrapolation)
$[NH_4^+]_- = k_{DOM}(!)$	0.227 <u>$1.0 \cdot 10^4$</u>	mM <u>$M^{-1} yr^{-1}$</u>
$k_{28}^f(!)$	<u>500</u>	<u>yr⁻¹</u>
$[PO_4^{3-}]^*(!)$	<u>75.0</u>	<u>μM</u>

- 5 **Table S5.** Organic carbon content (Brüchert, 2020) for a site offshore the Laptev Sea, Russia (core 14-3). The average density of the sediment matrix is 2.76 g cm^{-3} (Brüchert et al., 2018).

<u>Depth [cm]</u>	<u>Organic Carbon content [%]</u>
<u>3</u>	<u>0.88</u>
<u>5</u>	<u>0.29</u>
<u>7</u>	<u>0.51</u>
<u>9</u>	<u>0.84</u>
<u>11</u>	<u>0.59</u>
<u>14.5</u>	<u>0.72</u>
<u>17</u>	<u>0.74</u>
<u>19</u>	<u>0.4</u>

S6 Sensitivity study: model parameters and model boundary conditions. Tables

Table S6. Generic model parameters. The parameters below the red line at the bottom are the quantities involved in the bioenergetic formulation of AOM. Diffusion coefficients depends on temperature $T(^{\circ}\text{C})$, salinity S and porosity φ according to the relation $D(T, S, \varphi) = \frac{D(1+\mu T(^{\circ}\text{C}))}{1-\ln(\varphi^2)}$.

Quantity	Value	Units	Reference
ν	0.125	-	This study
SD	φ_s/φ	-	Athy (1930)
S	20	psu	This study
ρ	2.41	g cm^{-3}	Berg (2003)
D_b^0	29.8	$\text{cm}^2 \text{ yr}^{-1}$	Middelburg et al. (1997)
z_{bio}	5	$\text{cm}^2 \text{ yr}^{-1}$	Boudreau (1997)
z_{irr}	3.5	cm	Thullner et al. (2009)
T	0, 273.15	$^{\circ}\text{C}, \text{K}$	This study
C:N	106:16	-	Redfield ratio
C:P	106:1	-	Redfield ratio
$D_{\text{O}_2}, \mu_{\text{O}_2}$	380.45, 0.06	$\text{cm}^2 \text{ yr}^{-1}, \text{T}^{-1}$	Dale et al. (2012)
$D_{\text{NO}_3^-}, \mu_{\text{NO}_3^-}$	394.59, 0.038	$\text{cm}^2 \text{ yr}^{-1}, \text{T}^{-1}$	Van Cappellen and Wang (1996)

$D_{\text{SO}_4^{2-}}, \mu_{\text{SO}_4^{2-}}$	173.92, 0.045	$\text{cm}^2 \text{ yr}^{-1}, \text{ T}^{-1}$	Dale et al. (2012)
$D_{\text{CH}_4}, \mu_{\text{CH}_4}$	263.94, 0.052	$\text{cm}^2 \text{ yr}^{-1}, \text{ T}^{-1}$	Van Cappellen and Wang (1996)
$D_{\text{NH}_4^+}, \mu_{\text{NH}_4^+}$	395.87, 0.041	$\text{cm}^2 \text{ yr}^{-1}, \text{ T}^{-1}$	Van Cappellen and Wang (1996)
$D_{\text{PO}_4^{3-}}, \mu_{\text{PO}_4^{3-}}$	112.36, 0.054	$\text{cm}^2 \text{ yr}^{-1}, \text{ T}^{-1}$	Van Cappellen and Wang (1996)
$D_{\text{Mn}^{2+}}, \mu_{\text{Mn}^{2+}}$	123.39, 0.05	$\text{cm}^2 \text{ yr}^{-1}, \text{ T}^{-1}$	Van Cappellen and Wang (1996)
$D_{\text{Fe}^{2+}}, \mu_{\text{Fe}^{2+}}$	136.24, 0.044	$\text{cm}^2 \text{ yr}^{-1}, \text{ T}^{-1}$	Dale et al. (2012)
$D_{\text{H}_2\text{S}}, \mu_{\text{H}_2\text{S}}$	331.61, 0.06	$\text{cm}^2 \text{ yr}^{-1}, \text{ T}^{-1}$	Van Cappellen and Wang (1996)
$D_{\text{HS}^-}, \mu_{\text{HS}^-}$	392.02, 0.031	$\text{cm}^2 \text{ yr}^{-1}, \text{ T}^{-1}$	Van Cappellen and Wang (1996)
$D_{\text{CH}_4(\text{g})}, \mu_{\text{CH}_4(\text{g})}$	5000.0, 0.0	$\text{cm}^2 \text{ yr}^{-1}, \text{ T}^{-1}$	Van Cappellen and Wang (1996)
$D_{\text{H}_2\text{CO}_3}, \mu_{\text{H}_2\text{CO}_3}$	320.04, 0.06	$\text{cm}^2 \text{ yr}^{-1}, \text{ T}^{-1}$	Van Cappellen and Wang (1996)
$D_{\text{HCO}_3^-}, \mu_{\text{HCO}_3^-}$	217.22, 0.048	$\text{cm}^2 \text{ yr}^{-1}, \text{ T}^{-1}$	Van Cappellen and Wang (1996)
$D_{\text{CO}_3^{2-}}, \mu_{\text{CO}_3^{2-}}$	176.09, 0.047	$\text{cm}^2 \text{ yr}^{-1}, \text{ T}^{-1}$	Van Cappellen and Wang (1996)
$D_{\text{B}(\text{OH})_3}, \mu_{\text{B}(\text{OH})_3}$	110.05, 0.054	$\text{cm}^2 \text{ yr}^{-1}, \text{ T}^{-1}$	Van Cappellen and Wang (1996)
$D_{\text{B}(\text{OH})_4^-}, \mu_{\text{B}(\text{OH})_4^-}$	96.30, 0.041	$\text{cm}^2 \text{ yr}^{-1}, \text{ T}^{-1}$	Van Cappellen and Wang (1996)
$D_{\text{H}^+}, \mu_{\text{H}^+}$	600.0, 0.05	$\text{cm}^2 \text{ yr}^{-1}, \text{ T}^{-1}$	Van Cappellen and Wang (1996)
$D_{\text{Ca}^{2+}}, \mu_{\text{Ca}^{2+}}$	150.38, 0.045	$\text{cm}^2 \text{ yr}^{-1}, \text{ T}^{-1}$	Van Cappellen and Wang (1996)
$D_{\text{S}^0}, \mu_{\text{S}^0}$	173.92, 0.045	$\text{cm}^2 \text{ yr}^{-1}, \text{ T}^{-1}$	Van Cappellen and Wang (1996)
φ_0	0.45	-	LaRowe et al. (2017)
c_0	$0.5 \cdot 10^{-3}$	m^{-1}	LaRowe et al. (2017)
φ_∞	0.35	-	This study
K_{O_2}	8	μM	Thullner et al. (2009)
$K_{\text{NO}_3^-}$	5	μM	Van Cappellen and Wang (1996)
K_{MnO_2}	2	$\mu\text{mol/g}_d$	Thullner et al. (2009)
$K_{\text{Fe}(\text{OH})_3}$	5	$\mu\text{mol/g}_d$	Thullner et al. (2009)
$K_{\text{SO}_4^{2-}}$	100	μM	Dale et al. (2006)
k_7	$1.0 \cdot 10^7$	$\text{cm}^3 \text{ mol}^{-1} \text{ yr}^{-1}$	Van Cappellen and Wang (1996)
k_8	$2.0 \cdot 10^9$	$\text{M}^{-1} \text{ yr}^{-1}$	Thullner et al. (2009)
k_9	$2.0 \cdot 10^8$	$\text{M}^{-1} \text{ yr}^{-1}$	Thullner et al. (2009)
k_{10}	$1.0 \cdot 10^{11}$	$\text{cm}^3 \text{ mol}^{-1} \text{ yr}^{-1}$	Van Cappellen and Wang (1996)
k_{11}	$1.0 \cdot 10^9$	$\text{cm}^3 \text{ mol}^{-1} \text{ yr}^{-1}$	Van Cappellen and Wang (1996)
k_{12}	$1.0 \cdot 10^4$	$\text{M}^{-1} \text{ yr}^{-1}$	Thullner et al. (2009)
k_{13}	$1.0 \cdot 10^4$	$\text{M}^{-1} \text{ yr}^{-1}$	Thullner et al. (2009)
k_{14}	$1.0 \cdot 10^{13}$	$\text{cm}^3 \text{ mol}^{-1} \text{ yr}^{-1}$	Van Cappellen and Wang (1996)

k_{15}	$1.0 \cdot 10^9$	$\text{cm}^3 \text{mol}^{-1} \text{yr}^{-1}$	Van Cappellen and Wang (1996)
k_{16}	$1.0 \cdot 10^{-8}$	$\text{mol cm}^{-3} \text{yr}^{-1}$	Van Cappellen and Wang (1996)
k_{17}	$5 \cdot 10^{-9}$	$\text{mol cm}^{-3} \text{yr}^{-1}$	Van Cappellen and Wang (1996)
k_{18}	$1.0 \cdot 10^{-3}$	$\text{mol cm}^{-3} \text{yr}^{-1}$	Van Cappellen and Wang (1996)
k_{19}	$1.0 \cdot 10^{-9}$	$\text{mol cm}^{-3} \text{yr}^{-1}$	Van Cappellen and Wang (1996)
k_{20}	$6.0 \cdot 10^7$	$\text{cm}^3 \text{mol}^{-1} \text{yr}^{-1}$	Van Cappellen and Wang (1996)
k_{21}	$2.4 \cdot 10^4$	$\text{cm}^3 \text{mol}^{-1} \text{yr}^{-1}$	Van Cappellen and Wang (1996)
k_{22}	1	yr^{-1}	Van Cappellen and Wang (1996)
k_{23}	0.1	$\text{mol cm}^{-3} \text{yr}^{-1}$	Van Cappellen and Wang (1996)
k_{24}	24.16	$\text{M}^{-1} \text{yr}^{-1}$	Wallmann et al. (2006)
k_{25}	$1.0 \cdot 10^9$	$\text{cm}^3 \text{mol}^{-1} \text{yr}^{-1}$	Van Cappellen and Wang (1996)
k_{26}	$7.89 \cdot 10^2$	yr^{-1}	Pauss et al. (1990)
k_{27}	$1.0 \cdot 10^{-3}$	yr^{-1}	Van Cappellen and Wang (1996)
k_{28}^f	1.6	yr^{-1}	Van Cappellen and Wang (1996)
k_{28}^b	1.0	yr^{-1}	Van Cappellen and Wang (1996)
k_{29}^f	1.8	yr^{-1}	Van Cappellen and Wang (1996)
k_{29}^b	1.0	yr^{-1}	Van Cappellen and Wang (1996)
k_{30}^f	400	yr^{-1}	Van Cappellen and Wang (1996)
k_{30}^b	1.0	yr^{-1}	Van Cappellen and Wang (1996)
k_{31}^f	100	yr^{-1}	Van Cappellen and Wang (1996)
k_{31}^b	1.0	yr^{-1}	Van Cappellen and Wang (1996)
k_{32}	$8.470 \cdot 10^{-7}$	M	Millero (1995)
k_{33}	$4.300 \cdot 10^{-10}$	M	Millero (1995)
k_{34}	$1.602 \cdot 10^{-7}$	M	Millero (1995)
k_{35}	$1.318 \cdot 10^{-9}$	M	Millero (1995)
$[\text{CH}_4]^*$	5.46	mM	Dale et al. (2008a)
$[\text{PO}_4^{3-}]^*$	10	μM	This study
$K_{s\text{MnCO}_3}$	$3.2 \cdot 10^{-9}$	M^2	Van Cappellen and Wang (1996)
$K_{s\text{FeCO}_3}$	$4.0 \cdot 10^{-9}$	M^2	Van Cappellen and Wang (1996)
$K_{s\text{FeS}}$	$8.2 \cdot 10^{-4}$	M	Van Cappellen and Wang (1996)
$K_{s\text{CaCO}_3}$	$3.8 \cdot 10^{-7}$	M^2	Mucci (1983); Millero (1995)
μ_g	18.3	yr^{-1}	Dale et al. (2006, 2008b)
μ_d	0.1	yr^{-1}	Dale et al. (2006, 2008b)

γ	2.48	-	Dale et al. (2006, 2008b)
χ	8.0	-	Dale et al. (2006, 2008b)
ΔG_{BQ}	20	kJ/mol e ⁻	Dale et al. (2006, 2008b)
ΔG_r^0	-29.92	kJ/mol e ⁻	Regnier et al. (2011)
$K_m^{\text{CH}_4}$	$1.5 \cdot 10^{-3}$	M	Dale et al. (2006, 2008b)
$K_m^{\text{SO}_4^{2-}}$	$1.0 \cdot 10^{-3}$	M	Dale et al. (2006, 2008b)

Table S7. Generic model upper boundary conditions. The boundary condition for biomass is applied only in the bioenergetic formulation of AOM

Species	Value @ SWI	Units	Reference
POC	1.04	%	This study
O ₂	306.98	μM	Garcia et al. (2010a)
NO ₃ ⁻	11.51	μM	Garcia et al. (2010b)
MnO ₂	2.18	$\mu\text{mol cm}^{-2} \text{yr}^{-1}$	Dale et al. (2015); Glasby (2006)
Fe(OH) ₃	7.09	$\mu\text{mol cm}^{-2} \text{yr}^{-1}$	Dale et al. (2015); Glasby (2006)
SO ₄ ²⁻	28.0	mM	Thullner et al. (2009)
CH ₄	0.0	mM	This study
NH ₄ ⁺	0.0	mM	This study
PO ₄ ³⁻	1.0	μM	Sales de Freitas (2018)
Mn ²⁺	1.0	μM	Sales de Freitas (2018)
Fe ²⁺	1.0	pM	Sales de Freitas (2018)
H ₂ S	0.835	nM	Sales de Freitas (2018)
HS ⁻	9.17	nM	Sales de Freitas (2018)
CH ₄ (g)	0.0	nM	This study
H ₂ CO ₃	39	μM	Sales de Freitas (2018)
HCO ₃ ⁻	2150	μM	Sales de Freitas (2018)
CO ₃ ²⁻	15.3	μM	Sales de Freitas (2018)
B(OH) ₃	363.6	μM	Sales de Freitas (2018)
B(OH) ₄ ⁻	61.4	μM	Sales de Freitas (2018)
H ⁺	6.31	μM	Sales de Freitas (2018)
CaCO ₃	23	$\mu\text{mol cm}^{-2} \text{yr}^{-1}$	Sales de Freitas (2018)

Ca ²⁺	9.7	mM	Sales de Freitas (2018)
NH ₄ ⁺ (ads)	0	mM	Sales de Freitas (2018)
PO ₄ ³⁻ (ads)	0	mM	Sales de Freitas (2018)
FeS	0	$\mu\text{mol cm}^{-2} \text{yr}^{-1}$	Sales de Freitas (2018)
FeCO ₃	0	mM	Sales de Freitas (2018)
S ⁰	0	mM	Sales de Freitas (2018)
FeS ₂	0	$\mu\text{mol cm}^{-2} \text{yr}^{-1}$	Sales de Freitas (2018)
Fe ²⁺ (ads)	0	mM	Sales de Freitas (2018)
PO ₄ (ads _{Fe(OH)₃})	0	Mm	Sales de Freitas (2018)
B	$1.0 \cdot 10^8, 3.158 \cdot 10^7$	$\text{mol cm}^{-3}, \text{cells cm}^{-3}$	This study

Table S8. Name, location, water depth and linear sedimentation rate for cores used to inter- and extra-polate the sedimentation rates to the whole Laptev sea area via simple 3D kriging.

Core name	Lon (°)	Lat (°)	Water depth (m)	ω (cm/yr)	Reference
KD9502-14	133.117	76.192	46	0.003	Bauch et al. (2001)
PM9462-4	136.005	74.503	27	0.05	Bauch et al. (2001)
PM9499-2	115.545	75.501	48	0.004	Bauch et al. (2001)
PM9402-3	115.249	75.491	47	0.16	Strobl et al. (1998)
PM9417-4	130.014	75.503	51	0.08	Strobl et al. (1998)
PM9442-3	126.003	74.501	40	0.13	Strobl et al. (1998)
PM9462-1	136.004	74.502	27	0.12	Strobl et al. (1998)
PM9463-8	126.582	74.504	36	0.35	Strobl et al. (1998)
PM9481-2	134.004	73.750	17	0.17	Strobl et al. (1998)
PM9482-1	128.175	73.999	27	0.39	Strobl et al. (1998)
PS51/080-13	131.638	73.459	21	0.028	Bauch et al. (2001)
PS51/092-13	130.136	74.594	32	0.07	Bauch et al. (2001)
PS51/092-12	130.138	74.593	32	0.041	Bauch et al. (2001)
PS51/118-2	132.237	77.892	114	0.002	Bauch et al. (2001)
PS51/118-3	132.199	77.892	122	0.008	Bauch et al. (2001)
PS51/135-4	133.243	76.165	51	0.031	Bauch et al. (2001)

PS51/141-2	128.641	75.227	42	0.011	Bauch et al. (2001)
PS51/154-11	120.610	77.276	270	0.012	Bauch et al. (2001)
PS51/159-10	116.032	76.767	60	0.011	Bauch et al. (2001)
PS2458-4	133.398	78.167	983	0.027	Bauch et al. (2001)
L13-09-2	129.895	73.018	10	0.45	Han (2014)
L13-14-2	130.695	73.857	25	0.16	Han (2014)
L13-18-2	130.479	73.032	16	0.3	Han (2014)
L13-04-2	130.690	71.902	15	0.2	Han (2014)
C-37	130.367	71.617	10	0.024	Stein and Fahl (2000)
C-4	131.000	73.167	26	0.17	Stein and Fahl (2000)
C-7	129.983	74.883	37	0.159	Stein and Fahl (2000)
C-8	130.500	75.400	48	0.015	Stein and Fahl (2000)
C-11	130.083	76.867	66	0.011	Stein and Fahl (2000)
PS2725-5	144.135	78.656	77	0.013	Stein et al. (2001)
PS2778-2	113.065	77.978	341	0.038	Stein et al. (2001)
PS2476-4	118.193	77.39	521	0.05	Stein et al. (2001)
PS2742-5	103.815	80.788	1890	0.022	Stein et al. (2001)
PS2474-3	118.575	77.67	1494	0.02	Stein et al. (2001)
PS2741-1	105.395	81.105	2400	0.012	Stein et al. (2001)
PS2471-4	119.793	79.152	3047	0.002	Stein et al. (2001)

S6.1 Sensitivity study: model parameters and model boundary conditions. Figures

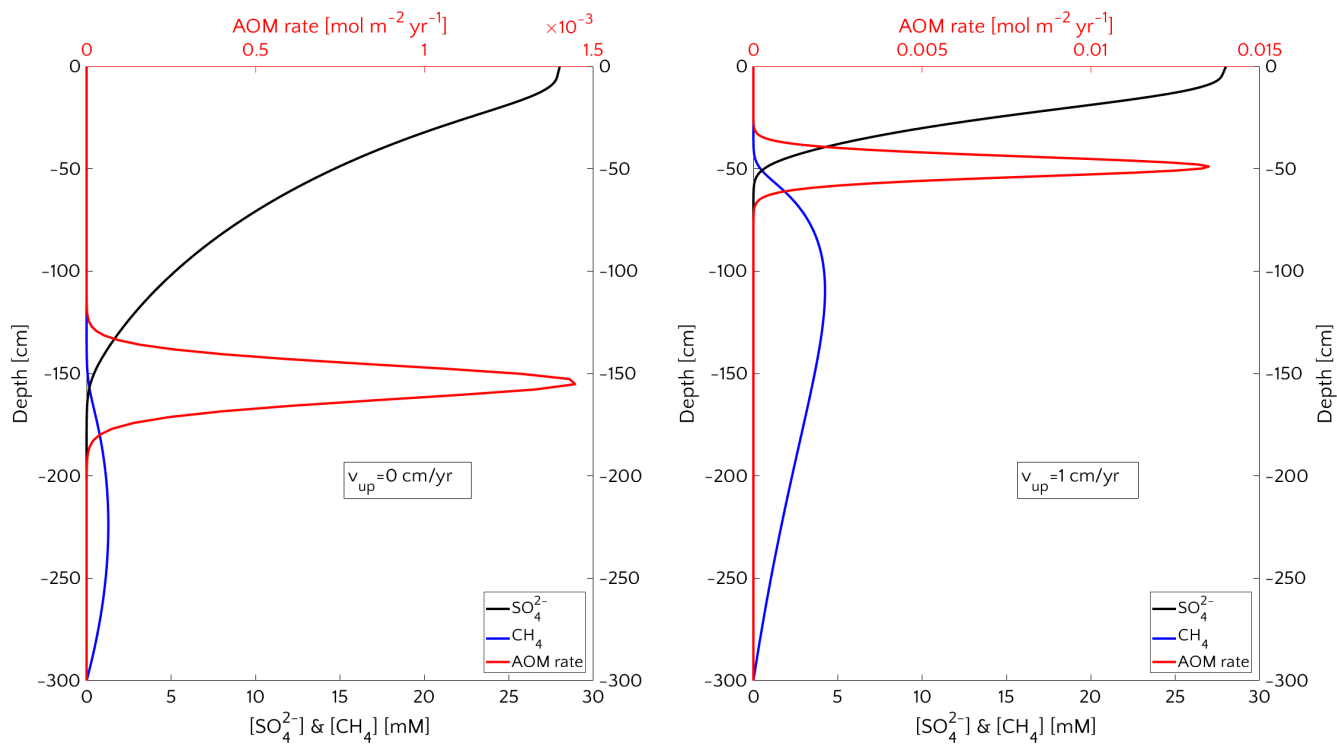


Figure S1. Outcomes for the baseline simulations at steady state. Passive case (left) and active case with $v_{up} = 1$ cm/yr (right). Typical SMTZ shoaling (from 155.2 cm to 48.9 cm) and squeezing (from 65 cm to 38 cm) from passive to active case.

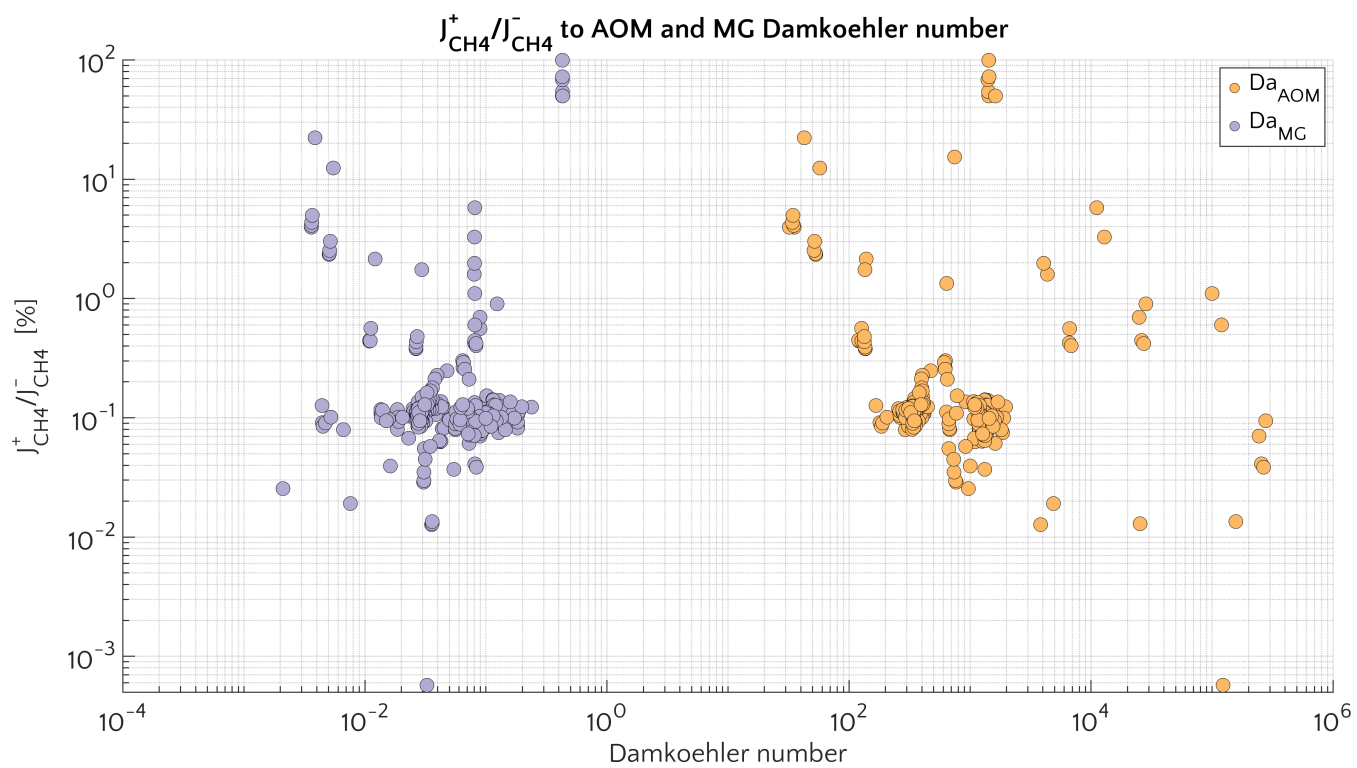


Figure S2. Ratio $J_{CH_4}^+ / J_{CH_4}^-$ (in %) as a function of the Damköhler numbers for AOM (orange) and for methanogenesis (purple)

AOM efficiency vs. sedimentation rate ω

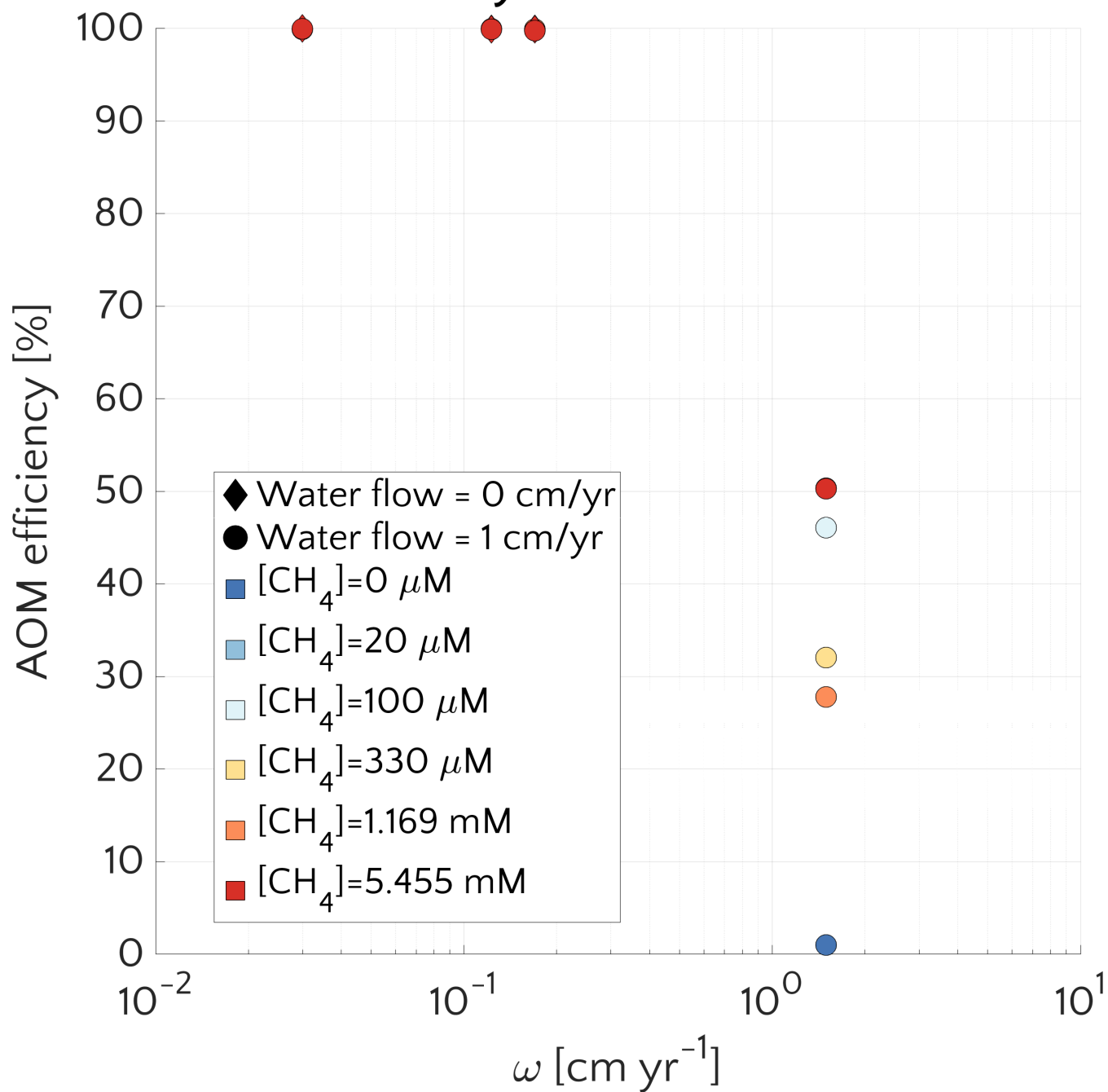


Figure S3. AOM filter efficiency η versus ω for passive cases (diamonds) and active cases (circles).

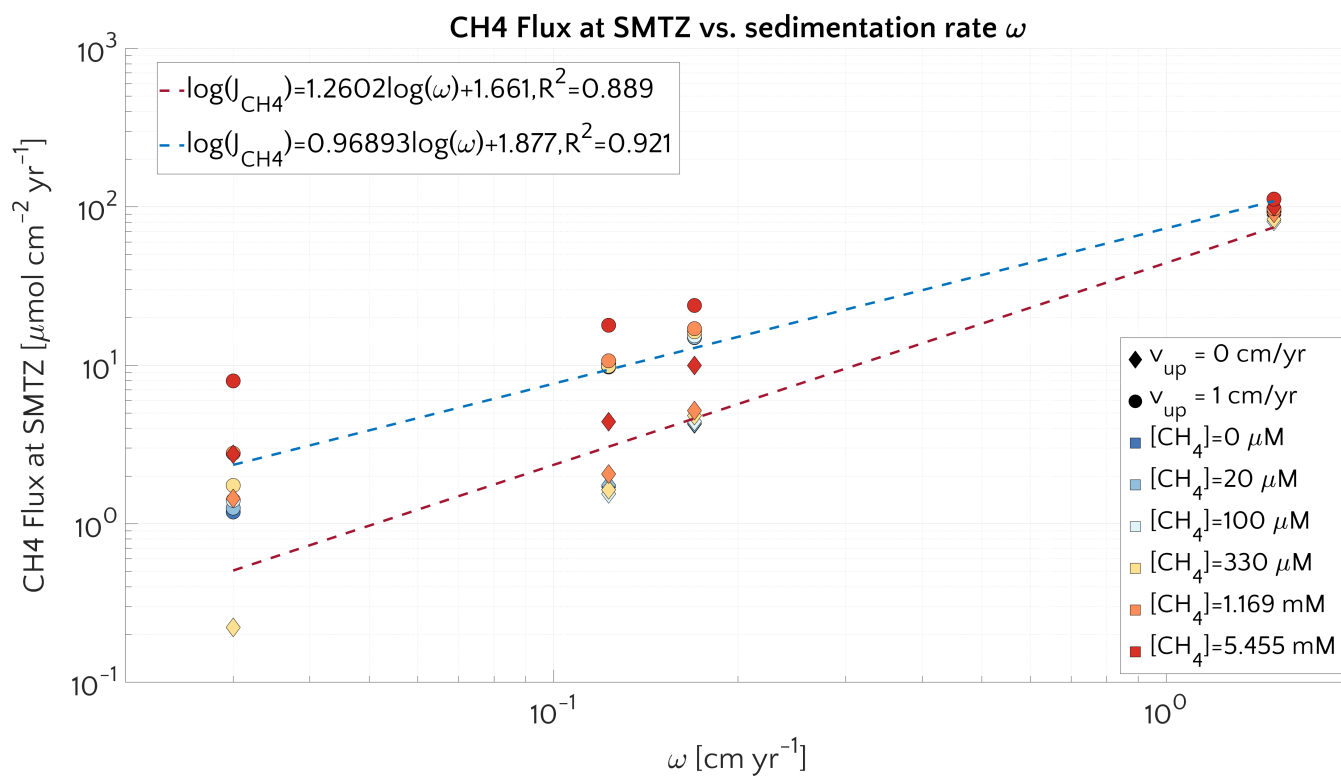


Figure S4. Methane flux at the centre of SMTZ versus ω for passive (diamonds) and active (circle) cases. Log-log fit is reported.

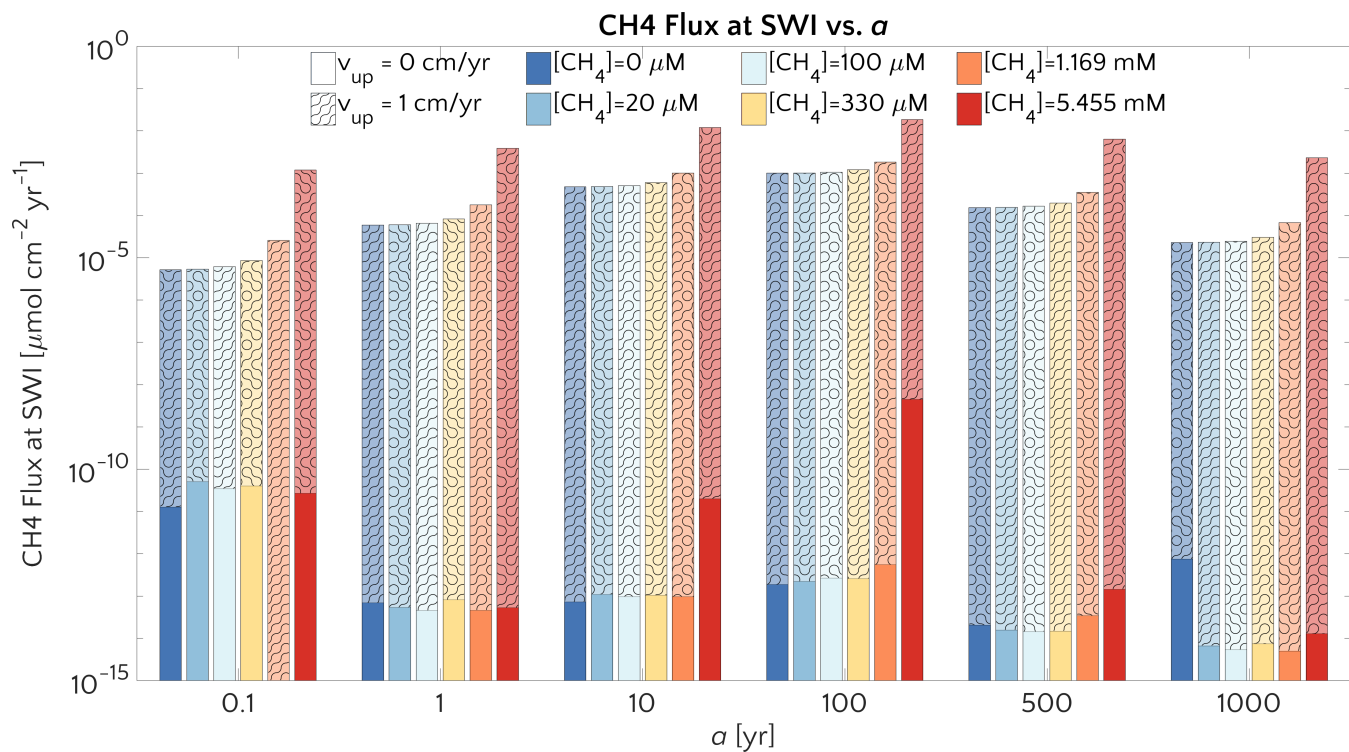


Figure S5. Barplot of the methane flux at the SWI versus a for passive case (plain) and active case (pattern) and the $[\text{CH}_4]_0$ reported in the text.

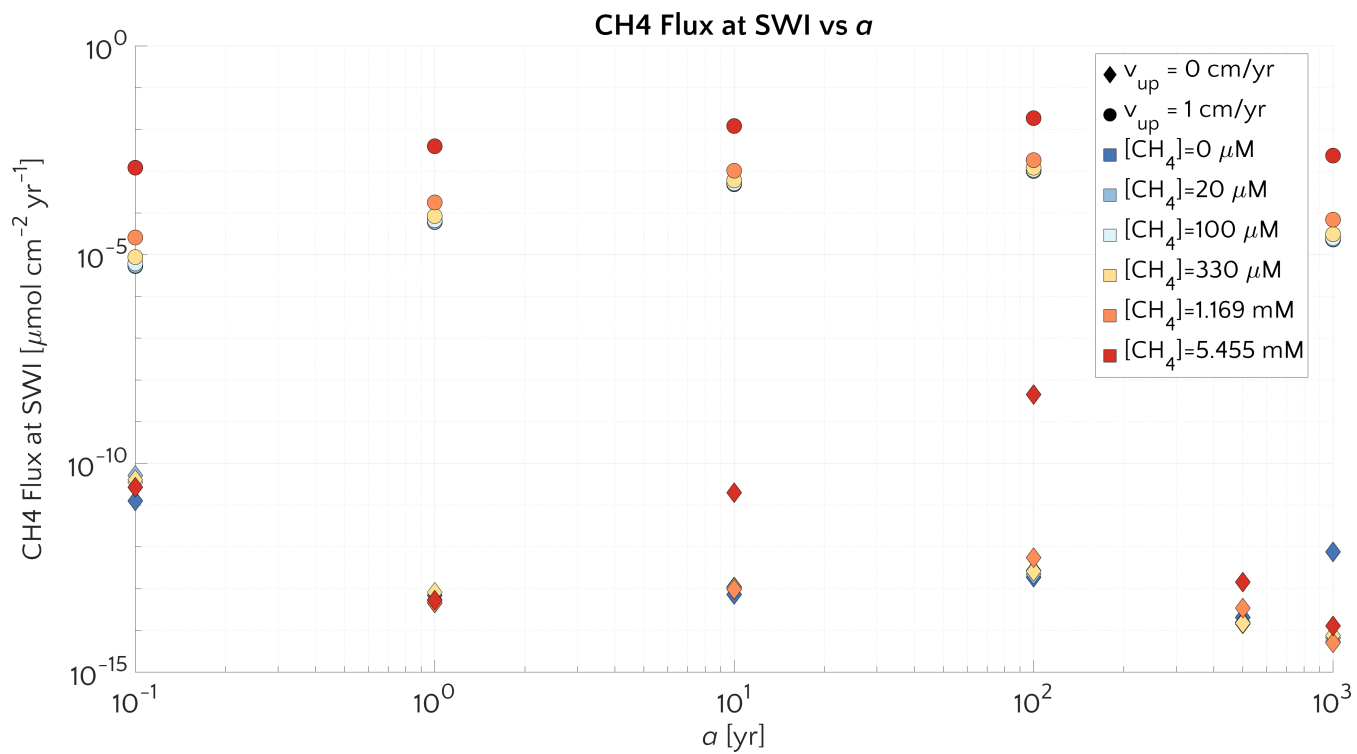


Figure S6. Methane flux at SWI versus a for passive (diamonds) and active (circle) cases.

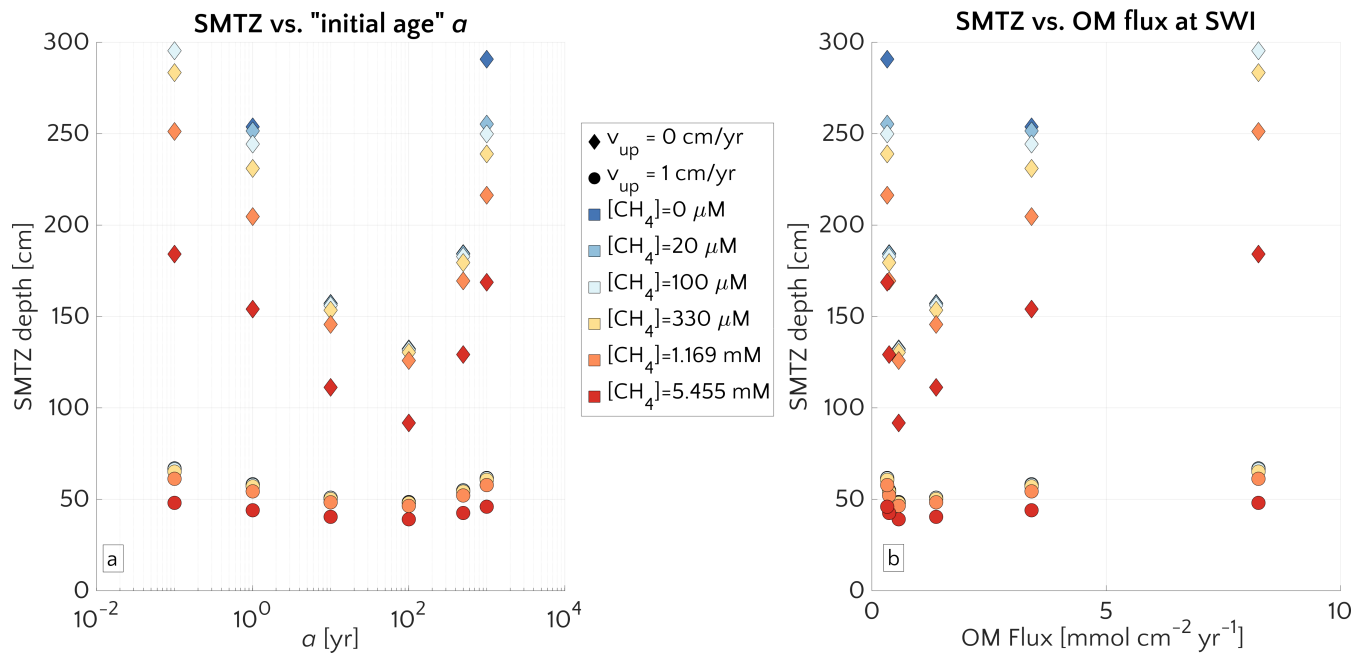


Figure S7. (a) SMTZ depth versus a . Passive (diamonds) and active (circle) cases for different $[CH_4]$. (b) SMTZ depth versus OM flux entering the system at the SWI.

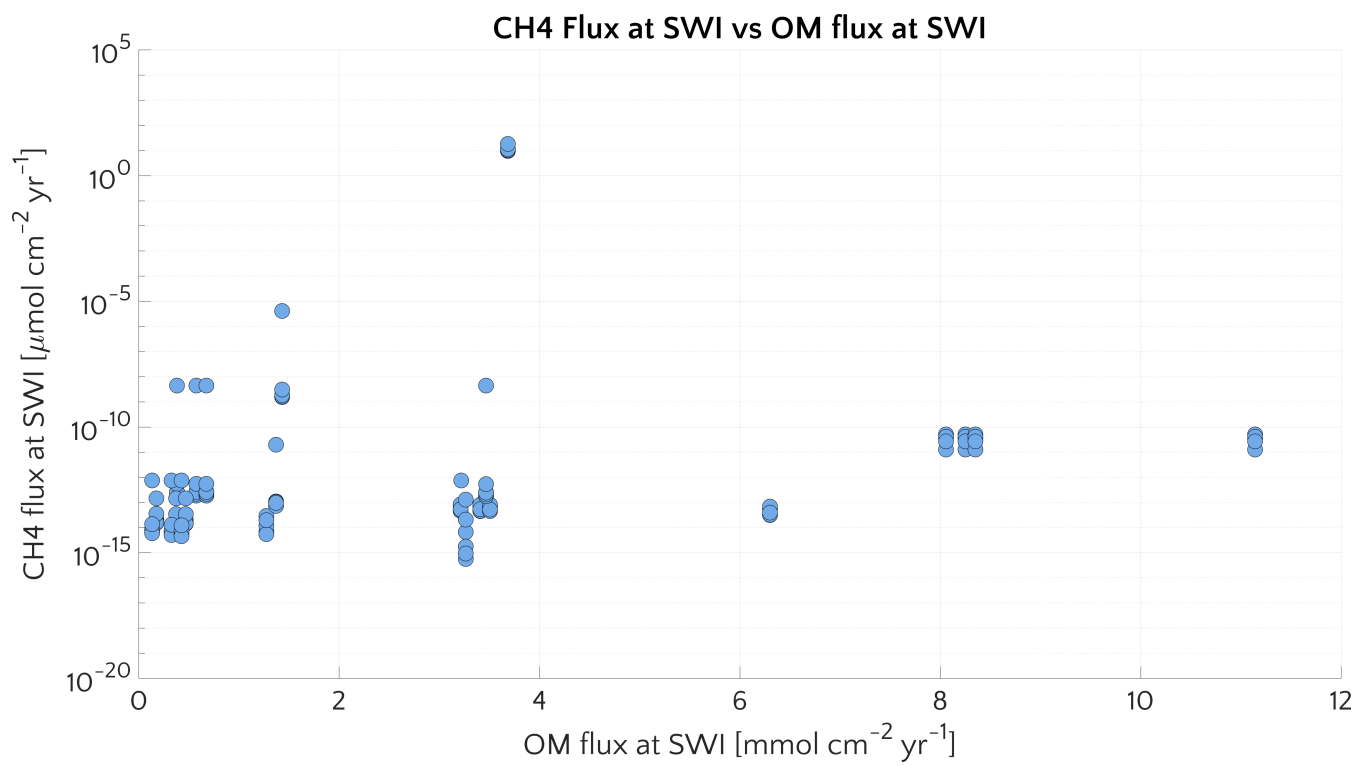
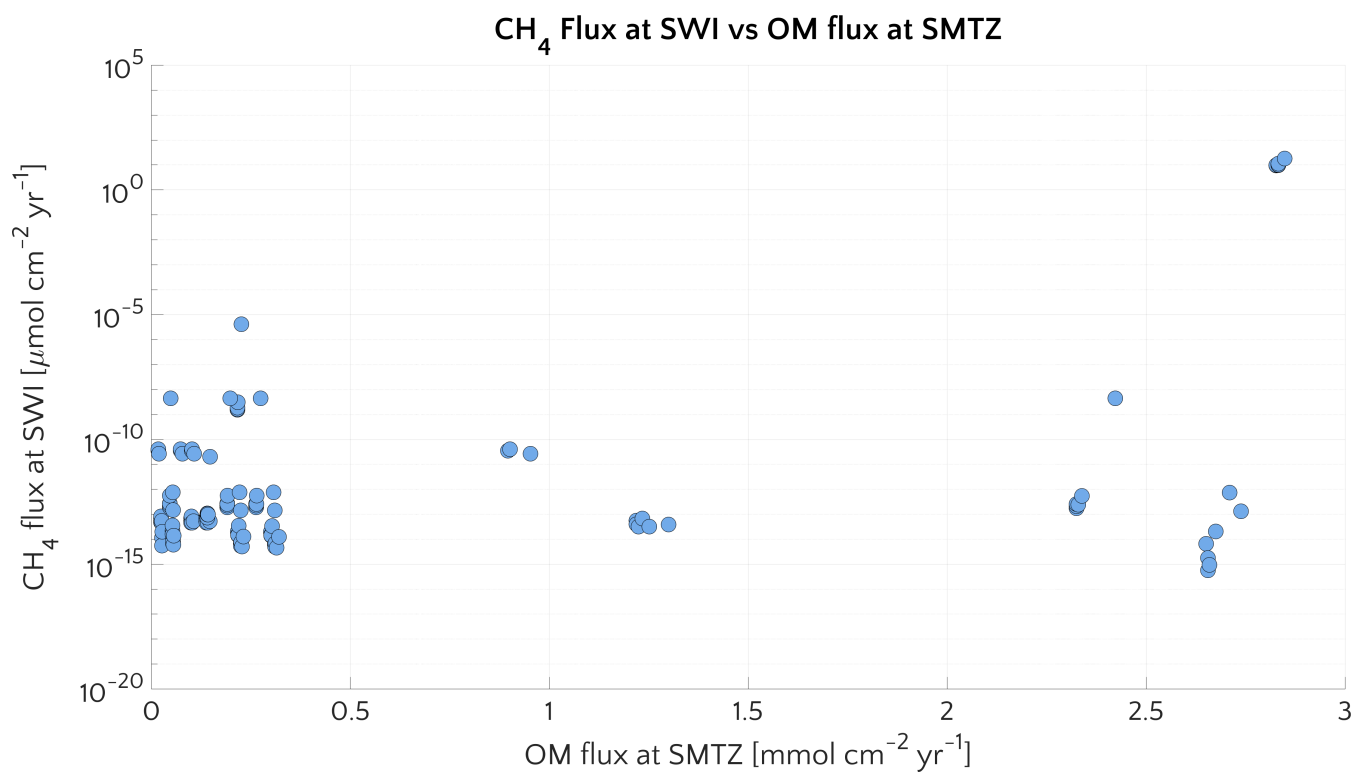


Figure S8. Methane flux at SWI versus OM flux at SWI



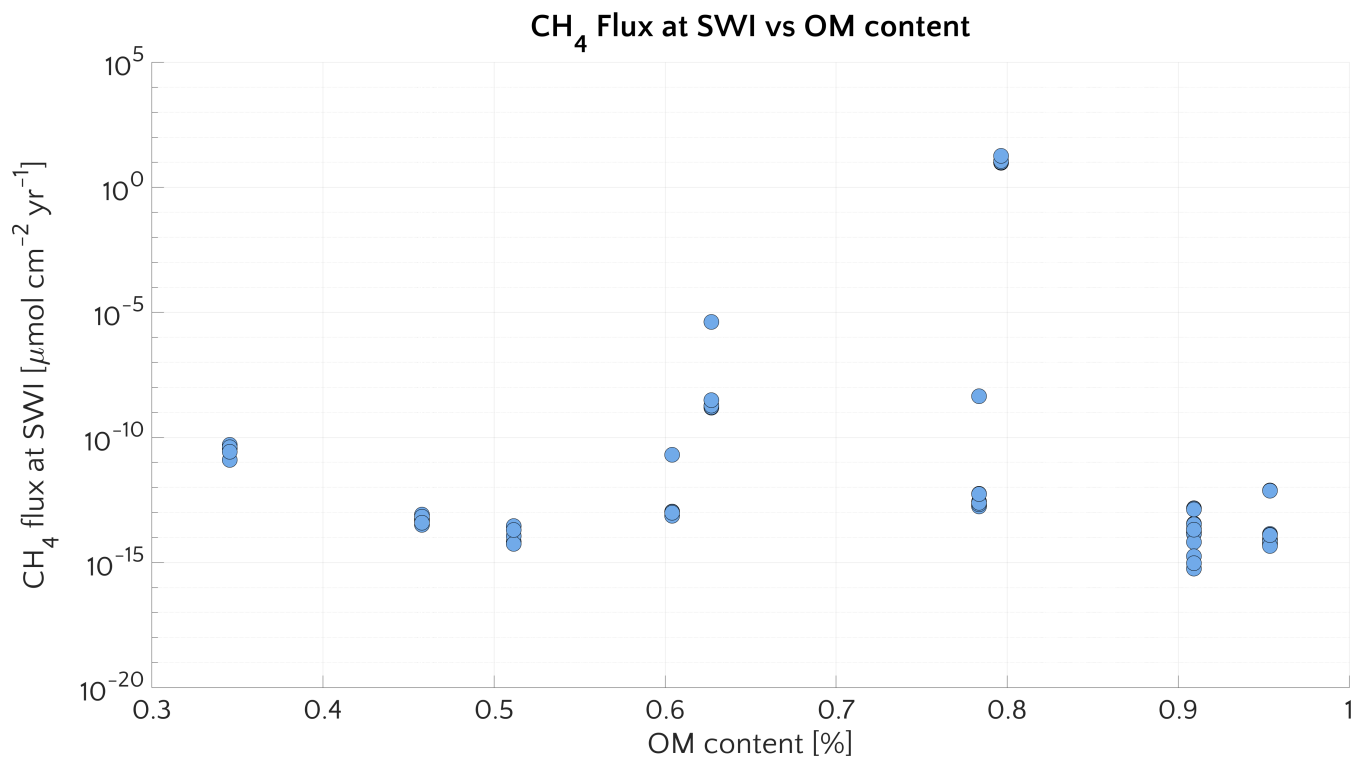


Figure S10. Methane flux at SWI versus OM sediment content

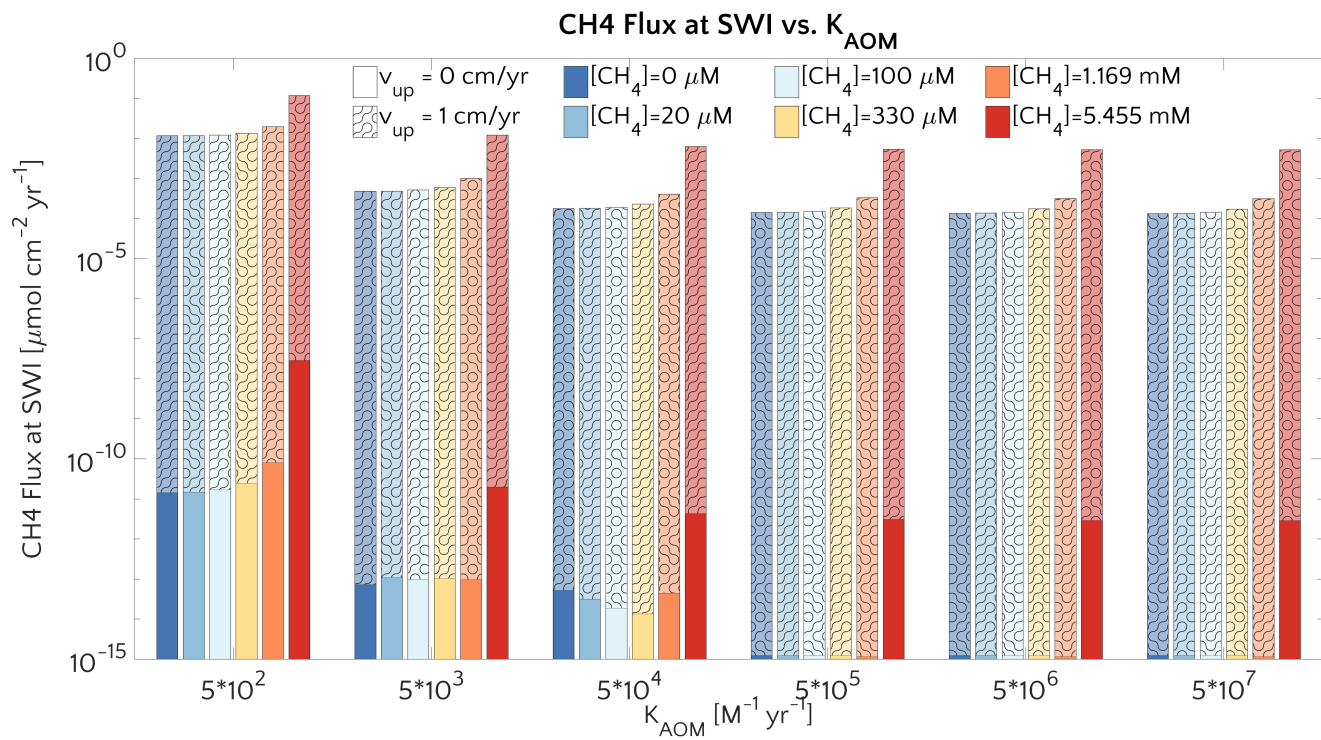


Figure S11. Methane flux at SWI versus AOM reactivity constant k_{AOM}

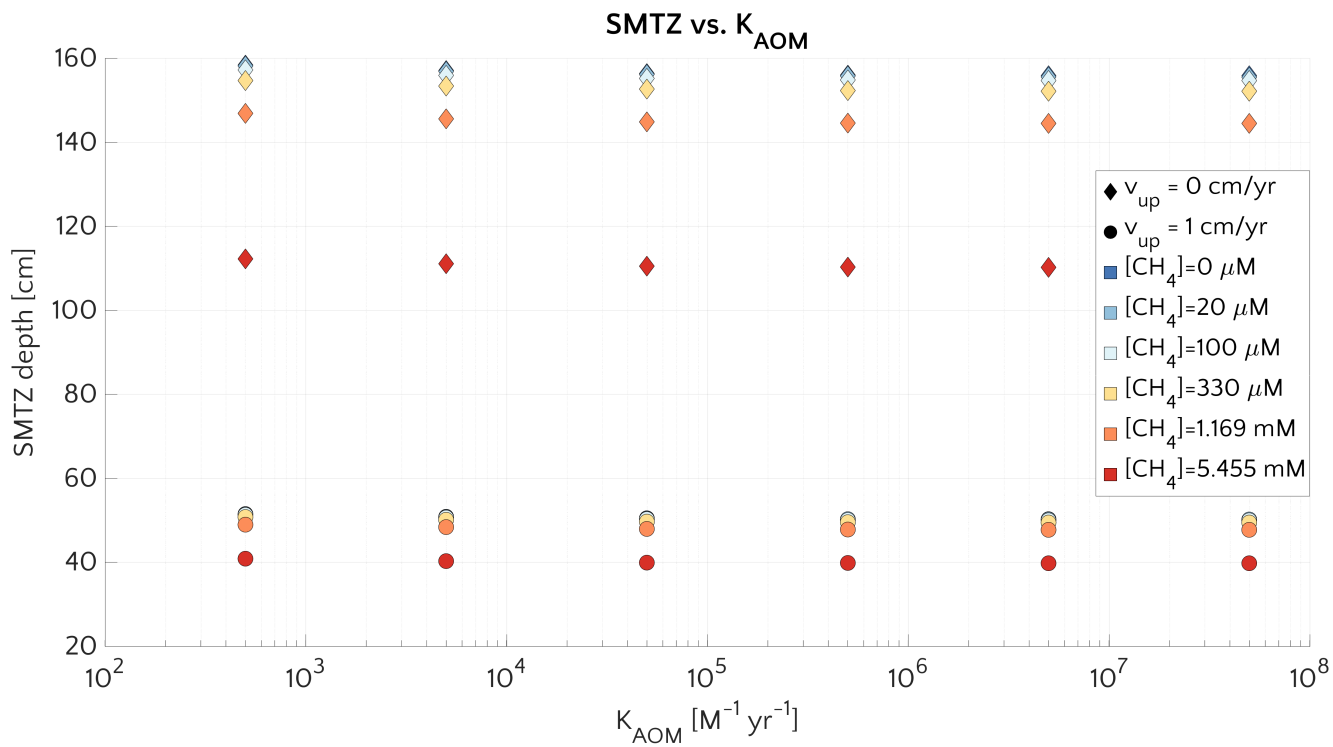


Figure S12. SMTZ depth versus k_{AOM} . Passive (diamonds) and active (circle) cases for different $[CH_4]_{-}$.

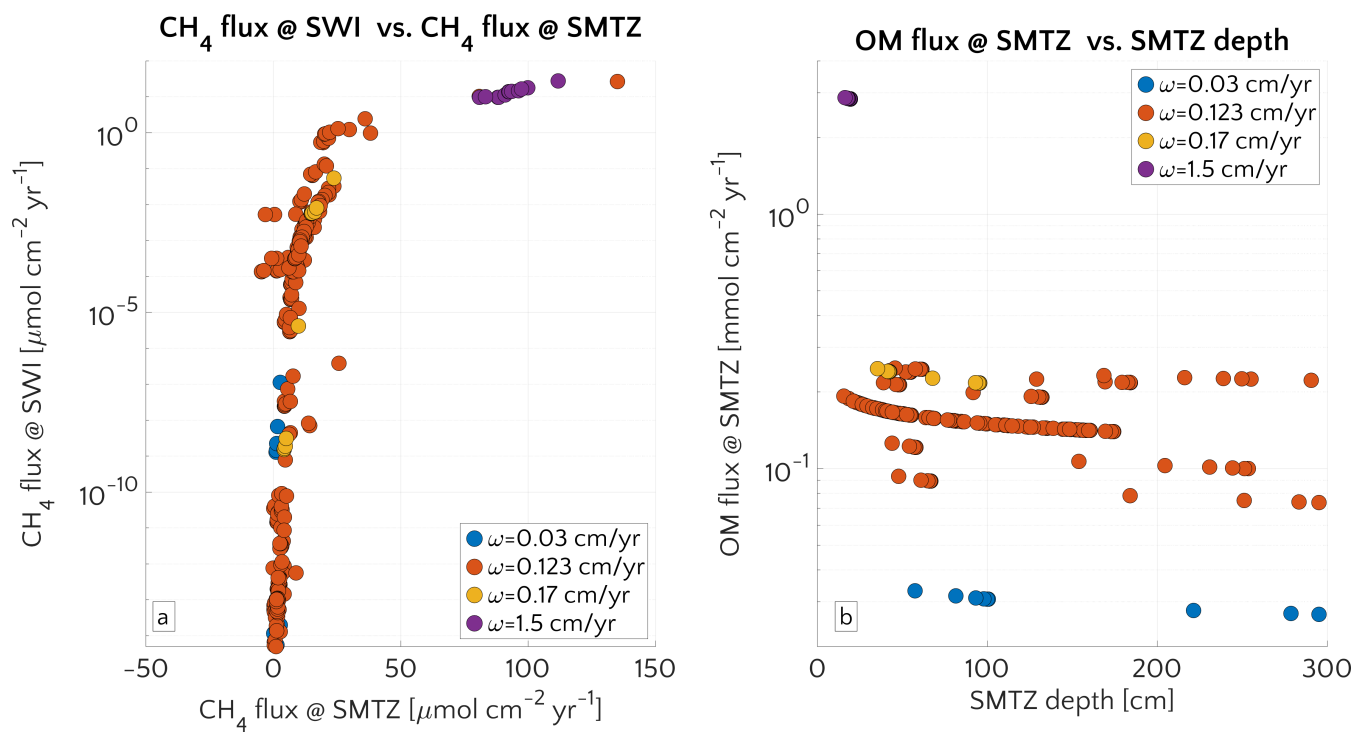


Figure S13. *a.* Flux of methane at SWI versus flux of methane at the SMTZ depth. *b.* OM flux at the SMTZ depth versus SMTZ depth itself. Colours identify simulations with different ω .

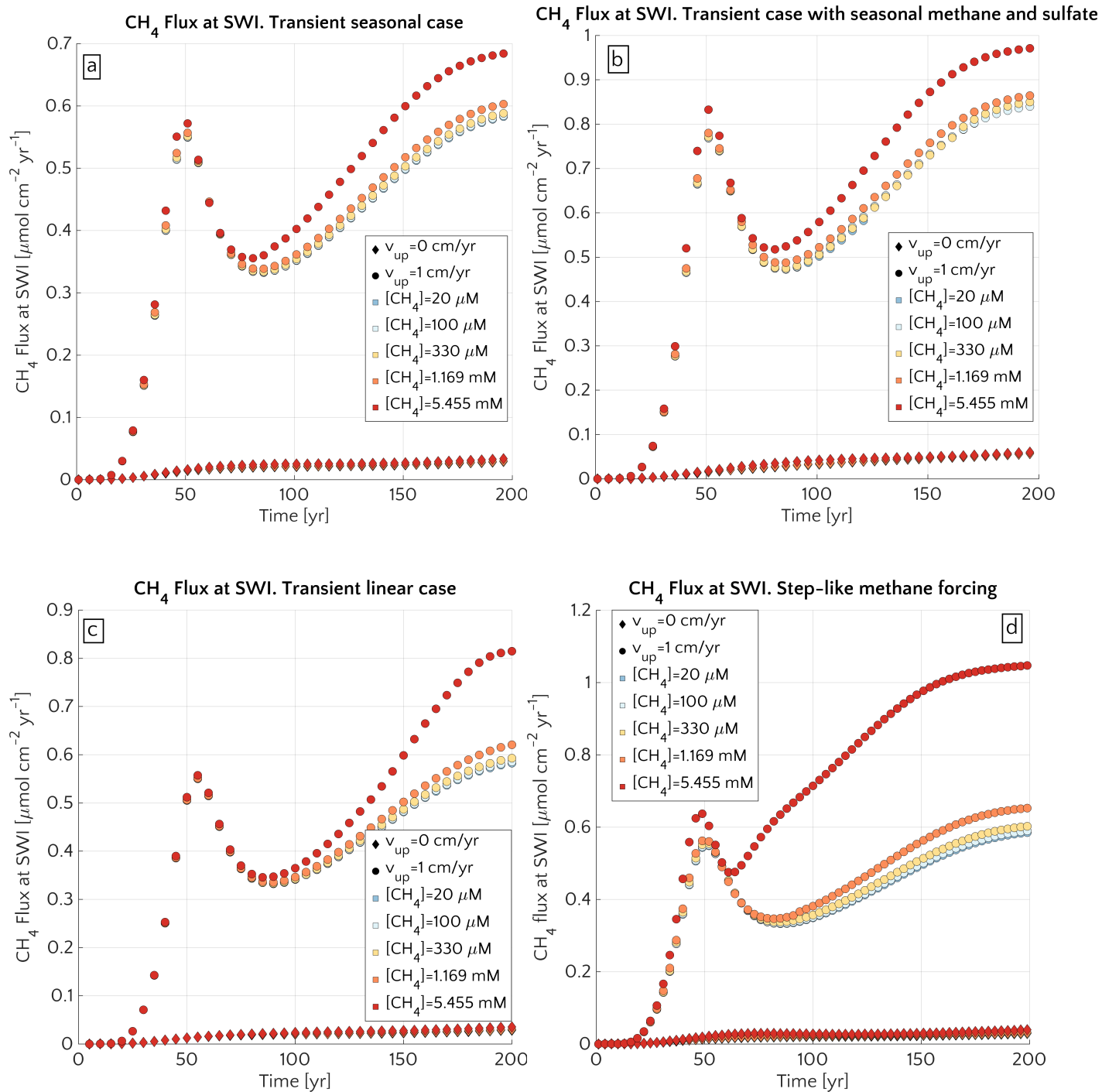


Figure S14. Flux of methane at SWI over time for passive (diamonds) and active (circle) setups and different $[CH_4]_0$. *a.* Seasonal methane forcing from below. *b.* Seasonal methane forcing from below and seasonal sulfate forcing from above. *c.* Linear methane forcing from below. *d.* Step-like methane forcing from below.

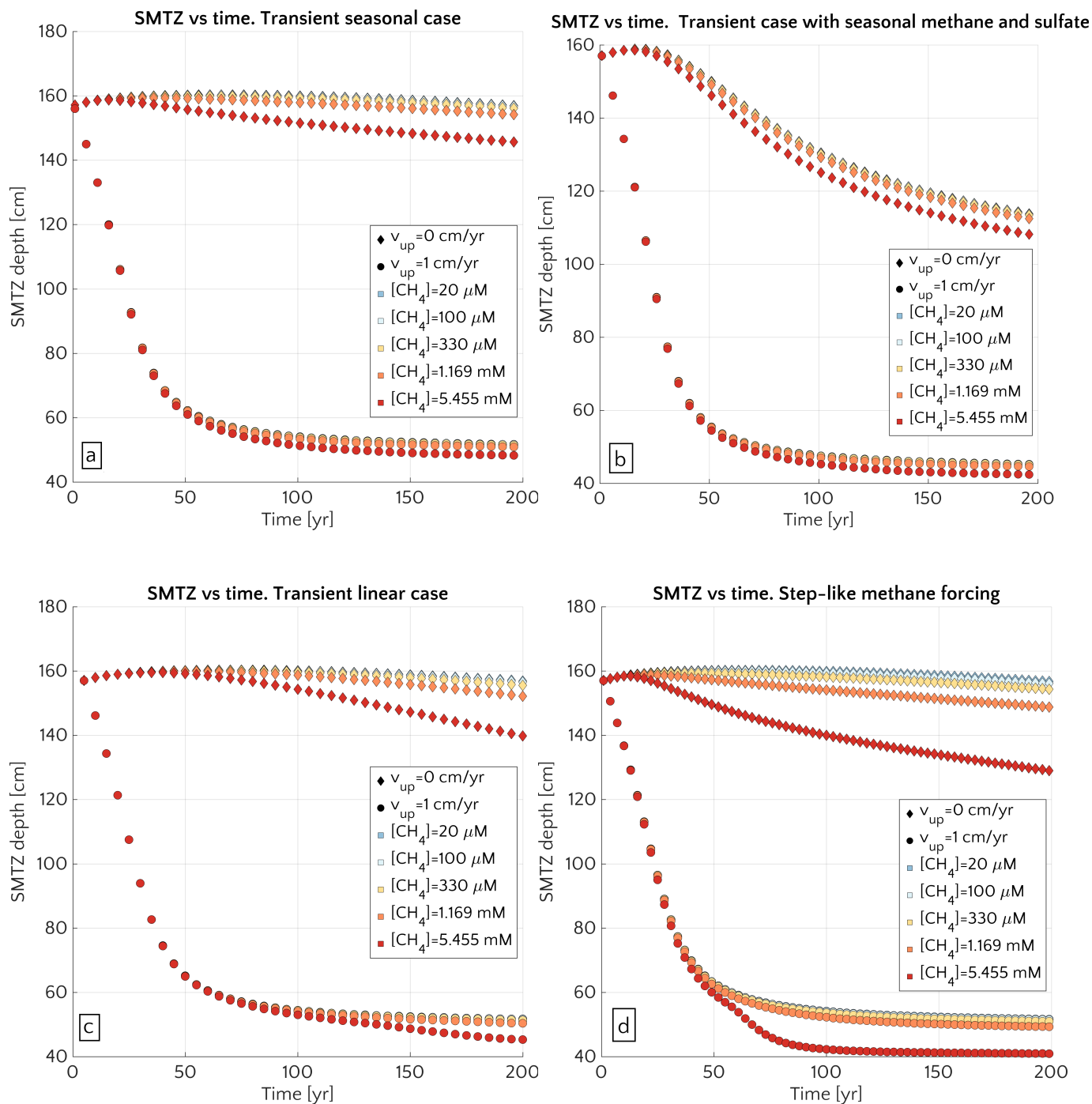


Figure S15. Movement of SMTZ over time for passive (diamonds) and active (circle) setups and different $[CH_4]$. *a.* Seasonal methane forcing from below. *b.* Seasonal methane forcing from below and seasonal sulfate forcing from above. *c.* Linear methane forcing from below. *d.* Step-like methane forcing from below.

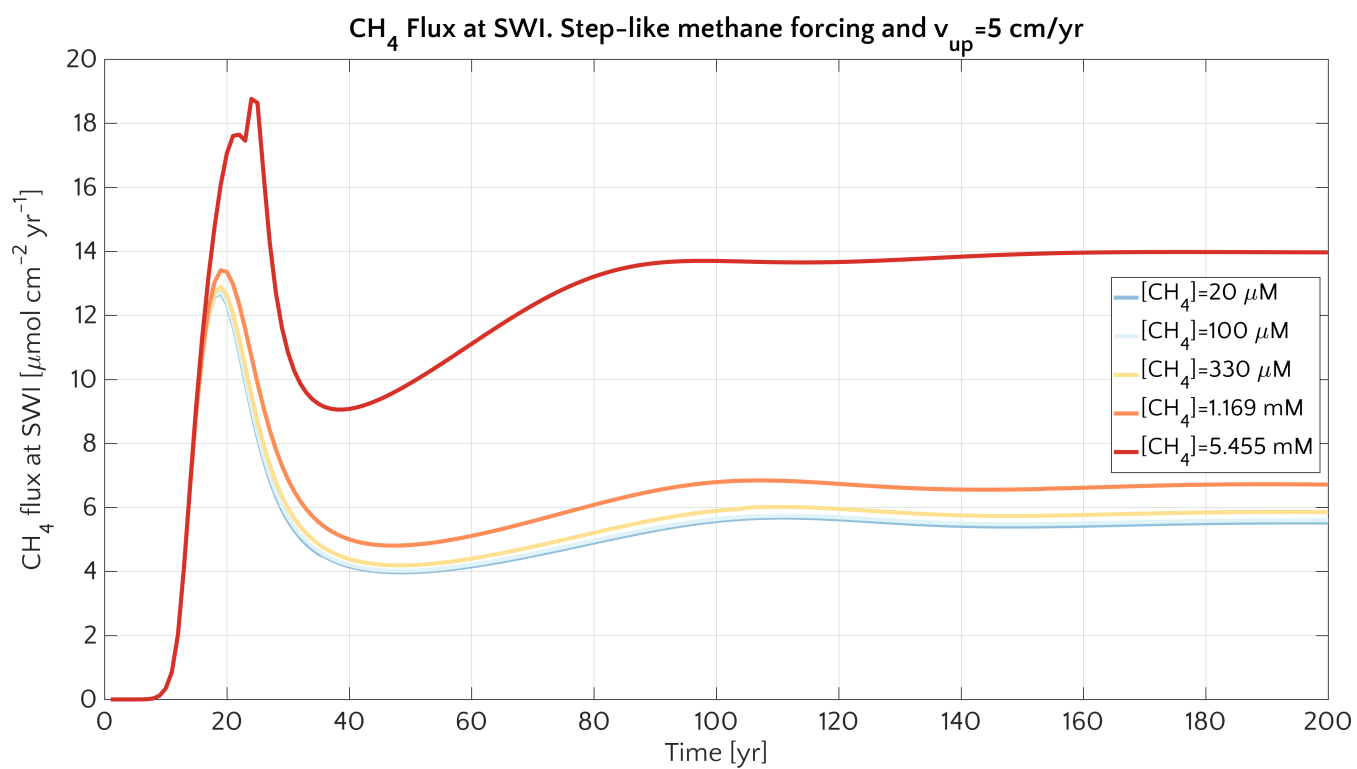


Figure S16. Flux of methane at SWI versus time for scenario 4 (step-like methane increase) and $v_{up} = 5$ cm/yr. Colours identify simulations with different CH₄ bottom concentrations.

Integrated AOM vs bottom CH_4 concentration

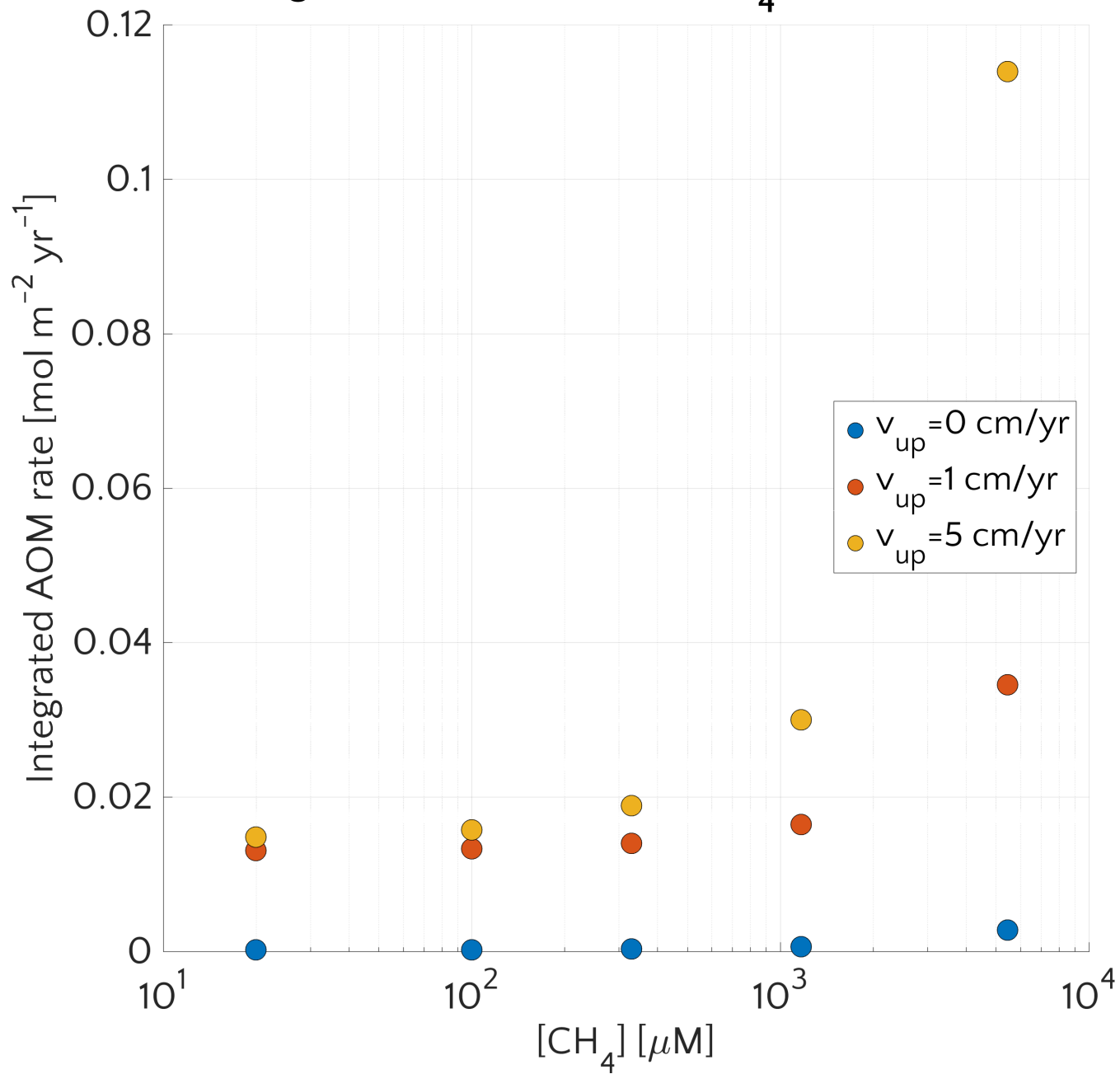


Figure S17. Vertically integrated AOM vs the bottom methane concentration $[\text{CH}_4]_{-}$ for three different v_{up} .

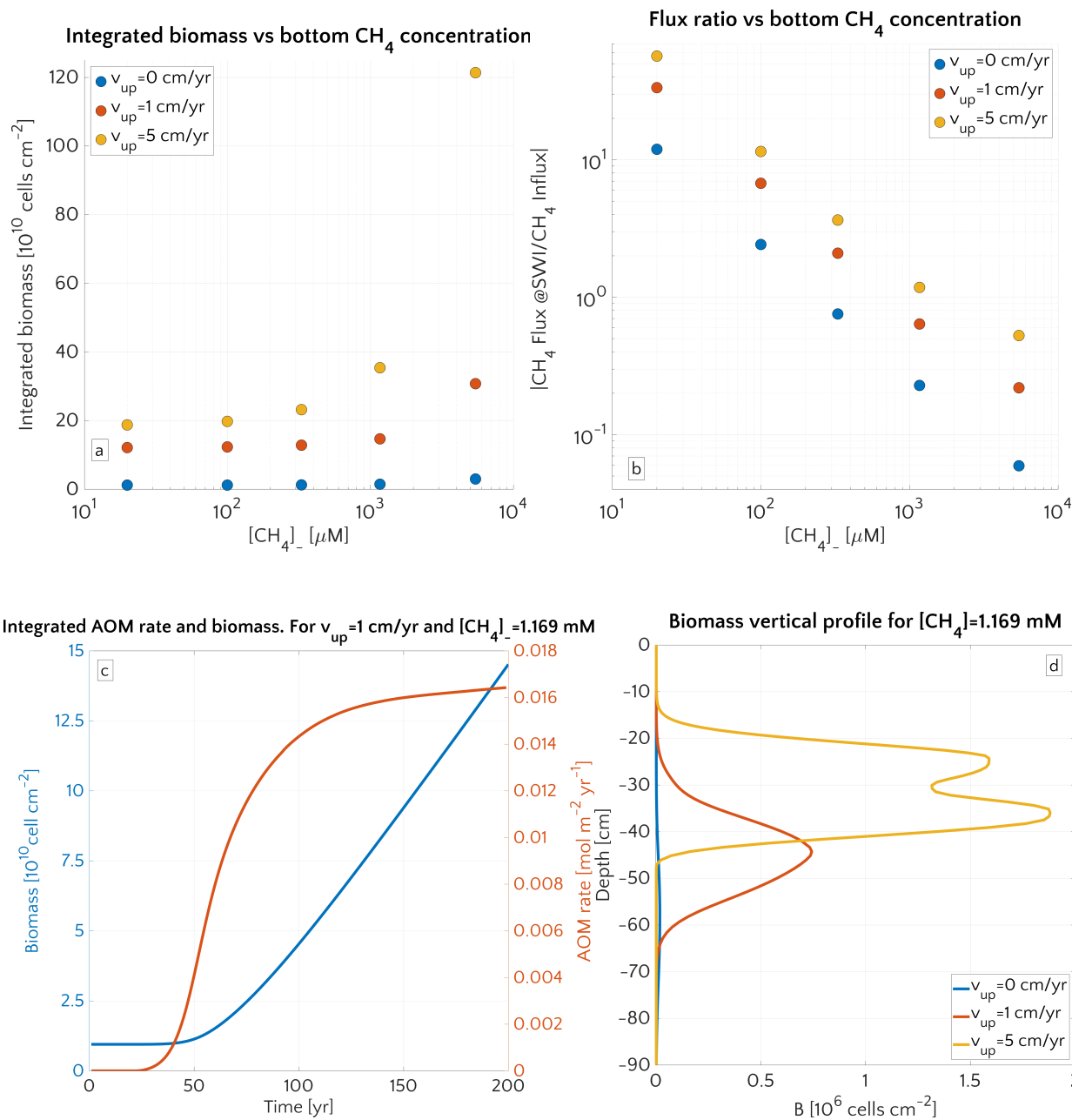


Figure S18. *a.* Vertically integrated biomass after 200 years vs the bottom methane concentration $[\text{CH}_4]_-$ for three different v_{up} . *b.* Absolute value of the ratio of the methane flux at the SWI to the advective methane flux at the base of sediment column vs the bottom methane concentration $[\text{CH}_4]_-$ for three different v_{up} . *c.* Time evolution of the vertically integrated AOM biomass (blue) and vertically integrated AOM rate (red) for the step-like simulation with $[\text{CH}_4]_- = 1.169$ mM and $v_{up} = 1$ cm/yr. *d.* AOM biomass vertical profile after 200 years for three different v_{up} in case of step-like simulation with $[\text{CH}_4]_- = 1.169$ mM.

5 References

- Aller, R. C. and Blair, N. E.: Early diagenetic remineralization of sedimentary organic C in the Gulf of Papua deltaic complex (Papua New Guinea): net loss of terrestrial C and diagenetic fractionation of C isotopes, *Geochimica et Cosmochimica Acta*, 68, 1815–1825, 2004.
- Arndt, S., Jørgensen, B. B., LaRowe, D. E., Middelburg, J., Pancost, R., and Regnier, P.: Quantifying the degradation of organic matter in marine sediments: a review and synthesis, *Earth-science reviews*, 123, 53–86, 2013.
- 10 Athy, L. F.: Density, porosity, and compaction of sedimentary rocks, *AAPG Bulletin*, 14, 1–24, 1930.
- Bauch, H. A., Mueller-Lupp, T., Taldenkova, E., Spielhagen, R. F., Kassens, H., Grootes, P. M., Thiede, J., Heinemeier, J., and Petryashov, V.: Chronology of the Holocene transgression at the North Siberian margin, *Global and Planetary Change*, 31, 125–139, 2001.
- Berg, P.: Dynamic Modeling of Early Diagenesis and Nutrient Cycling. A Case Study in an Arctic Marine Sediment, *American Journal of Science*, 303, 905–955, 2003.
- 15 Berner, R. A.: *Early diagenesis: a theoretical approach*, 1, Princeton University Press, 1980.
- Boudreau, B. P.: *Diagenetic models and their implementation*, vol. 505, Springer Berlin, 1997.
- Boudreau, B. P. and Ruddick, B. R.: On a reactive continuum representation of organic matter diagenesis, *American Journal of Science*, 291, 507–538, 1991.
- Brüchert, V.: Unpublished raw data, 2020.
- 20 Brüchert, V., Bröder, L., Sawicka, J. E., Tesi, T., Joye, S. P., Sun, X., Semiletov, I. P., and Samarkin, V. A.: Carbon mineralization in Laptev and East Siberian sea shelf and slope sediment, *Biogeosciences*, 15, 471–490, 2018.
- Claypool, G. E. and Kaplan, I.: The origin and distribution of methane in marine sediments, in: *Natural gases in marine sediments*, pp. 99–139, Springer, 1974.
- Dale, A. W., Regnier, P., and Van Cappellen, P.: Bioenergetic controls on anaerobic oxidation of methane (AOM) in coastal marine sediments: a theoretical analysis, *American Journal of Science*, 306, 246–294, 2006.
- 25 Dale, A. W., Aguilera, D., Regnier, P., Fossing, H., Knab, N., and Jørgensen, B. B.: Seasonal dynamics of the depth and rate of anaerobic oxidation of methane in Aarhus Bay (Denmark) sediments, *Journal of Marine Research*, 66, 127–155, 2008a.
- Dale, A. W., Van Cappellen, P., Aguilera, D., and Regnier, P.: Methane efflux from marine sediments in passive and active margins: Estimations from bioenergetic reaction–transport simulations, *Earth and Planetary Science Letters*, 265, 329–344, 2008b.
- 30 Dale, A. W., Meyers, S. R., Aguilera, D. R., Arndt, S., and Wallmann, K.: Controls on organic carbon and molybdenum accumulation in Cretaceous marine sediments from the Cenomanian–Turonian interval including Oceanic Anoxic Event 2, *Chemical Geology*, 324–325, 28–45, 2012.
- Dale, A. W., Nickelsen, L., Scholz, F., Hensen, C., Oschlies, A., and Wallmann, K.: A revised global estimate of dissolved iron fluxes from marine sediments, *Global Biogeochemical Cycles*, 29, 691–707, <https://doi.org/10.1002/2014gb005017>, <https://doi.org/10.1002/2014gb005017>, 2015.
- 35 Froelich, P., Klinkhammer, G., Bender, M. L., Luedtke, N., Heath, G. R., Cullen, D., Dauphin, P., Hammond, D., Hartman, B., and Maynard, V.: Early oxidation of organic matter in pelagic sediments of the eastern equatorial Atlantic: suboxic diagenesis, *Geochimica et cosmochimica acta*, 43, 1075–1090, 1979.
- Garcia, H. E., Boyer, T. P., Locarnini, R. A., Antonov, J. I., Mishonov, A. V., Baranova, O. K., Zweng, M. M., Reagan, J. R., Johnson, D. R., and Levitus, S.: *World Ocean Atlas 2009, Volume 3: Dissolved Oxygen, Apparent Oxygen Utilization, and Oxygen Saturation*, 2010a.

- 5 Garcia, H. E., Locarnini, R. A., Boyer, T. P., Antonov, J. I., Baranova, O. K., Zweng, M. M., Reagan, J. R., Johnson, D. R., Mishonov, A. V., and Levitus, S.: World Ocean Atlas 2009, Volume 4: Nutrients (phosphate, nitrate, silicate), 2010b.
- Glasby, G. P.: Manganese: predominant role of nodules and crusts, in: Marine geochemistry, pp. 371–427, Springer, 2006.
- Han, P.: Characteristics and sedimentation rates at the shallow Laptev Sea, Master's thesis, University of Bremen, 2014.
- LaRowe, D. E., Burwicz, E., Arndt, S., Dale, A. W., and Amend, J. P.: Temperature and volume of global marine sediments, *Geology*, 45, 275–278, 2017.
- Meile, C. and Van Cappellen, P.: Particle age distributions and O₂ exposure times: Timescales in bioturbated sediments, *Global biogeochemical cycles*, 19, 2005.
- Middelburg, J. J., Soetaert, K., and Herman, P. M.: Empirical relationships for use in global diagenetic models, *Deep Sea Research Part I: Oceanographic Research Papers*, 44, 327–344, 1997.
- 15 Millero, F. J.: Thermodynamics of the carbon dioxide system in the oceans, *Geochimica et Cosmochimica Acta*, 59, 661–677, [https://doi.org/10.1016/0016-7037\(94\)00354-o](https://doi.org/10.1016/0016-7037(94)00354-o), <https://doi.org/10.1016%2F0016-7037%2894%2900354-o>, 1995.
- Mucci, A.: The solubility of calcite and aragonite in seawater at various salinities, temperatures, and one atmosphere total pressure, *American Journal of Science*, 283, 780–799, <https://doi.org/10.2475/ajs.283.7.780>, <https://doi.org/10.2475%2Fajs.283.7.780>, 1983.
- Pauss, A., Andre, G., Perrier, M., and Guiot, S. R.: Liquid-to-gas mass transfer in anaerobic processes: inevitable transfer limitations of methane and hydrogen in the biomethanation process, *Appl. Environ. Microbiol.*, 56, 1636–1644, 1990.
- 20 Regnier, P., Dale, A. W., Arndt, S., LaRowe, D., Mogollón, J., and Van Cappellen, P.: Quantitative analysis of anaerobic oxidation of methane (AOM) in marine sediments: a modeling perspective, *Earth-Science Reviews*, 106, 105–130, 2011.
- Sales de Freitas, F.: Deciphering the relationships between reactivity and sources of organic matter in marine sediments: a coupled large-scale model and lipid biomarker analysis, Ph.D. thesis, School on Earth Sciences, University of Bristol, 2018.
- 25 Stein, R. and Fahl, K.: Holocene accumulation of organic carbon at the Laptev Sea continental margin (Arctic Ocean): sources, pathways, and sinks, *Geo-Marine Letters*, 20, 27–36, <https://doi.org/10.1007/s003670000028>, <https://doi.org/10.1007%2Fs003670000028>, 2000.
- Stein, R., Boucsein, B., Fahl, K., de Oteyza, T. G., Knies, J., and Niessen, F.: Accumulation of particulate organic carbon at the Eurasian continental margin during late Quaternary times: controlling mechanisms and paleoenvironmental significance, *Global and Planetary Change*, 31, 87–104, 2001.
- 30 Strobl, C., Schulz, V., Vogler, S., Baumann, S., Kassens, H., Kubik, P., Suter, M., and Mangini, A.: Determination of depositional beryllium-10 fluxes in the area of the Laptev Sea and beryllium-10 concentrations in water samples of high northern latitudes, in: *Land-Ocean Systems in the Siberian Arctic*, pp. 515–532, Springer, 1998.
- Stumm, W. and Morgan, J. J.: *Aquatic Chemistry: Chemical Equilibria and Rates in Natural Waters* {Environmental Science and Technology}, Wiley, 1996.
- 35 Thullner, M., Dale, A. W., and Regnier, P.: Global-scale quantification of mineralization pathways in marine sediments: A reaction-transport modeling approach, *Geochemistry, geophysics, geosystems*, 10, 2009.
- Van Cappellen, P. and Wang, Y.: Cycling of iron and manganese in surface sediments; a general theory for the coupled transport and reaction of carbon, oxygen, nitrogen, sulfur, iron, and manganese, *American Journal of Science*, 296, 197–243, 1996.
- Wallmann, K., Aloisi, G., Haeckel, M., Obzhairov, A., Pavlova, G., and Tishchenko, P.: Kinetics of organic matter degradation, microbial methane generation, and gas hydrate formation in anoxic marine sediments, *Geochimica et Cosmochimica Acta*, 70, 3905–3927, 2006.
- 215